Universitat Autònoma de Barcelona

In vitro natural remineralization of enamel: Characterization by conventional and synchrotron radiation-based techniques

Sandra Diez García

Universitat Autònoma de Barcelona

In vitro natural remineralization of enamel: Characterization by conventional and synchrotron radiation-based techniques

Sandra Diez García

Doctoral Thesis

PhD programme in Chemistry

Directors:

Prof. Manuel Valiente Malmagro

Dr. María Jesús Sánchez Martín

Department of Chemistry

Faculty of Sciences

2021

Universitat Autònoma de Barcelona

Doctoral Thesis

PhD programme in Chemistry

In vitro natural remineralization of enamel: Characterization by conventional and synchrotron radiation-based techniques

Sandra Diez García

2021

This PhD thesis has been carried out in the Centre GTS (Grup de Tècniques de Separació en Química) at the Department of Chemistry of the Universitat Autònoma de Barcelona, under the supervision of Professor Manuel Valiente and Dr. Maria Jesús Sánchez Martín.

Prof. Manuel Valiente Malmagro

Dr. María Jesús Sánchez Martín

“Si yo no quería ser científica, quería ser bibliotecaria…”

BMQ

AGRADECIMIENTOS

First of all, I want to thank the entire GTS group for being the most amazing group I have ever been part of and for making this thesis period an unforgettable part of my life. Even with a pandemic situation, the wonderful spirit of GTS has been maintained with virtual coffees and vermouths, with the bonus of allowing us to recover our pre-GTS weight (although the traditional welcomes and farewells were really missed). It is wonderful to know that in this group there will always be someone willing to help you when you need it, either with moral support or with hard work. And above all, it makes me happy to be aware that once you are part of GTS, you will always be part of GTS. For all this and for many other reasons, I will be eternally grateful to all of you.

And here comes the most important and difficult part of writing a thesis and the one that most people want to read, thank you all from the bottom of my heart:

Manolo, muchas gracias por darme esta oportunidad de crecer científicamente y como persona a lo largo de la tesis. Ha sido un honor poder aportar mi toque biotecnológico a este grupo de químicos que me ha enseñado tantísimo. Intentaré no olvidar nunca todo lo que he aprendido, tanto de ciencia en los dental hubs como otras lecciones importantísimas para la vida (véase la técnica correcta para cortar jamón o cómo llegar a tiempo para cualquier deadline imposible). Juro que extrañaré de verdad el maravilloso jamón de las celebraciones GTS y me acordaré de ti cada vez que pruebe uno bueno.

Gracias Mari por acogerme bajo tu ala de jefa de dientes. No sé qué habría sido de mí sin tu ayuda, tus consejos y tus eficientísimas correcciones. Sin cortar con que has sido una gran amiga con la que he podido compartir muchas cervezas y buenos momentos a lo largo de estos años. Y por supuesto, espero que siga siendo así muchos muchos años más, de momento en cuanto mi tobillo se recupere te advierto de que nos veremos en la pista de pádel, y deseandito estoy de la escapada dental a Bilbao. Por cierto, cómo olvidar tu papel como secuestradora de unicornios jaja gracias por montar semejante circo que tan entretenidos nos tuvo a todos, y sobre todo por ser magnánima y devolverlo para el viaje familiar.

Jorge, mi rey de Biomat, tengo tanto tanto que agradecerte… Han sido muchos años trabajando codo con codo y compartiendo también la vida fuera del lab, incluyendo todas las rutinacas en el SAF como mi compañero deportivo por excelencia que eres. Has estado ahí en las buenas y en las malas, compartiendo risas o jornadas interminables según tocara. Gracias por apoyarme siempre, aunque nos tuviéramos que ir a Suecia desde el sincrotrón literalmente sin dormir y acabáramos con un tatuaje (por cierto, ya solo quedas tú para el próximo). Nos han dicho muchas veces que parecemos salidos de escenas de matrimonio y no me extraña con la de cosas que hemos vivido juntos. Ya sabes que te quiero un montón, aunque a veces seas un poco gruñón y me intentases echar al sofá en Bilbao jaja al menos no fue al suelo que conociéndote no me habría extrañado.

Mil gracias a mi Manu por ser tú, visir de Biomat y rey del ICP al que quiero con locura. Porque eres una persona increíble que nos ha alegrado la vida en el laboratorio día tras día lloviera o nevase y siempre has estado dispuesto a echar una mano a quien lo necesitara por mucho trabajo que tuvieses (y sabemos de sobra que lo tenías). Sé que ha sido poco tiempo sin ti, pero de verdad de la buena que se te ha extrañado muchísimo en Biomat. Solo espero que la OTB tenga éxito pronto. Que sepas que siempre serás mi Masqueperra, te guste o no. Cuida de Raffaella y dale las gracias a Joan por su deliciosa tarta de tres chocolates que nos alegraba los cafés.

A Sergi, el padre de mi Gorka y ahora de dos gatetes con su Toni que estoy deseando conocer, gracias por los maravillosos ratos que compartimos en Biomat al principio de este viaje que es la tesis y por los que hemos compartido fuera después. Hemos vivido aventuras increíbles, como viajar sin fecha ni destino conocido y acabar en tu "amada" Francia de la que casi no podemos salir sin pasar por el cuartelillo, o ser chantajeados por secuestradores que piden galletas hasta hacerte perder la paciencia y la cordura. Porque se te quiere, aunque seas una perra mala que cotillea sus propios regalos y se alegra de que llamase a la gente ratas traicioneras (aún sin estar presente, solo por amor al caos).

Gracias Clara por encima de todo por enseñarme a pulir dientes jaja es broma, muchas gracias por ser la más increíble hermana de dientes que se puede tener. Porque vivir contigo en Estocolmo fue toda una experiencia, lo bien que lo pasamos, las locuras que hicimos y lo poco que gastamos en comida (no así en cervezas que madre mía que precios). Porque quién si no iba a ir por la vida conmigo sacando fotos divertidas de Bob y haciendo su muñeco de nieve, o se iba a preocupar por si me enfrío haciendo angelitos nada más salir de nuestra maravillosa casa o por si me hundo en el mar. Y ya sabes que si hace falta le tendrás que decir a mi madre que he muerto por gili, pero espero que antes de eso vivamos juntas mil divertidas aventuras más.

Iris, sabia reina de las piedras y mi querida vikinga canaria, mil gracias por estar siempre dispuesta a compartir tus amplios conocimientos con los necesitados a cambio de una sonrisa y un café o lo que surja. De verdad que los brainstorming contigo y unas bravas han sido fundamentales para llegar hasta aquí. Gracias por ser la instigadora de la locura Ginfaxi, has sido una gran compañera de fatigas celulares y espléndidos fikas en Suecia (no sé qué habríamos hecho sin ti). Espero que nunca olvides la fantástica canción de remover la salsa. Gracias también por ofrecerte como profe de boxeo, aunque te desesperen mis tendencias kungfucianas.

A Mon, mi amada sexy April, cómo darte las gracias por todo lo que me has apoyado durante estos años. Porque tu puerta siempre ha estado abierta para tomar un té y hablar cuando ha sido necesario. Espero que pronto podamos revivir nuestro maravilloso viaje por China en el que compartimos tantas cosas (prisas y pétalos de rosa incluidos) y en el que tanto dinero perdimos por no poner en marcha el negocio de la GoPro o el otro. Por no mencionar que fuiste la otra secuestradora de unicornios jaja escondida a plena vista ya que eras la sospechosa número uno, pero siempre nos lograste dar esquinazo como una profesional. Y sin olvidar tampoco tu gran habilidad con los disfraces para el carnaval del vino, me quito el sombrero.

Gracias a Montse, Cristina y Gus por tanta amabilidad y sabios consejos para esta biotecnóloga infiltrada, porque siempre estáis ahí para echar una mano con las presentaciones o lo que sea cuando hace falta. Y a Roberto y Víctor por vuestra inestimable ayuda en el sincrotrón, porque siempre es una paliza, pero con ayuda se sobrevive así que gracias. Por cierto, gracias por traer esas hormigas Roberto, es la cosa más rara que he tenido el gusto de probar. A Marilyn y Marcia, las chicas de plantas, gracias por llegar a este grupo tan loco y animaros a todo en vez de asustaros jaja sois geniales. Y mil gracias por el delicioso aguacate cubano Marcia. Laia, pastelera por excelencia, gracias por todos los deliciosos e increíbles postres. Nithya, the synchrotron girl, thank you for always being so sweet and best of luck in your next journey. And special mention also to all the wonderful foreign visitors I have had the pleasure to meet in this international group and who have taught me so much about the world.

Thanks to my entire Chinese colony, JingJing, Jun, TingTing, Wei, Lou and Dong, because you have all been great friends. JingJing, darling, you were the first to leave and I miss you infinitely but I sincerely hope to see you again soon, the SAF spa is not the same without you and I also miss going to museums together. TingTing, my dear queen of plants, my crazy and amazing girl, I also miss you already and I've tried to take care of your Male but I'm afraid it will come back to you with a couple of adjustments (at least your plants are fine, I promise). And of course, thank you to Jun and Wei for all your super delicious dumplings, I miss you too (not only your food) and the Chinese New Year is not the same without you. Lou (Juanlu) and Dong (Don Juan), thanks for my Chinese name (格格桑), I plan to enjoy very much the time we have left to share, although I have to confess that I'm crying inside because Lou's departure is approaching and that I also like your dumplings Dong don't worry. By the way, TingTing and Wei, your wedding was gorgeous so thanks for letting me be part of it. Also thank you all for welcoming us so warmly in your cities during our trip and introducing us to your culture (we will visit your hometown next time Dong so don't be sad).

Evidentemente no puede faltar aquí ninguno de los maravillosos antiguos miembros de GTS, que como bien he dicho antes siempre serán parte del grupo lo quieran o no. A Vero, Mangi y su Gina, eternas compañeras del carnaval de Haro, gracias por los buenos momentos que compartimos cuando estabais aquí y por los que han venido después. Vero, gracias por llevarme de croquetas en mi primerísimo miércoles aquí, eso es un buen recibimiento y lo demás son tonterías jaja y dale las gracias a Kike por descubrirme que el pollo con Coca-Cola es un manjar. Mangi, jefaza de las plantas y los sincrotrones, gracias por sacar siempre un rato para charlar con un té después de comer jaja aunque siempre trabajaras hasta horas intempestivas y te extrañáramos en el café. Albert, Javi y Elena de mis amores, ha sido un placer compartir con vosotros todas esas muy necesarias cervezas afterwork a lo largo de estos años, y que no paren porfa que esta pandemia ha sido muy mala pero ya se ve la luz y se os extraña. Por cierto Javi querido, me disculpo nuevamente por el evento paranormal de los Power Rangers en tu tesis jaja pero gracias por tomártelo con buen humor. Gracias Marta por ser mi compañera de pádel por excelencia y espero volver a jugar contigo pronto. A Olga, mi madre de dientes, que te apuntas a un bombardeo si hace falta y este año nos has adelantado a todos con las fotazas del calen. Pilar, mi abuela de dientes, gracias por esas

charlas sobre el mundo dental que hicieron más cortos esos viajes interminables por toda China, y fue un placer conocer al adorable gruñón de tu perro en Miranda. Aunque en realidad tengo que dar las gracias a todo el equipo del China Express (Mon, Mangi, Elena y Pilar), porque nunca olvidaré las aventuras que vivimos por China, fue el mejor viaje de mi vida y no habría sido lo mismo sin vosotras.

Y llegamos a los inestimables minions jaj son muchos y seguro que me dejo a alguien, pero de verdad que gracias a todos. Primero mis niñas, Anna y Mariona, muchas gracias por haber pensado que un TFG de dientes sería divertido y aparecer así en mi vida para alegrarme la cansada vida de pulidora de dientes solitaria. No se me olvida Anna que la idea original de secuestrar unicornios fue tuya y solo tuya. Alejandro, compi de piso sincrotroniano, gracias por toda la historia que me enseñaste (quisiera o no aprender) y los buenos ratos que pasamos en Biomat o en la pulidora. JT, nombrado biomatiano honorario a pesar de ser de plantas, gracias por las anécdotas fabulosas y las aventuras que están siempre garantizadas contigo (aunque no te vuelvo a llevar de karaoke). Anna, la alumna que se convirtió en paciente maestra en el SAF, eres increíble y espero que sigamos haciendo mil cosas más juntas, y dale las gracias a Marc por su paciencia en aquel partido de pádel. A Paula, porque tú también eres genial, y no creas que no sé que lo de Pokémon fue cosa vuestra que me lo confesó Anna, pero sois mis alumnas favoritas igualmente. Óscar, porque ya sabes que eres mi súbdito favorito, gracias por ofrecerte voluntariamente para la locura sincrotoniana (jabalíes incluidos) y dejarte secuestrar un día más de lo prometido para que tus reyes no murieran en el intento, y gracias también a tu hermana por las arepas que nos preparaba. María y Montsita, gracias por traer tanta alegría a Biomat. Y Adrià, solo tengo que decirte que ya apuntas maneras. Serena, thank you very much for the tiramisu and the coconut balls, I hope your little plant arrived safely to Italy and see you in Eurovision. Thanks Indira, because I am very happy that you are coming back. Lovely Fa, thanks for always being willing to learn and help. Georgious and Andreas, thank you for helping me brush so many teeth, you saved me and I know you won't forget it.

Associate Professor Pontus Blomberg and Professor Moustapha Hassan, thank you for welcoming me with open arms at Karolinska. And also thanks to Ying, Rui, Wenji, Qiang, Ibrahim, Fadwa, Risul and Kim. I remember you a lot when I go to a hot pot. Of course, I have to thank the Erasmus group that made my time in Sweden so pleasant and loved Bob so much, thanks Nora, Linde, Niels, Vassilis, Ana, Elena, André, Félix, Mufasa, Emma, Marija and Marloes.

Mil gracias a Maria Dolors, Alba y Elena por ayudarme con toda la locura de papeleos que te encuentras a lo largo de una tesis. Que puede parecer cosa fácil, pero sin vosotras no lo habría sido. Maria Dolors, te extraño mucho cada vez que Manolo trae jamón.

A la planta de Analítica, especialmente a Anna y Marta que empezaron conmigo y con las que he compartido muchas aventuras y desventuras. Espero que acabéis bien esta gran misión tesiana y mucha suerte en la siguiente sea cual sea.

José Manuel Amigo, infinitas gracias por descubrirme el maravilloso mundo de la quimiometría y la buena cerveza, nos vemos pronto. A Pau Solsona, mil gracias por el tiempo

que hemos pasado juntos nanoindentando dientes. Gracias también a la maravillosa gente del SEM, Martí, Emma, Pau y Cris, que se desesperaban conmigo cada vez que un diente se revelaba contra nosotros. And thank you to Ibraheem and Oriol, my synchrotron local contacts, for the invaluable help.

Thanks to the past, present and I hope future Sexy Scientific Calendar team for making special each day 1 along these years, and my special gratitude to the customers for helping us in our solidarity purpose.

Y muchas gracias a la Pizarrita de Juanlu y la cafetería de Ingeniería por alimentarme y proveerme de energía tantos años, da mucha alegría que siempre te reciban con una sonrisa. Gracias también por ayudarnos a vender calendarios, sois los mejores.

A mis Albas de la moneda, especialmente a ti locatis que estoy muy feliz de que estés bien y muy orgullosa de ti. Hicisteis de esa fábrica un lugar mucho más divertido, aunque éramos un desastre encolando hojas juntas y mejor no hablemos de limpiar el chisme ese.

Y a mis amigas de la universidad Irantzu, Nagore, Sara, Alba e Irene, por empezar conmigo este camino y seguir a mi lado desde entonces. Iran de mi alma, que te quiero mucho, aunque abandonaras la química en la que he acabado yo metida para seguir tu vocación de ser profesora, y que estoy orgullosa porque eres una profe genial. Por cierto Nago e Iran, espero seguir saliendo de muchos escape rooms juntas, porque aquella resi de monjas de locos (que puede considerarse el primero de todos) mereció la pena solo por teneros a vosotras como compinches. Nago y Sara, gracias por ser las mejores compañeras de piso que pude soñar (aunque seáis bioquímicas adoradoras de los hámsteres como Darwin). Y a mis biotecnólogas Alba e Irene, fue una bonita carrera y una gran suerte por haberme llevado a conoceros. Queridas Nago y Alba, no os olvidéis de que tenemos una serotonina pendiente.

Por supuestísimo, gracias a toda mi estupenda gran familia llena de gente locamente maravillosa, os quiero a todos. Gracias especialmente a mis padres y a mi hermano que me han animado siempre a perseguir mis sueños. Alberto, papá, tú sí que resplandeces. Gracias por apoyarme siempre con todo tu corazón, aunque toque hacer locuras como tirar para el monte pertrechados con cepillos de dientes eres el primero en apuntarse y disfrutar como un enano. Arturo y mamá, muchas gracias por seguirnos en la loca caza fotográfica de vacas y convertirlo en una divertida excursión familiar (sin mencionar que tenéis mucho mejor ojo para el encuadre que yo). Mar, la mejor madre del mundo, gracias por cuidarme tanto y querer siempre lo mejor para mí. Porque aunque a veces refunfuñe las dos sabemos que no estaría aquí si no es por ti, así que mil gracias. Artur, gracias por ser mi little bro, que es duro tenerte tan lejos, pero sé que estás ahí si te necesito y que me quieres tanto como yo a ti, aunque no me lo digas mucho porque no te gustan las cursiladas (estoy cursi, te aguantas). Y a ver si ahora que ambos acabamos la uni sacamos tiempo para ese viaje a Grecia que nos ha dejado pendiente el virus este. Y creo que puedo hablar en nombre de todo GTS para daros las gracias por el suministro constante cada vez que voy a veros de delicatessen culinarias (véase delgadillas o salmorejo a tutiplén) y esquejes de árbol de jade (se supone que trae suerte y dinero, de suerte bien de momento, pero el dinero ya veremos). Gracias

también por acoger a toda la tropa con tanta alegría cuando vamos al carnaval o de viaje turístico a Miranda, y por ser incondicionales del café GTS cuando venís a Barcelona.

Y a Borja, mi compañero en esta vida desde hace más años de los que se pueden contar con ambas manos, gracias por todo. Por estar esperándome en casa con tu paciencia infinita cuando llego cansada y estresada, por alimentarme con rica comida casera en vez de dejar que sobreviva como pueda, por tus ideas que a veces son pepitas de oro, y sobre todo por quererme tanto. Porque eres único e irrepetible para mi, aunque a veces cortocircuite y te llame Gorka o Jorge jaja pero me quieres igual. Porque si hemos sobrevivido a una tesis juntos creo que ya podemos con lo que sea. Gracias por dejarme llenar la casa de plantas, porque aunque pongas cara de circunstancias cuando aparezco con una nueva sé que no nos vas a echar de casa jaja te amo mi gruñoncín. Y gracias también por haber acabado queriendo a los locos de GTS casi tanto como los quiero yo.

With all my love,

Biomat Queen

FINANCIAL SUPPORT

This Doctoral Thesis has been developed with public funding through:

- Pre-doctoral grant, Universitat Autònoma de Barcelona (UAB).
- FI-2017 fellowship, Agència de Gestió d'Ajuts Universitaris i de Recerca (AGAUR).
- CHEMNEXUS, CTM2015-65414-C2-1-R, Ministerio de Economía y Competitividad de España (MINECO).
- NEOSETAC, GA778325, H2020-MSCA-RISE-2017, European Union funding for Research & Innovation.
- Synchrotron granted proposals, 2018093150 and 2020024308, ALBA Synchrotron.

Chemistry Department
Universitat Autònoma de Barcelona, Spain

Fons Social Europeu, Agència de Gestió d'Ajuts Universitaris i de Recerca (Generalitat de Catalunya)

CHEMNEXUS (CTM2015-65414-C2-1-R)
Ministerio de Economía y Competitividad de España

NEOSETAC (GA778325)
Horizon 2020, European Union funding for Research & Innovation, Marie Curie Actions

MIRAS and MSPD beamlines
ALBA Synchrotron, Spain

SHORT-TERM STAYS

Three short-term stays have been carried out during the period of this Doctoral Thesis, where valuable collaborations have taken place, along with the acquirement of novel insights in several areas of knowledge:

- 01/03/2018-30/04/2018. Karolinska Cell Therapy Center, Karolinska Institutet and Karolinska University Hospital, Stockholm, Sweden. Under the European Union funded H2020-MSCA-RISE-2017 project NEOSETAC (New Selenium-based Targeted Nanocapsules to treat Breast Cancer).

- 14/06/2019-02/07/2019. Karolinska Cell Therapy Center, Karolinska Institutet and Karolinska University Hospital, Stockholm, Sweden. Under the European Union funded H2020-MSCA-RISE-2017 project NEOSETAC (New Selenium-based Targeted Nanocapsules to treat Breast Cancer).

- 27/09/2019-07/10/2019. Karolinska Cell Therapy Center, Karolinska Institutet and Karolinska University Hospital, Stockholm, Sweden. Under the European Union funded H2020-MSCA-RISE-2017 project NEOSETAC (New Selenium-based Targeted Nanocapsules to treat Breast Cancer).

RESUMEN

El desarrollo de tecnologías para reconstruir el esmalte dental y restaurar la estructura del diente es de vital importancia teniendo en cuenta la incapacidad del esmalte maduro para regenerarse tras un daño sustancial. Los productos con flúor ampliamente utilizados pueden prevenir la desmineralización y promover la remineralización en las superficies de los dientes sustituyendo los iones hidroxilo por iones fluoruro. Esta interacción forma fluorapatita en el esmalte dental, más resistente a los ácidos y estable, en lugar de hidroxiapatita (mineral original del esmalte).

En el presente estudio se utiliza un enfoque diferente para inducir la remineralización, a fin de evitar las altas concentraciones de flúor con sus efectos secundarios y prolongar el tiempo de contacto entre los iones fluoruro y los dientes. Este trabajo pretende desarrollar un material dental innovador para remineralizar el esmalte dental mediante una combinación apropiada de resinas de intercambio iónico para la liberación controlada de los iones minerales que forman el esmalte dental, en presencia de amelogenina humana para guiar un adecuado crecimiento de los cristales. El novedoso producto propuesto consiste en una combinación de resinas de intercambio iónico (ácido débil y base débil) cargadas individualmente con los iones remineralizantes: Ca^{2+}, PO_4^{3-} y F^-, incluyendo también Zn^{2+} en una cantidad menor como agente antibacteriano, junto con la proteína amelogenina. Dicho cóctel proporciona una liberación controlada *in situ* de los iones necesarios para la remineralización del esmalte que evita la precipitación de compuestos indeseados por el encuentro masivo de iones fuera de la superficie del esmalte, y al mismo tiempo, una guía para el crecimiento de los cristales por la proteína indicada. La proteína amelogenina está implicada en el desarrollo estructural del esmalte natural y desempeña un papel clave en el control de la morfología y la alineación del crecimiento de los cristales en la superficie del esmalte dental.

Los dientes tratados se evaluaron utilizando técnicas convencionales y técnicas basadas en la fuente de luz de sincrotrón. Las limitaciones para evaluar la remineralización del esmalte dental se han superado gracias a una metodología resultante de la combinación adecuada de la radiación de sincrotrón, aplicada tanto a la microespectroscopia infrarroja como a la microdifracción de rayos-X, con la ayuda de la aplicación específica de minería de datos. Estos datos de sincrotrón, analizados con método quimiométrico adecuado, nos permiten

estudiar la evolución de la estructura de las apatitas y su distribución tras el proceso de remineralización. De este modo, pudimos alcanzar la resolución espacial necesaria para determinar los cambios en la remineralización en función de la profundidad gracias a la calidad de los datos proporcionada por la fuente de luz de sincrotrón, particularmente gracias a la excepcional relación señal/ruido. Los datos de sincrotrón se trataron mediante el análisis de componentes principales y la resolución multivariante de curvas para analizar la capa mineral formada en presencia y ausencia de amelogenina, con el fin de determinar la influencia de la proteína en los cambios morfológicos del esmalte remineralizado.

Este innovador material induce la remineralización dental creando una capa de fluorapatita libre de impurezas de carbonato, con una dureza equivalente a la del esmalte sano y la adecuada alineación de los correspondientes nanocristales gracias a la contribución de la amelogenina, siendo la fluorapatita más resistente a los ácidos que el mineral original. Los resultados sugieren que el nuevo producto muestra potencial para inhibir la desmineralización y promover la remineralización a largo plazo, lo que supondría la inhibición de la progresión de la caries y la protección de las estructuras dentales.

SUMMARY

Developing technologies to reconstruct dental enamel and restore tooth structure is of vital importance considering the inability of mature enamel to regenerate itself after substantial damage. Widespread fluoride products can prevent demineralization and promote remineralization on tooth surfaces by replacing hydroxyl ions with fluoride ions. This interaction forms more acid-resistant and stable fluorapatite in the dental enamel instead of hydroxyapatite (original natural enamel mineral).

A different approach to induce remineralization is used in the present study to avoid high concentrations of fluoride with its side effects and prolong the contact time between fluoride ions and teeth. This work aims to develop an innovative dental material to remineralize tooth enamel by a proper combination of ion-exchange resins as controlled release of mineral ions forming dental enamel, in presence of human amelogenin to guide the appropriate crystal growth. The novel product proposed consists of a combination of ion-exchange resins (weak acid and weak base) individually loaded with the remineralizing ions: Ca^{2+}, PO_4^{3-} and F^-, also including Zn^{2+} in a minor amount as antibacterial agent, together with the protein amelogenin. Such cocktail provides onsite controlled release of the ions necessary for enamel remineralization avoiding the precipitation of undesired compounds by massive encounter of related ions outside of the enamel surface, and at the same time, a guiding tool for crystal growth by the indicated protein. Amelogenin protein is involved in the structural development of natural enamel and takes a key role in controlling the crystal growth morphology and alignment at the dental enamel surface.

Treated teeth were evaluated by using conventional techniques as well as techniques based in synchrotron light source. The limitations to assess dental enamel remineralization have been overcome by a methodology resulting from the appropriate combination of synchrotron radiation-based techniques on both, infrared microspectroscopy and micro X-ray diffraction, with the help of specific data mining. The appropriate synchrotron data obtained, analysed with the proper chemometric method, allow us to study the evolution of the structure of apatites and their distribution after the remineralization process. Thus, we could reveal the spatial resolution required to determine the changes in the remineralization as a function of the depth thanks to the goodness of data provided by the synchrotron source, in particular the unique enhanced signal-to-noise ratio. The

synchrotron data were treated using principal component analysis and multivariate curve resolution to analyze the mineral layer formed in the presence and absence of amelogenin in order to determine the protein influence on the morphological changes of the remineralized enamel.

The innovative material induces the dental remineralization creating a fluorapatite layer free of carbonate impurities, with a hardness equivalent to sound enamel and the appropriate alignment of the corresponding nanocrystals thanks to amelogenin contribution, being the fluorapatite more acid-resistant than the original mineral. Our results suggest that the new product shows potential for inhibiting demineralization and promoting long-term remineralization leading to the inhibition of caries progression and protection of dental tissues structures.

GLOSSARY

µFTIR	Fourier transformed infrared microspectroscopy
µXRD	Micro X-ray diffraction
2D	Two dimensions
ACFP	Amorphous calcium fluoride phosphate
ACP	Amorphous calcium phosphate
ANOVA	Analysis of variance
CPP	Casein phosphopeptide
CSM	Continuous stiffness measurement
DEJ	Dentino-enamel junction
DPJ	Dentino-pulpal junction
EDX	Energy dispersive X-ray spectroscopy
FA	Fluorapatite
FE-SEM	Field emission scanning electron microscopy
FTIR	Fourier transformed infrared spectroscopy
HA	Hydroxyapatite
HEPES	4-(2-hydroxyethyl)-1-piperazine-ethanesulfonic acid
LINAC	Linear accelerator
MCR	Multivariate curve resolution
MMP20	Matrix metalloproteinase-20
NMTD	New dental treatment material
PC	Principal component
PCA	Principal component analysis
SEM	Scanning electron microscopy
SR-µFTIR	Synchrotron radiation-based Fourier transformed infrared microspectroscopy
SWOT	Strengths, weaknesses, opportunities and threats
tts-µXRD	Through-the-substrate micro X-ray diffraction
XRD	X-ray diffraction

TABLE OF CONTENTS

1. INTRODUCTION

1.1. Tooth anatomy and physiology

Teeth are hard anatomical pieces rooted in the jaw bones. In the adult human there are usually 32 teeth that are symmetrically distributed in two arches: the upper (maxilla) and the lower (mandible). According to their position in the arch, the teeth can be incisors and canines, which allow cutting food, or premolars and molars, which are the posterior teeth and assist in the food digestion. Human teeth have a layered structure and are divided into a crown, that is the visible part of the tooth, and one or more roots, that are placed in the dental alveoli situated in the jaw. The crown is composed of the tooth pulp, which is an inner soft tissue surrounded by a relatively harder tissue known as dentin, which is enveloped by the enamel that is the hardest biological substance in the human body and protects the dentin. The junction between the pulp chamber and the dentin is known as the dentino-pulpal junction (DPJ), while the junction between the dentin and the enamel is the dentino-enamel junction (DEJ) [1]. The structure of a human tooth observed with a stereomicroscope can be observed in Figure 1.

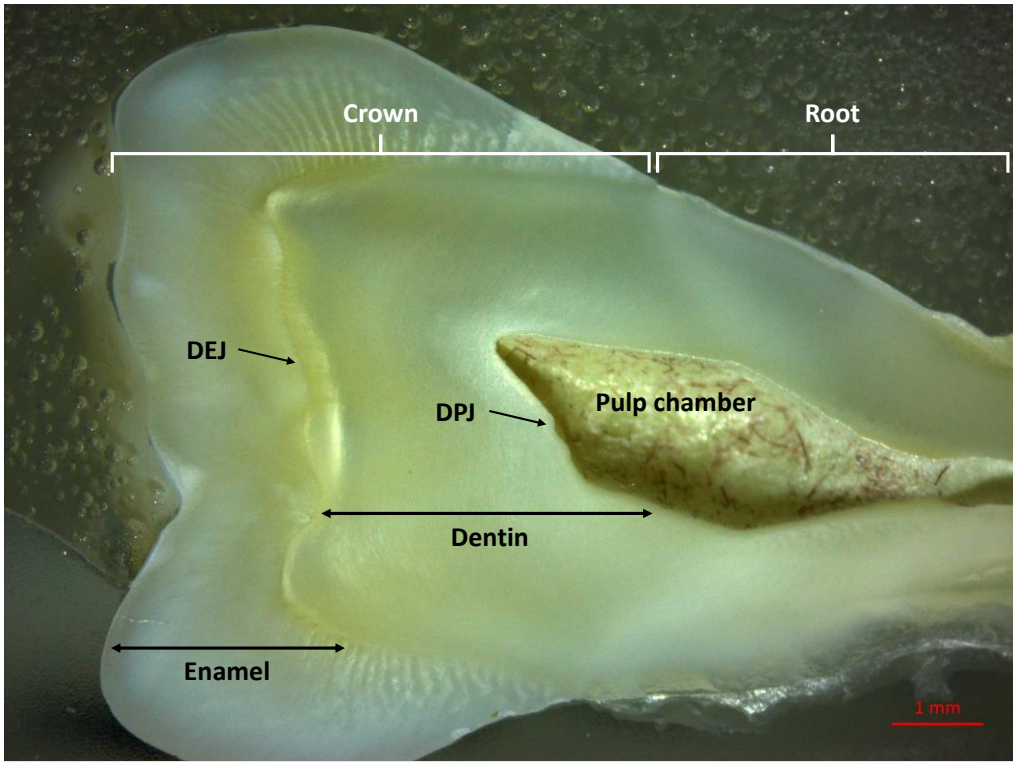

Figure 1. Stereomicroscope image of a human tooth.

Enamel contains around 96% by weight of hydroxyapatite (HA) with 3% of water and 1% of protein, which makes it a highly mineralized tissue, hence its high hardness without being

brittle. This enamel strength is essential to withstand chewing forces, extreme temperature variations and chemical changes. Dentin is a less mineralized organic matrix containing approximately 70% hydroxyapatite crystallites (more randomly oriented than in the enamel) and with significant amounts of proteoglycans, phosphoproteins and collagenous proteins. Dentinal tubules are microscopic fluid-filled channels in the dentin, radiating out from the DPJ. The tooth dentin is innervated and the pulp connects the tooth to the vascularization. The dental pulp is an extremely sensitive tissue since the pulp chamber holds blood vessels and nerves that extend into the roots as root canals. The roots are formed by dentin with a cementum surface, which is a relatively soft matrix containing about 50% hydroxyapatite and also collagen. Cementum anchors the periodontal ligaments, which are responsible for attaching the teeth to the jaw [2,3]. Figure 2 shows the enamel and dentin of a tooth observed by scanning electron microscopy (SEM), dentinal tubules can be appreciated in the dentin.

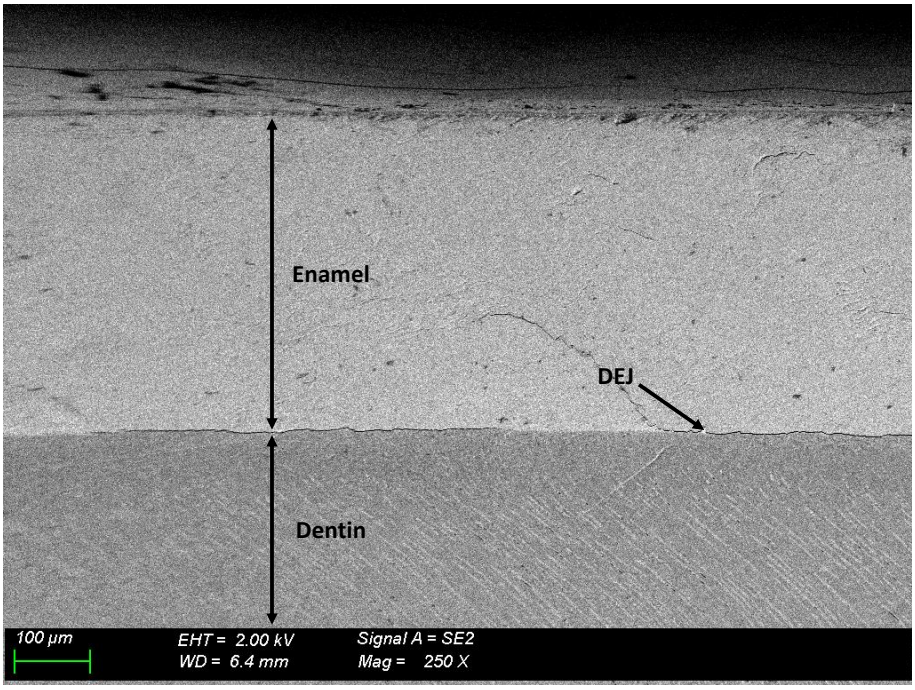

Figure 2. SEM image of a bovine tooth longitudinal cut showing enamel and dentin.

1.2. Tooth enamel

Dental enamel, the outer layer of the teeth, is the most long-lasting mineralized tissue present in the human body, capable of fulfilling its biological function throughout life. Protecting the tooth structure from external damage, despite the fact that it is susceptible

to adverse chemical and mechanical environmental influences with no remodeling capacity and a very restricted ability for remineralization and repair [4].

1.2.1. Dental enamel histology

The enamel is an acellular mineralized tissue composed of highly oriented carbonated calcium hydroxyapatite crystals with a ribbon-like structure grouped in clusters called prisms or rods. The rods start at the DEJ and extend perpendicular to it through the whole enamel length. Each rod composed of a few thousands of nanocrystals is surrounded by organic matter and they are connected by interrods, which are interprismatic crystallites oriented in different directions. The main orientation of the interrods progressively deviates from the rod direction and the farthest interrod crystal is oriented at a 60º angle in relation to the enamel rods. However, the crystals of the prisms do not grow uninterruptedly parallel between them and perpendicular to the surface, instead they present discontinuities in orientation [5,6].

Enamel prisms are structures of about 5 µm wide formed by really thin apatite fibers with a diameter of 50 nm and several hundred micrometers in length to cover the entire enamel [7]. The pattern prevailing in enamel prisms is the keyhole shape, with the prism's core being wider than the tail. Hunter-Schreger bands are groups of enamel prisms with different directionality, which produces an optical phenomenon of dark and light bands. These bands increase the resistance of the dental enamel to wear and fracture, hence the dentition evolution has increased their packing [8].

Healthy primary enamel has a well-preserved outer layer with a microstructure without enamel rods. Its average thickness is 50-100 µm, but can reach values of up to 220 µm, whereas in mature enamel this prism-free layer is reduced to less than 5 µm or is absent [4]. Mature human enamel thickness varies, increasing from a tapered edge to as much as 2.5 mm at the cusps [8].

1.2.2. Chemical composition of dental enamel

During tooth germination, the enamel mineral is a highly substituted carbonated apatite. The composition of enamel hydroxyapatite differs slightly from the stoichiometric HA ($Ca_{10}(PO_4)_6(OH)_2$) since it is carbonated and may contain other cations such as magnesium, sodium, potassium, zinc or strontium. The mineral is related to hydroxyapatite but is much more soluble in acid, as well as calcium deficient (calcium is replaced by the other cations),

and contains between 3 to 6% of carbonate ions replacing phosphate ions in the crystal lattice [4,9]. Although the carbonate ion can also substitute for two hydroxyl ions to a lesser extent. In both types of carbonate substitution, variations in the crystal lattice parameters are induced because the O-O distance of carbonate ion is different from the O-H distance of hydroxyl ion and the O-O distance of phosphate ion. Table 1 shows the major constituents of dental enamel, as well as minor constituents and trace elements that are incorporated into the tooth enamel structure during its mineralization. The stability of the apatite structure, as well as the resistance of apatite to acid attack, may be influenced by minor constituents and trace elements. In addition, these elements may also play a role in inhibiting or promoting calcification. Their concentrations change from the outer surface of the enamel to the DEJ and some elements can alter the lattice parameters even being present in small amounts [5].

Table 1. Major and minor constituents of dental enamel and trace elements [5].

Constituent	*Average concentration (dry weight, %)*
Ca	36.6
P	17.7
CO_3	3.2
Na	0.67
Mg	0.35
Cl	0.35
K	0.04
Trace element	*Mean concentration (dry weight, µg/g)*
Zn	179
Sr	156
Si	136
F	120
S	59
Al	51
Fe	33

Mineral composition of mature enamel is a mixture of compounds, primarily hydroxyapatite. This HA of mature enamel is not stable and suffers changes due to chemical interactions. The major change is produced when phosphate is substituted by carbonate because this substitution increases the solubility of the enamel. However, fluorapatite (FA) is generated if the hydroxyl ions of HA are replaced by fluoride ions, being this compound with fluoride less soluble and more resistant to acid attack [10].

1.2.3. Morphogenesis of dental enamel

Dental enamel formation or amelogenesis consists of a series of well-organized extracellular processes controlling the nucleation, growth and arrangement of the developing enamel apatite crystals [11].

The enamel mineral is primarily produced at the DEJ. The crystals, once nucleated, elongate in a direction defined as the c-axis of the crystal that is perpendicular to the junction, and form the rods. The ameloblasts are the cells derived from the embryonic ectoderm that secrete an extracellular protein matrix, which is involved in the formation and mineralization of tooth enamel. This protein matrix consists of two protein types, amelogenins and non-amelogenins. The amelogenin proteins constitute the majority of the organic matrix during the development of enamel, followed by enamelin and ameloblastin [5,6]. Ameloblasts form a monolayer around the developing enamel tissue and move as a single front as they secrete and deposit the protein matrix that serves as a template for crystal growth [12].

The formation of apatite crystals has three stages called secretion, transition and maturation. Following the differentiation of ameloblasts during the presecretory stage, they reach the secretory stage with a morphology characterized by a cellular process called the Tomes' process [3]. It is based on triangular-shaped cell projections that are located at the distal end and penetrate the enamel matrix. The Tomes' process is crucial for the exocytosis of secretory vesicles and is also involved in the determination of the boundaries between rod and interrod regions [12]. A continuous calcium supply is required for crystal formation and growth and this calcium most likely comes from the ameloblasts through an active calcium pump. A high local calcium concentration is obtained as a result of this ameloblast mechanism, leading to a calcium phosphate precipitation in the proximity of the cells, which then initiate the amelogenin secretion [5].

Enamel matrix proteins play a vital part during the development of enamel in the regulation of mineralization and crystal organization. The organic matrix of proteins secreted by the ameloblasts provides a scaffold for the enamel minerals to grow. The importance of the amelogenin protein is well known because amelogenin self-assembly controls the morphology, size and orientation of the growing crystals [13–16]. The filamentous protein structures present during enamel development are formed by amelogenins. The interaction of amelogenin scaffolds with acidic non-amelogenin proteins induces an amorphous calcium phosphate (ACP) precursor formation, that is progressively transformed into oriented apatite fibers along the protein scaffold [17].

Today, the molecular mechanisms of the protein matrix to synthesize the distinctive enamel architecture are still unclear. The self-assembly of amelogenin *in vitro* has been investigated to gain a better understanding of this superstructure. Amelogenin is a little hydrophobic protein of 175 amino acids with a hydrophilic C-terminus. This hydrophilic tail on a protein otherwise hydrophobic causes amelogenin to self-assemble into nanospheres with a diameter of 20-25 nm. The observation of these nanospheres *in vitro* has led to the hypothesis that the filamentous structures observable *in vivo* are amelogenin nanosphere chains [5,6,18].

Nevertheless, during the last decade, the drastic effect of calcium and phosphate ions found *in vivo* on the amelogenin self-assembly properties has been demonstrated. The presence of calcium and phosphate seems to favor the formation of amelogenin nanoribbons. In physiological circumstances, formation of ion bridges between the amelogenin chains results in amyloid-like protein fibers, which are also consistent with the filamentous structures found in the developing dental enamel [6,7]. The influence of the proteolytic enzyme matrix metalloproteinase-20 (MMP20), which binds to the protein amelogenin, on the resultant protein superstructure has also been considered. The C-terminus of the amelogenin is cleaved by this MMP20 [11,17].

Two different models proposed for the process by which amelogenin proteins regulate the tooth enamel formation are shown in Figure 3.

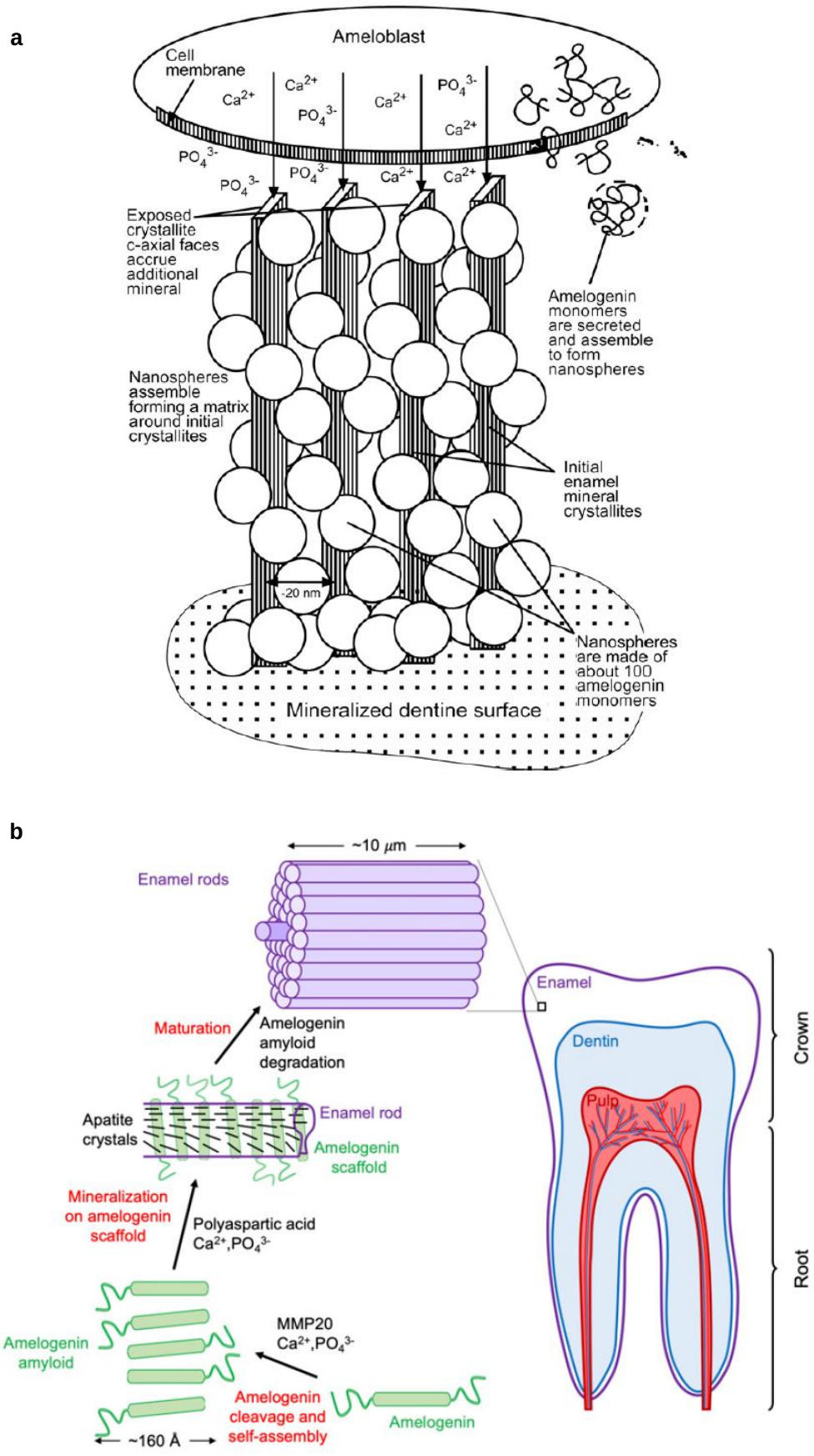

Figure 3. Proposed molecular processes behind the development of oriented apatite crystals in the dental enamel: amelogenin nanosphere chains [5] (a) and amelogenin protein fibers [6] (b).

In the transition stage, the reduction of ameloblast height begins, disappearing the Tomes' process as ameloblasts change their apical cell morphology. Moreover, the secretion of enamel matrix is stopped by the down-regulation of genes coding for the extracellular protein matrix in ameloblasts, and the majority of the organic matter is degraded. The protein content decreases during the process of enamel mineralization from the 20-30% present at the early amelogenesis stage. Once the crystal enters into the maturation stage, when the enamel bulk formation is finished, the protein component concentration has decreased up to 1% of weight of mature enamel. This loss is related to the growth in thickness and width of the enamel crystals, which involves the removal of the protein matrix as the mineral occludes the majority of the tissue volume. To facilitate the elimination of amelogenins in the maturation stage, it has been hypothesized that these proteins are proteolytically degraded to small fragments by serine proteases. During this elaborated process of enamel formation, which requires years to be accomplished, dental enamel changes from a cellular tissue abundant in functional proteins to a completely mineralized tissue with outstanding functional properties [5,6].

1.3. Bovine incisors as *in vitro* model

The caries-free human teeth needed for dental research are really challenging to find, as the teeth extracted by dentists are usually damaged or endodontically treated molars. Fortunately, the enamel structure is strongly preserved across species in contrast to other biomaterials like bone, indicating important evolutionary advantages [6]. Bovine mandibular incisors have a great macroscopic and microscopic similarity to human teeth, so they have been commonly used as a model in dental studies [19–21].

Human and bovine incisors have certain small differences that are important to consider when conducting physical or chemical studies of dental specimens. For example, bovine enamel crystals present larger diameter than human enamel crystals and bovine prisms differ in shape compared to human prisms. In addition, calcium distribution is more homogeneous in bovine enamel than in human enamel. However, there are no significant differences in fluoride uptake or in carbonate content between human and bovine enamel. Moreover, both kinds of teeth have also similar hardness, porosity and amount of interprismatic enamel [22–25].

These healthy bovine teeth are obtained easily from the butchery without the need for an ethical review. Figure 4 shows the structure of a bovine tooth observed with a stereomicroscope.

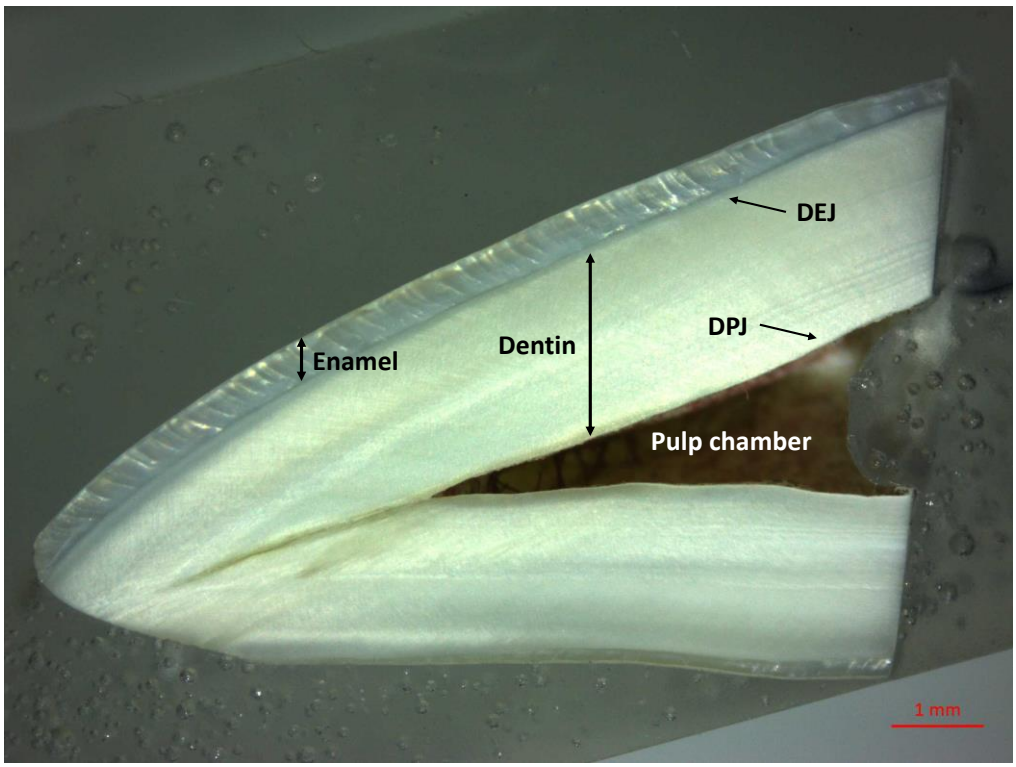

Figure 4. Stereomicroscope image of a rootless bovine tooth.

1.4. Hydroxyapatite versus fluorapatite

Enamel HA is crystalline calcium phosphate that has a hexagonal crystal system with the $P6_3/m$ space group, and its unit cell dimensions are a=b=0.9432 nm and c=0.6881 nm [26–28]. Each unit cell of the HA crystal contains 10 Ca^{2+}, 6 PO_4^{3-} and 2 OH^- ions. There are channels formed by the hexagonal packing of the PO_4^{3-} ions. The OH^- ions are placed along the channels, each of them surrounded by three Ca^{2+} ions at the same level forming a triangle with a 120º symmetry. There is a 60º shift between two calcium triangles, each of these six Ca^{2+} ions having an accompanying PO_4^{3-} ion [5].

FA belongs to the same space group of HA and has a quite similar atomic structure, with the only difference being the substitution of the hydroxyl groups by fluoride (Figure 5). When converting from HA to FA, as the fluoride ion is smaller than the hydroxyl ion, the triangle formed by the three coordinating calcium ions shrinks, resulting in a symmetry-conserving contraction of the unit cell in the a,b-plane to 0.9368 nm but with no change in the c-axis

dimension (long axis of apatite crystal). This reduction in the volume of about 1% is responsible for the greater mechanical strength of FA compared to HA and the enhanced chemical stability by the electrostatic bond between fluoride and the adjacent ions [28–32].

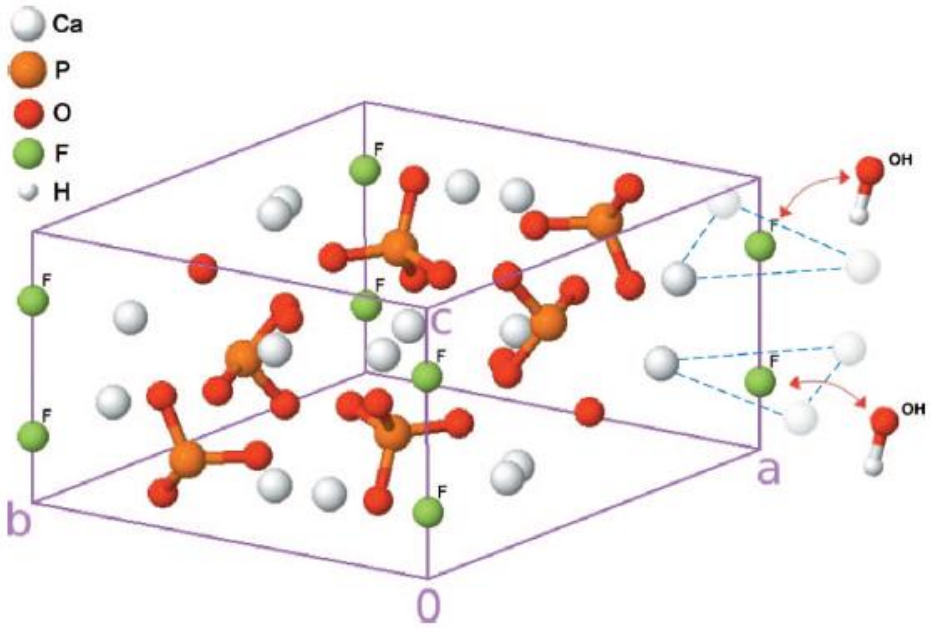

Figure 5. Model of fluorapatite crystal, hydroxyapatite has an identical hexagonal structure but with all fluoride ions replaced by hydroxyl ions as indicated in the image [32].

Fluorapatite can grow in solution taking the form of FA spherulites when a large dipole field along the FA c-axis causes the spherulites fractal grow, as can be appreciated in Figure 6.

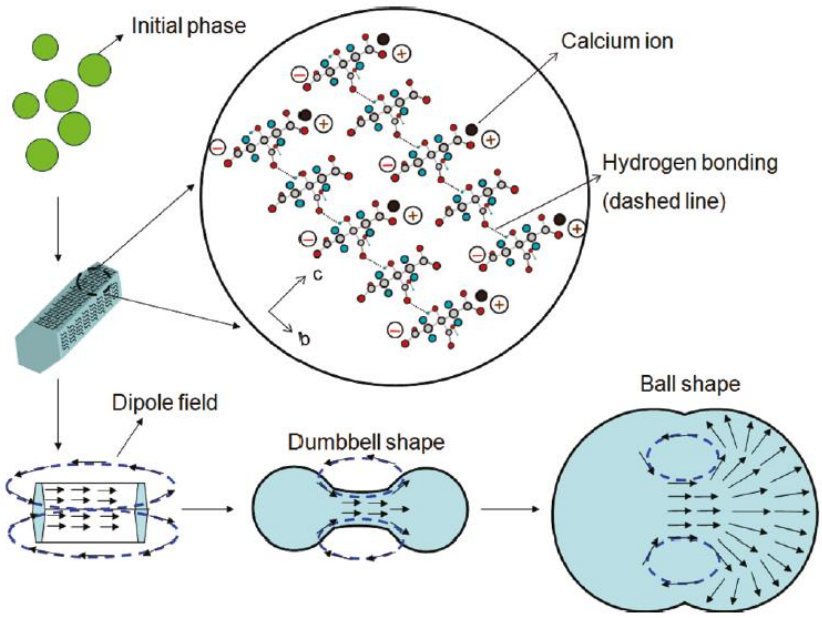

Figure 6. Proposed diagram for the formation mechanism of fluorapatite spherulites [33].

1.5. Dynamic process of demineralization and remineralization

Demineralization and remineralization can be contemplated as dynamic processes (Equation 1). On the one hand, demineralization is basically the mineral apatite loss from the enamel. On the other hand, remineralization is the natural process of the body to repair the enamel rod structure after acidogenic episodes producing net mineral gain.

$$Ca_{10}(PO_4)_6(OH)_2 + 8H^+ \leftrightarrow 10Ca^{2+} + 6HPO_4^{2-} + 2H_2O \quad \text{(Equation 1)}$$

Normally, the dissolution is balanced by the effect of saliva, which is supersaturated in respect to the majority of solid calcium phases and also contains buffering agents to control the pH. The supersaturation of calcium and phosphate in saliva inhibits mineral dissolution. Calcium phosphate phases does not precipitate because of the presence of salivary proteins, specifically statherin and proline-rich phosphoproteins [2]. The suggested action mechanism consists of protein segments containing phosphoseryl residues, particularly the statherin sequence, bind to clusters of calcium and phosphate ions, inhibiting the ion clusters from growing to the critical size necessary to precipitate and transform into a crystalline phase. The saliva's capacity to remineralize demineralized enamel is derived from its ability to deliver bioavailable calcium and phosphate ions to the dental surface thanks to this critical stabilization of the ions by salivary proteins, which also prevents surface deposition forming calculus. Nevertheless, the net remineralization caused by saliva is limited and rather slow, tending to mineral gain in the superficial part of the lesion as a consequence of the low ion concentration gradient into the dental lesion [34].

The calcium-deficient and carbonate-rich regions of the enamel crystal are markedly susceptible to be attacked during demineralization. The carbonate is preferentially lost during the demineralization process, and it is excluded during remineralization. When the hydroxyl groups in pure hydroxyapatite are completely replaced by fluoride ions, it results in mineral fluorapatite, which is really resistant to dissolution by acid (Equation 2). Therefore, the remineralization process implies the diffusion of calcium and phosphate from saliva, and the reaction of fluoride with hydroxyapatite, to build a hypermineralized fluorapatite-like veneer over the remains of existing crystal, which function as remineralization nuclei. Mature enamel is mostly a mixture of hydroxyapatite and fluorapatite, and for this reason it is much less soluble than the original mineral, leading to a post-eruptive resistance to demineralization [9,35,36].

$$Ca_{10}(PO_4)_6(OH)_2 + 2F^- \rightarrow Ca_{10}(PO_4)_6F_2 + 2OH^- \quad \text{(Equation 2)}$$

1.6. Dental health history and significance of dental remineralization

Teeth have great importance in a variety of aspects of life, as they are responsible for the mechanical fragmentation of food, allow the production of sound by acting as resonance boxes and provide a beautiful smile that is crucial for esthetic reasons.

There are several factors that put oral health at risk, such as the popularity of whitening systems with their side effects or the excessive consumption of acidic foods and beverages [37–41]. Numerous children and young adults suffer from erosive tooth wear, which has been linked to the trend towards increased consumption of acidic beverages [42]. Moreover, certain medicines for oral application, like acetylic salicylic acid, can produce dental erosions. The principal intrinsic factor that leads to dental lesions is the contact of gastric juice with the teeth, particularly in people affected by chronic regurgitations, bulimia or anorexia nervosa. The gastric juice erosive potential is mostly caused by hydrochloric acid and there is evidence of a substantially higher erosive capacity of gastric juice compared to carbonated acidic beverages [43].

Nevertheless, the main risk to dental health has always been tooth decay, also known as dental caries or cavities. This illness afflicts about 3 billion people worldwide, inflicting pain and a serious impact on life quality [44]. It is one of the most prevalent preventable childhood diseases and people are susceptible to it during their entire life, being the leading cause of oral pain and tooth loss. Dental caries is a complex disease process that afflicts a large proportion of the world's population, regardless of gender, age and ethnicity, although it is more likely to be present in individuals with a low socioeconomic status and with limited access to healthcare [45–47]. Despite the fact that the prevalence of dental caries has descended over the last decades through advances in dental care, the disease is still a major problem for adults and children, and an improved approach to prevention and therapy is currently needed [9,48]. The teeth themselves become more resistant to demineralization as they age with the incorporation of fluoride into the enamel, which is related to caries being a disease with a high prevalence in childhood [2]. Caries in children is a major global issue and it has been reported that the caries prevalence in children in the United States, Europe and Asia is respectively 28%, as high as 32% and from 36 to 85% [49].

Tooth surface formed by dental enamel is required to have a high resistance to abrasion and corrosion. Mechanical properties of the macroscopic enamel tissue are highly dependent on the alignment and orientation of the crystals. Therefore, changes in surface structure as

a result of caries or microscopic damage can cause significant impairment of the dental function. Moreover, if this damage exposes dentinal tubules to the exterior, it can produce painful tooth hypersensitivity, and ultimately, the tooth loss [50]. More than 12 million dental implants are needed annually worldwide as part of routine oral rehabilitation [51].

However, one of the main purposes of modern dentistry is to treat non-cavitated caries lesions in a non-invasive manner by remineralization with the aim of preventing disease progression and improving esthetics, strength and tooth functionality [34]. The development of technologies to rebuild tooth enamel and preserve tooth structure is of great interest due to the inability of the acellular mature tooth enamel to regenerate itself after substantial mineral loss [52–56].

1.7. Dental caries prevention and treatment

Dental caries is an infectious dentition disease that is characterized by the localized destruction of the tooth. It progresses when organic acids, produced by bacterial action from biofilms of dental plaque on dietary fermentable carbohydrates, diffuse into the tooth and dissolve the mineral. *Streptococcus mutans* is the microbial biofilm member most associated with this disease [57–64]. Dental caries is a dynamic process, which can be stopped and reversed in its initial stages. If left untreated, the early reversible lesion can progress from a stage of an early reversible lesion to an irreversible collapse of the enamel surface [65,66]. The untreated caries will progress to affect the dentin and finally the pulp chamber, which becomes necrotic. The infection may spread to the periodontal tissue at the root apex, resulting in periapical abscesses, and also severe systemic infection may occur in rare cases [2].

The mature enamel has no residual cellular components that can carry out the repair when it is damaged, so the restoration depends on physicochemical events at the tooth surface [45,46]. There are protective factors that can prevent or reverse demineralization in early caries lesions, such as salivary proteins, salivary flow, calcium, phosphate and fluoride in saliva [67–70].

Therefore, preventive treatments are necessary to reduce dental cavities and its associated risks. Non-invasive therapy for the early caries treatment through remineralization has the potential capacity to be a significant breakthrough in the disease's clinical management. The usual treatments for severe caries involve filling the hole with chemically and mechanically

resistant biocompatible materials. Nevertheless, new restorative techniques are currently being developed with the purpose of reconstructing the tissue [48].

1.7.1. Use of fluoride

Fluoride is the most popular agent for enhancing remineralization since fluoride topical administration has proven to be an effective anticaries treatment. Fluoride is widely used in dental products because it has a cariostatic effect inhibiting the demineralization at the crystal surfaces, enhancing the opposite process of remineralization, interfering with plaque formation and inhibiting bacterial metabolism [71–73].

When early enamel lesions are fluoride-enhanced, the fluoride provides remineralization and acid resistance to enamel. The presence of fluoride in saliva has been associated with increased remineralization rates and decreased caries incidence. Therefore, fluoride is added to toothpastes, varnishes, mouthwashes, drinking water and even orthodontic adhesives as an anticaries agent [9,74].

The presence of fluoride ions restricts the formation of acidic, more soluble calcium phosphates, as dicalcium phosphate dihydrate or octacalcium phosphate, and facilitates the creation of more acid-resistant fluorapatite or fluorhydroxyapatite (partial substitution of fluoride by hydroxyl groups) in the presence of salivary calcium and phosphate ions. Fluorapatite or fluorhydroxyapatite are formed when low levels of fluoride ions are present, and calcium fluoride will be created with high levels of fluoride ions, as it can be seen in Figure 7. This calcium fluoride layer, that acts as a reservoir source for fluoride and protects the enamel from the formation of caries, will hydrolyze to fluorhydroxyapatite in the presence of acid phosphate or phosphate ions. Moreover, fluoride is more effective in inhibiting hydroxyapatite dissolution when calcium and phosphate ions are also present in the solution [46,75]. With fluoride availability, demineralization is reduced because part of the calcium and phosphate lost by the dissolution of hydroxyapatite returns to the enamel as more acid-resistant fluorapatite [76].

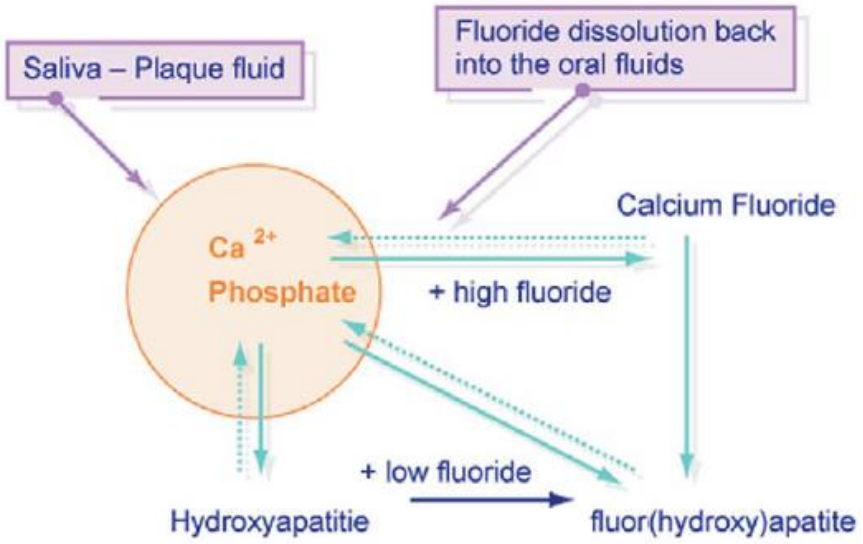

Figure 7. Scheme of the dynamic chemical process of the tooth when fluoride intervenes [77].

Even though systemic fluoride by means of water fluoridation has been promoted in the past for the decline in dental caries, it has been found that the systemic benefits of fluoride are minimal and the primary reduction in dental caries is due to the topical effect of water fluoridation and the availability of fluoridated toothpastes. In several European countries without water fluoridation, a caries reduction has been seen after the introduction of fluoridated toothpastes [47]. Toothpastes are probably the most widespread products in health care and are one of the most effective ways to deliver free or soluble fluoride [78]. Topical fluoride varnish, another widely used dental product, provides a fluoride deposit adjacent to the enamel surface with prolonged contact time. The varnish delivers fluoride to the enamel while forming a calcium fluoride-like complex with a reservoir of free fluoride ions [44].

Despite its benefits, high concentrations of fluoride can cause numerous undesirable side effects. Unfortunately, due to the excessively short oral application time of many fluoride products, fluoride ions are released too rapidly producing high concentrations in a brief period [35,79]. Millions of people around the world are affected by excess of fluoride that can lead to problems such as osteosclerosis and osteoporosis [80]. Overexposure to fluoride during the development of teeth leads to irreversible dental fluorosis with enamel structural and compositional changes due to its hypomineralization [3,12]. In recent times, there has been an increase in the exposure to fluoride ingestion in children, increasing the risk of

toxicity and dental fluorosis because of the high levels of fluoride released into biological fluids [81].

1.7.2. Use of calcium and phosphate

Remineralization by clinical application of calcium and phosphate ions has been ineffective as a result of the poor calcium phosphate solubility, especially with fluoride ions present, since calcium and phosphate ions are not available for enamel remineralization. Insoluble calcium phosphates do not have an easy application, are not efficiently localized on the enamel surface and need acidic conditions for their dissolution in order to generate ions able to diffuse into the subsurface of enamel. In addition, the presence of substantial amounts of solid calcium phosphate phases on the enamel surface is problematic. Meanwhile, soluble calcium and phosphate ions can be employed only at minimal amounts because of the inherent insolubility of calcium phosphates, especially calcium fluoride phosphates. Therefore, soluble calcium and phosphate ions are not sufficiently localized on the enamel surface to induce an efficient concentration gradient to promote diffusion into subsurface dental lesions [34,48].

A technology used to overcome these solubility problems is based on the stabilizing properties of the casein phosphopeptide (CPP). This remineralizing system uses nanocomplexes of casein phosphopeptide-amorphous calcium phosphate (CPP-ACP) to stabilize and deliver bioavailable ions [34]. These CPPs stabilize the raised levels of calcium and phosphate ions on the tooth enamel surface through binding to dental plaque and pellicle that is an organic film on the surface of the teeth. Therefore, the CPP-ACP complexes can attach to dental biofilm, inhibiting bacterial colonization and creating a calcium and phosphate supersaturated environment. Nevertheless, there are disappointing results from clinical research showing few outcome differences in relation to fluoride use. CPP-ACPs have been introduced in toothpastes, mouthwashes, lozenges, chewing gums and even in bovine milk [48,74,82]. This system can also be combined with fluoride resulting in an enhanced dental remineralization due to the synergistic effect of fluoride with CPP-ACP in the remineralization of eroded dental enamel. CPP-ACP complexes have been reported to interact with fluoride ions producing a new amorphous calcium fluoride phosphate (ACFP) phase [42,48].

Another significant technique to consider is the direct application of casein phosphopeptide-amorphous calcium fluoride phosphate (CPP-ACFP) instead of the simple

combination of CPP-ACP with fluoride. CPPs prevent the promotion of dental calculus, which consists of dental plaque mineralization, by stabilizing the calcium, phosphate and fluoride ions. Yet the ions are freely bioavailable to induce remineralization by their diffusion through concentration gradients into enamel subsurface lesions [48]. CPP-ACP and CPP-ACFP are the technologies with most supporting evidence to sustain their use among those commercially available for dental remineralization [34].

Other dental therapy is the addition of bioactive glasses to demineralized enamel. Bioactive glasses are a subset of bioactive inorganic ceramics, capable of reacting with physiological fluids to form strong and stable bonds with mineralized tissue. These bonds are due to the formation of a thin apatite layer at the interface between the glass and the mineralized tissue after implantation, which denotes their effective integration with the surrounding tissue [83]. Therefore, bioactive glasses made up of amorphous sodium calcium phosphosilicate have potential utility in the promotion of enamel remineralization since calcium and phosphate ions can be released intraorally by the particles of glass, but more clinical research is needed to explore their clinical efficacy in inducing dental remineralization [74].

1.7.3. Use of amelogenin and self-assembling peptides

The protein amelogenin, that is the most abundant protein in the forming enamel constituting more than 90% of the protein matrix, plays a central role in guiding the hierarchical organization of apatite crystals observed in mature enamel [84–87]. It is known that the crystal morphology and alignment of enamel, as well as the correct enamel thickness, are the result of a protein-guided uniaxial growth process. The exact mechanism guiding this process remains undetermined due to the rapid degradation of the underlying protein matrix during tissue maturation. However, the role of self-assembly of enamel matrix proteins, particularly amelogenin, has been widely recognized as a key factor in controlling enamel structural development [17,53,84].

Ameloblasts die as soon as the teeth have erupted as their task has been accomplished and the organic matrix is degraded during enamel maturation [8]. As amelogenin is no longer present or replenished after the mature enamel is formed, tooth enamel is unable to regenerate optimally once it has been demineralized or damaged [18]. Therefore, there is considerable interest in the use of amelogenin and other similar self-assembling peptides for dental remineralization [88–94].

1.8. Controlled release by ion-exchange resins

1.8.1. Ion-exchange mechanism

Ion exchange consists of the replacement between labile ions immobilized in a matrix and ions from an electrolyte solution. The uptake of ions by the exchange material will cause it to simultaneously release a stoichiometric amount of ions with the same charge in order to maintain electroneutrality. Thus, ion-exchange materials are polyelectrolytes containing fixed charge sites neutralized by counter ions, ions of opposite charge, which are the ones interchanged. Cation exchangers contain cations as counter ions, while anion exchangers contain anions [95,96]. The application of ion-exchange materials has advantages compared to conventional chemical reagents, since the release of ions is only due to the ion-exchange mechanism so they do not introduce undesirable ions into the solution, and they are characterized by practically neutral pH values [97].

There are many different natural and synthetic materials presenting ion-exchange properties, being ion-exchange resins one of the most important ones. These resins are synthetic organic crosslinked polyelectrolytes. Their ion-exchange behavior and selectivity are mainly determined by the fixed ionic groups. The ion-exchange capacity is established by the number of groups, while the chemical nature of the groups influences the ion-exchange equilibrium, being a relevant factor the acid or base strength [95]. Most of these resins are non-toxic and are used in the pharmaceutical industry, in medical applications and also in the food industry [97]. Their capacity for substituting one type of ion for another supports the potential use of these materials in dental remineralization [98].

1.8.2. New dental treatment material (NMTD)

This research employs an innovative approach against dental demineralization to avoid the side effects of high fluoride concentrations in the oral environment and extend the contact time between the ions and the tooth surface, enabling successful remineralization. The product called NMTD [99] (*Nuevo Material de Tratamiento Dental* in Spanish) provides a controlled release system for the anticaries treatment and it is composed of a combination of weak acid and weak base ion-exchange resins loaded with calcium, fluoride, phosphate and zinc. This agent allows the formation of FA by controlling the rate of fluoride released into the oral environment thanks to the weak resin character, in conjunction with the controlled release of calcium and phosphate ions to induce remineralization avoiding the precipitation of undesired compounds. Thus, the remineralized layer made of FA shows

lower mineral solubility, higher mechanical strength and greater resistance to caries diseases than enamel HA. The molar ratio of the calcium, fluoride and phosphate ions has to be close to that of the organomineral tissue to be remineralized. In contact with NMTD, the organomineral tissues are remineralized in a fast and effective way, especially in the presence of zinc ions, thanks to the bioavailability of the structural ions. These zinc ions act as initiators of the ionic release of the structural ions. In addition, zinc incorporation into enamel may accelerate its remineralization and reduce the rate of enamel demineralization, zinc also has antibacterial and odor-control properties [69,100]. A toothpaste containing NMTD has demonstrated efficacy in limiting enamel demineralization and enhancing remineralization *in vitro* [77].

Table 2 shows a SWOT (strengths, weaknesses, opportunities and threats) analysis to assess the advantages and disadvantages of the NMTD agent.

Table 2. SWOT analysis of the NMTD product developed by the GTS research group.

Strengths	*Weaknesses*
• Product with competitive advantages over the competence because of its *in vitro* efficacy. • Expected absence of side effects due to the slow release of fluoride in the oral environment. • Novel composition with relevant potential for commercial impact. • User-friendly application for at-home use. • Low-cost and industrially scalable production.	• Discomfort due to its slow action and long treatment times. • Technology readiness level 6 of technology demonstration in a relevant environment. • Lack of marketing strategy to differentiate from the competitors. • Production and distribution capacity.
Opportunities	*Threats*
• Socioeconomic impact of dental caries and lack of a permanent solution. • Continuous growth of the dental market. • Dental companies in pursuit of new ingredients to stand out from the competitors.	• Risks arising from *in vivo* testing, manufacturing testing and stability. • Legislation regulating the entry of new products on the market. • Potential market interest in alternative technologies and strong competition.

2. OBJECTIVES

Since mature tooth enamel does not regenerate after substantial loss, finding a suitable solution for the dental problems is essential. The main objective of this thesis is to study and to understand the remineralizing effect of the NMTD agent in presence and absence of amelogenin on tooth enamel in order to develop a suitable remineralizing product. This objective is projected to be accomplished through the performance of the following specific tasks:

- To evaluate the NMTD effect in saliva solution to determine the type of crystal generated by the release of ions from the ion-exchange resins.
- To develop a proper methodology for the analysis of the remineralization of hard dental tissues, understanding the fundamentals of the techniques used to achieve relevant knowledge and accurate conclusions.
- To study the NMTD remineralizing effect *in vitro* using a bovine tooth model.
- To assess the NMTD remineralization capacity in presence of human amelogenin, in order to understand the influence of this protein on the crystal morphology and alignment during the remineralization process.
- To validate the new remineralizing system (NMTD with amelogenin) on human tooth samples since the ultimate goal is the application of this product in humans.

3. EXPERIMENTAL SECTION

3.1. Experimental techniques

3.1.1. Scanning electron microscopy (SEM)

Scanning electron microscopy is one of the most widely employed methods in the surface characterization of materials. This technique scans the surface of the samples with a focused electron beam produced by an electron gun and multiple condenser lenses, allowing the surface structure of the teeth to be studied. The focused beam of high-energy electrons produces a variety of signals scattered from the surface of solid samples that are represented on the SEM image. The signals derived from the interaction between the specimen and the electrons provide information about the specimen, such as external morphology, chemical composition or crystalline structure and orientation of the materials [101,102].

In the first place, the electrons are accelerated by the electron gun, the narrow beam of primary electrons collides with the sample, and then the backscattered and secondary electrons are reflected from the surface and collected in the detector. Backscattered electrons are beam electrons emerged from the sample having a high fraction of their incident energy still intact after undergoing scattering and deflection by the electric fields of sample atoms. While secondary electrons are the electrons escaping from the surface of the sample after the beam electrons have ejected them from the sample atoms [102]. Field emission guns, which are used for field emission scanning electron microscopy (FE-SEM), provide the highest gun brightness among all gun technologies [103].

In the past, samples were severely damaged or altered by the electron beam, requiring the sample to be conductive in order to be observed by SEM. In the case of non-conductive materials, the samples had to be coated with a thin layer of a conductive material like gold [101]. Nonetheless, it is nowadays feasible to process samples in a low conductivity configuration without metallization. The charge compensation systems of the new SEM instruments allow the acquisition of high-resolution images of non-conductive samples. The electrons accumulated on the sample surface are removed by a gentle flux of nitrogen gas to prevent overcharging [104].

The main parts of a SEM equipment and the imaging process are shown in Figure 8.

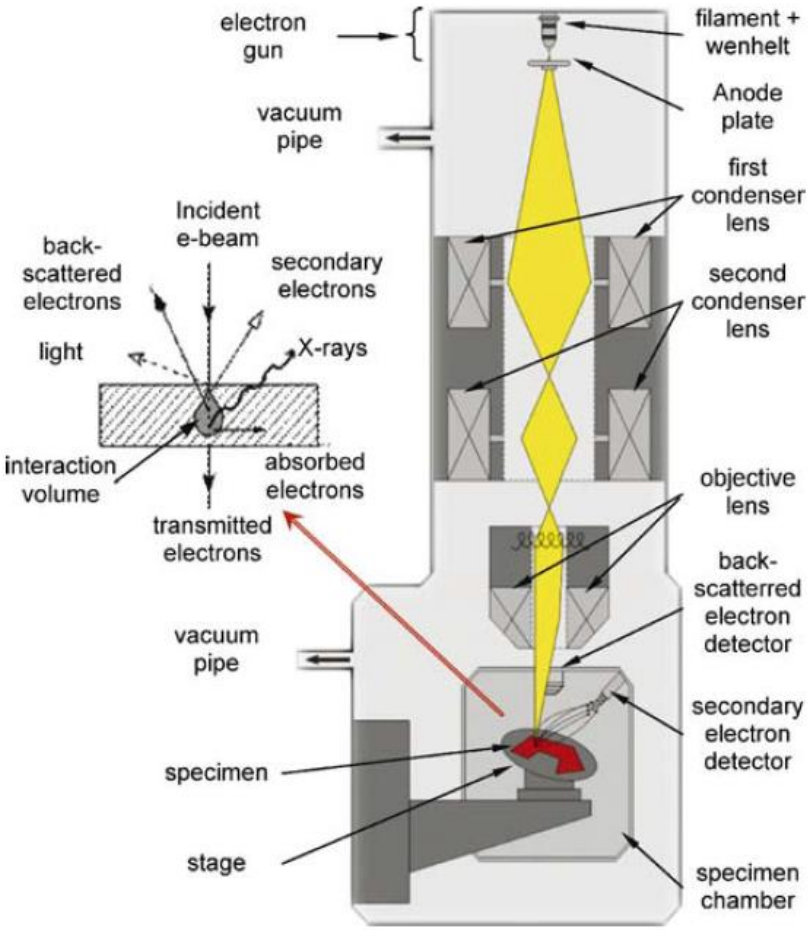

Figure 8. Scanning electron microscope set up and imaging process [105].

3.1.2. Energy dispersive X-ray spectroscopy (EDX)

Energy dispersive X-ray spectroscopy is an analytical technique commonly applied for elemental analysis or chemical characterization of specimens, making possible the determination of fluorine, oxygen, phosphorus and calcium in dental enamel. Each element has a unique atomic structure that allows its electromagnetic emission spectrum to have a single set of peaks, being the basis for the characterization capability of this method. In this technique, a high-energy beam of charged particles is focused into a specimen to stimulate the emission of X-rays distinctive of the sample. An electron can be excited from the ground state by the incident beam, ejecting it as it creates an electron hole. Then, an electron from a high-energy outer state fills the hole, and the energy difference between the energetic states is released as an X-ray. Since the energies of the X-rays are characteristic of the energy difference between the two states and of the atomic structure of the emitting element, the EDX technique allows the evaluation of the elemental composition of the sample by measuring the number and energy of the X-rays emitted by a sample with an energy

dispersive spectrometer [102]. A scanning electron microscope equipped with an EDX detector can be seen in Figure 9.

Figure 9. Zeiss Merlin FE-SEM with an EDX Oxford INCA X-Max detector.

3.1.3. Nanoindentation

Given the relationship between hardness and other physical properties, hardness is significant in the characterization of dental restorative materials. Macroindentation, microindentation or nanoindentation can be used to quantify the hardness of a sample. Nanoindentation is an ideal technique for analyzing dental samples due to the small sample size. The nanoindentation technique determines the hardness and Young's modulus of materials by performing indentation hardness tests, which are perhaps the most commonly employed tools for testing the mechanical properties of materials. Indentation hardness tests have the benefit of being inexpensive, simple, reproducible and fairly non-destructive. The nanoindentation technique avoids the visualization and measurement of indentations. In a nanoindentation test, a loading process up to maximum load and a posterior unloading are applied to the surface of the material by means of an indenter of known geometry. Load and displacement are continuously monitored along the sequence of loading and unloading, and hardness is calculated from the load-displacement curve considering the indenter geometry [106,107]. For measurements on a small scale, the Berkovich triangular pyramidal tip is preferable to the four-sided Vickers or Knoop since a three-sided pyramid is easier to

grind to a sharp point. This nanoindentation technique also allows to perform continuous stiffness measurement (CSM) test, which is the measurement of material properties as a function of depth by applying cyclic loading [108]. Nanoindentation is a technique commonly used in dental science to characterize the mechanical properties of teeth, as they can be accurately assessed with fine spatial resolution in the submicron scale [109–112]. Figure 10 shows a nanoindentation equipment.

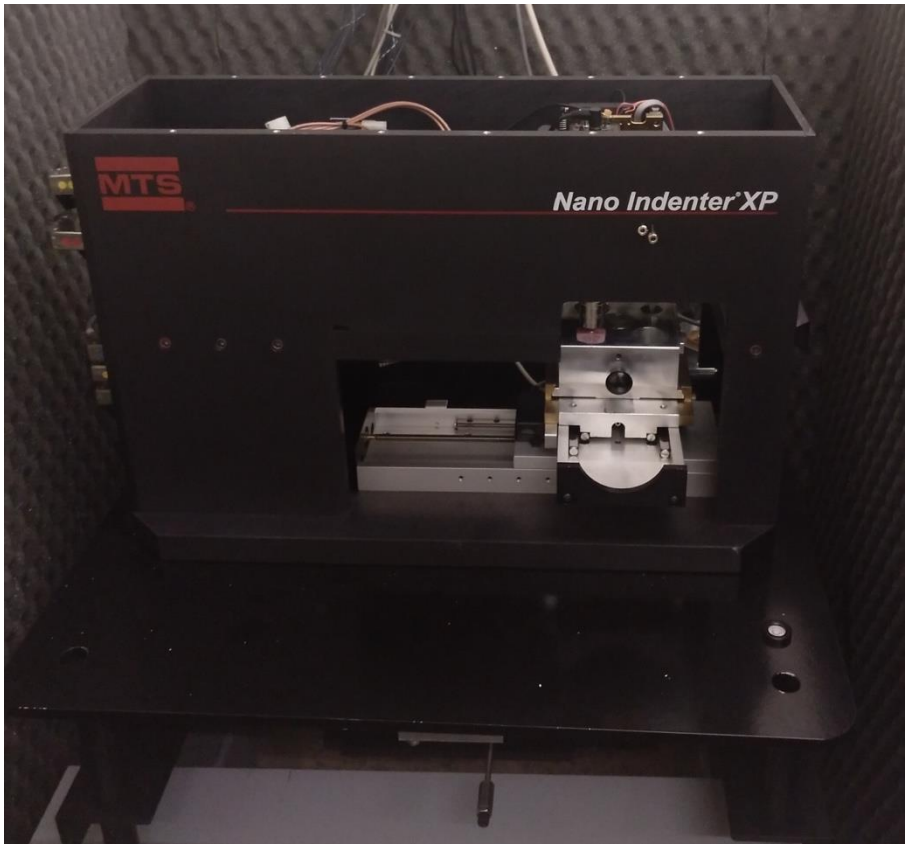

Figure 10. MTS Nano Indenter XP.

3.1.4. Micro X-ray diffraction (μXRD)

X-ray diffraction (XRD) is one of the physical phenomena that occurs when an X-ray beam of a certain wavelength interacts with a crystalline substance. It is based on the coherent scattering of the X-ray beam by the sample (maintaining the wavelength of the radiation) and on the constructive interference (in-phase) of the waves that are scattered in certain spatial directions. Miller indices are assigned to the lattice planes to designate them in a consistent manner and are universally represented by (*hkl*) values [113]. In powder XRD, the Bragg condition (Figure 11) is simultaneously satisfied for a number of atomic planes of numerous crystals randomly oriented [114].

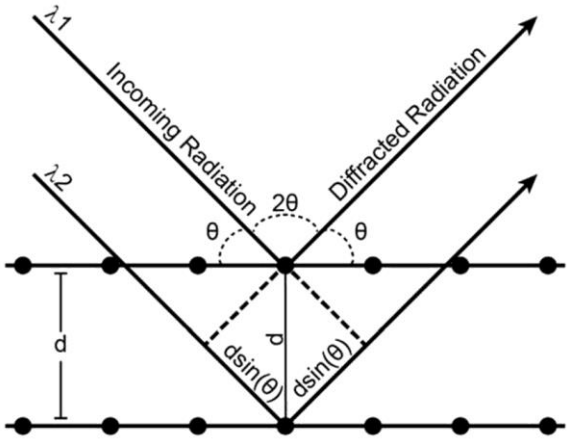

Figure 11. Scheme of Bragg's law conditions [114].

As apatite has a well-defined hexagonal crystal structure, diffraction methods can be used to analyze the crystal structure in teeth [50]. The crystallographic properties of enamel and fluoridated enamel have been investigated using X-ray diffraction. Incorporating fluoride into the enamel structure may lead to crystallographic changes in enamel (contraction of a,b-axis, increase in apatite crystal size and reduction of crystal defects). Nevertheless, enamel crystallinity varies at different layers and if it is ground into powder mixing the layers, it may affect the accuracy of the measurement [115]. The micro X-ray diffraction analysis overcomes the limitations of conventional powder XRD and can obtain site-specific data directly from the tooth allowing the study of the enamel crystallinity at different levels [116].

3.1.5. Fourier transformed infrared microspectroscopy (μFTIR)

The three main regions of the infrared spectrum are the near-infrared (13000–4000 cm^{-1}), the mid-infrared (4000–400 cm^{-1}) and the far-infrared (<400 cm^{-1}). The infrared technique focuses on the vibrations of the atoms that form the molecule. The infrared radiation interacts with a specimen and the portion of the incident radiation absorbed at a given energy is determined. A spectrum peak represents the molecule's vibration and has a specific frequency. The infrared determination process can be considered as a change in the dipole moments related to the molecule's vibrations and rotations. Common molecule movements that lead to this change are stretching and bending of the molecular bond, resulting in a change in bond length or angle. Stretching can be symmetric (in-phase) and antisymmetric (out-of-phase) [117,118].

Fourier transformed infrared (FTIR) spectroscopy led to a major breakthrough in the evolution of infrared instrumentation. The spectra quality and the measurement time were

significantly improved by this technique. It is based on the interference of radiation between two beams and the interferogram is the signal generated by the pathlength change between both beams. This kind of equipment employs an interferometer and performs the Fourier transformation, a well-known mathematical operation [117]. The scheme of a common Michelson interferometer can be seen in Figure 12.

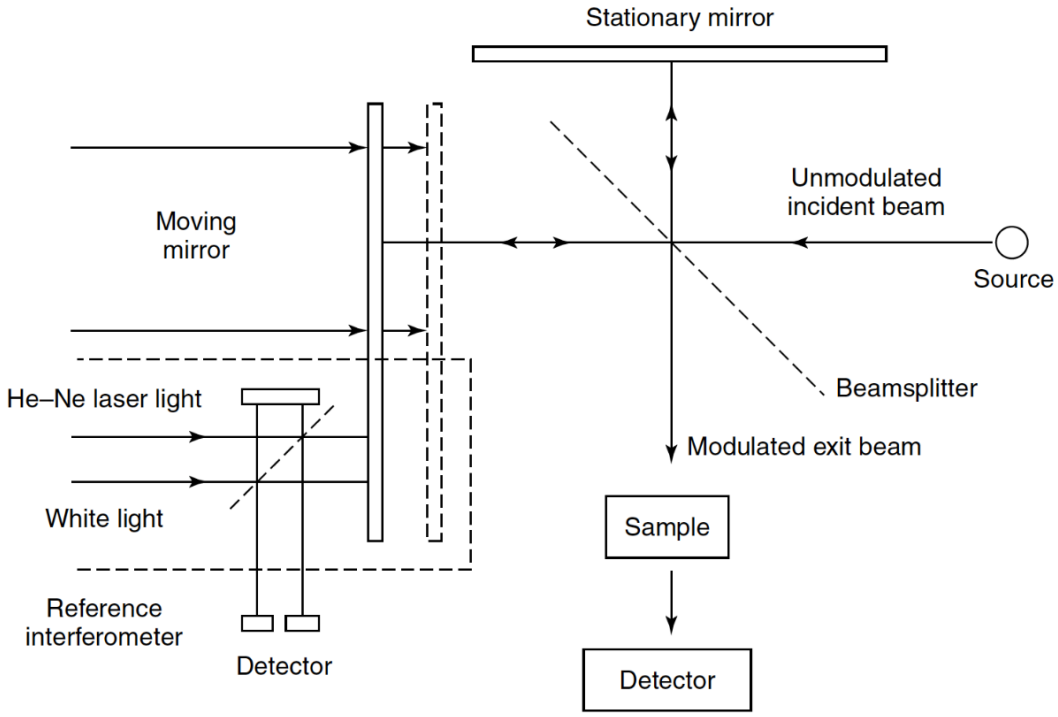

Figure 12. Michelson interferometer scheme [117].

FTIR is a well-recognized molecular vibrational technique widely used to investigate the chemical structural properties of natural materials [119,120]. It has been extensively utilized for mapping the material properties of mineralized tissues such as dental enamel, including mineralization, crystallinity or carbonate substitution [121,122]. The incorporation of a microscope in FTIR microspectroscopy has introduced the possibility of combining biochemical and spatial information [123]. For samples difficult to measure by the conventional transmittance method, reflectance can be employed [118].

Infrared spectroscopy of apatites generally provides two different types of information. The crystalline quality is evaluated from the width of the absorption bands due to the phosphate vibrational modes. The other type of information is based on the presence of molecular species, like carbonate groups, which are detected by specific vibrational bands [124].

3.1.6. Use of synchrotron radiation

Synchrotron light is electromagnetic radiation generated by accelerating bunches of charged particles (usually electrons), which are circulating within an accelerator, through magnetic fields used to bend their trajectory to maintain them inside a circular orbit [125].

Electrons are produced in the electron gun, by thermionic emission from a hot filament, and then accelerated to about 100 MeV by a linear accelerator (LINAC). These electrons are regularly supplied to the booster ring, which accelerates the electrons up to the energy of the storage ring, where they are periodically injected [126]. As can be appreciated in Figure 13, the storage ring is not circular, but is a higher order polyhedron with bending magnets (red cubes) at each vertex. These magnets are crucial to generate radiation, as they deflect the path of electrons (blue line), which travel almost at the light speed, resulting in the liberation of radiation in a broad spectrum of photon energy. Electromagnetic radiation (yellow line) is emitted tangentially and utilized in the adjacent beamlines [127,128]. These beamlines can be used for different techniques according to the radiation energy adapted in the beamline optical hutch [126].

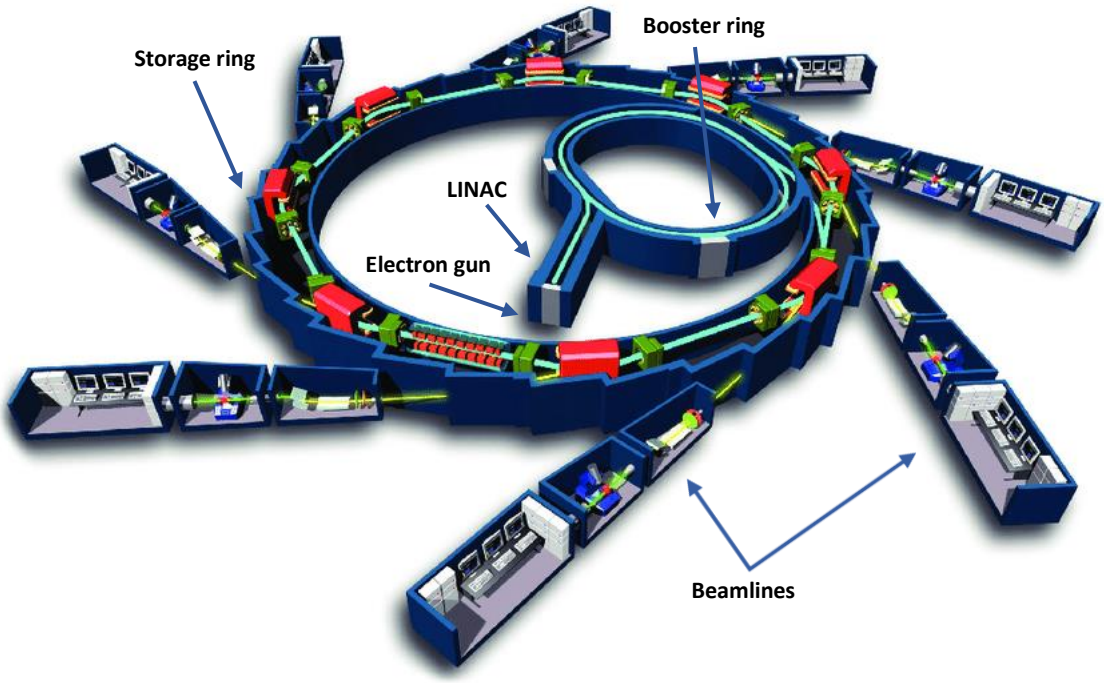

Figure 13. Scheme of a modern synchrotron [128].

The synchrotron through-the-substrate micro X-ray diffraction (tts-μXRD) allows performing punctual analysis in thin sections with a spot size of few micrometers. Therefore, this

technique enables data collection directly on thin tooth sections preserving the textural context and allowing local identification of mineral phases [129].

Coupling µFTIR technique to a synchrotron radiation light source, synchrotron radiation-based FTIR microspectroscopy (SR-µFTIR), allows a much better signal-to-noise ratio and the use of a smaller beam size without losing signal efficiency, since one of the most outstanding properties of a synchrotron radiation source is its high brightness compared with a traditional globar source [123]. The use of µFTIR with synchrotron radiation makes it possible to examine human dental tissues with higher lateral resolution at data acquisition and a high signal-to-noise ratio, avoiding long-term accumulation of the signal, which is essential for the analysis of biological samples. This allows to elucidate the molecular composition of enamel mineral and to observe local changes in areas of a few microns [80].

3.2. Experimental procedures

3.2.1. Reagents

4-(2-hydroxyethyl)-1-piperazine-ethanesulfonic acid (HEPES, 99.5%), magnesium chloride hexahydrate (99%), calcium fluoride (95%) and chloramine T trihydrate (98-103%) were purchased from Sigma Aldrich (Steinheim, Germany); potassium dihydrogen phosphate (99.5%), calcium chloride dihydrate (74-78%) and tricalcium phosphate (35-40% (Ca)) from Panreac (Barcelona, Spain); potassium chloride (99-100.5%) from J. T. Baker (Deventer, Holland), all in powder form. Potassium hydroxide pellets (85%) and hydrochloric acid (37%) were purchased from Panreac (Barcelona, Spain). The hydroxyapatite reference powder was of analytical grade and was used as received without any further purification (>90%, Fluka, Sigma-Aldrich, Steinheim, Germany).

Deionized water was purified using a Millipore purification system (Millipore, Milford, MA, USA).

Food grade ion-exchange resins charged with different ions (Zn^{2+}, Ca^{2+}, F^- and PO_4^{3-}) were purchased from MionTec (Leverkusen, Germany). The base of the weak acid cation-exchange resins is a copolymer from acrylic acid, divinylbenzene and aliphatic diene with carboxylic acid functional groups (Lewatit S 8528, Lanxess, Leverkusen, Germany). While the base of the weak base anion-exchange resins is a styrene-divinylbenzene-copolymer with tertiary amine functional groups (Lewatit S 4528, Lanxess, Leverkusen, Germany). The different resins, ground to a particle size below 50 μm, were mixed to form the NMTD product, with a molar ratio between Ca^{2+}, F^- and PO_4^{3-} of 2:1:1, respectively. In addition, resin charged with Zn^{2+} ions was added, representing 0.2% of the dry weight of the resulting product.

3.2.2. Fluorapatite reference synthesis

The fluorapatite sample was synthetized by a solid phase reaction [28] mixing calcium fluoride (95%) and tricalcium phosphate (35-40% (Ca)) in the agate miller at the ratio of 1.67 Ca/P. Subsequently, the reagents were placed in the muffle furnace Selecta 366 PE (Selecta, Barcelona, Spain) to heat them at 1200 ºC for 2 hours. The solid fluorapatite was then ground into powder for 15 minutes.

3.2.3. Artificial saliva preparation

Artificial saliva was prepared by mixing the following compounds in the indicated concentrations: potassium chloride 0.24 g/l, calcium chloride dihydrate 0.078 g/l, potassium dihydrogen phosphate 0.544 g/l, magnesium chloride hexahydrate 0.041 g/l, HEPES 4.77 g/l. After complete dissolution of the saliva components, the pH was adjusted to 7.1±0.4 with potassium hydroxide pellets.

3.2.4. Mineral growth in solution

In order to form FA in solution, 0.6 g of NMTD were mixed with 1 ml of artificial saliva and placed in a closed container inside an incubator at 37 ºC for 24 hours. The resultant paste is filtered with the aid of a funnel and a Kitasato flask under vacuum, and dried at room temperature.

The structure and elemental composition of the resulting powder were analyzed by SEM-EDX with a Zeiss Merlin FE-SEM equipped with an EDX Oxford INCA X-Max detector. This microscope has a charge compensation system that allows the high-resolution imaging of non-conductive samples, electrons which accumulate on the sample surface are swept away by a fine jet of nitrogen. The images were taken with the secondary electron detector with a low voltage of 1-3 kV and the EDX measurements were taken at 10 kV. The powders from the HA and FA references were characterized under the same conditions. All the analyses were performed at room temperature.

3.2.5. Amelogenin production

A human 175 amino acid amelogenin (Swissprot Q99217, isoform 1, excluding the signal peptide) was expressed in *Escherichia coli* strain BL21 (DE3) and purified by an acid/heat treatment as described previously Svensson Bonde and Bulow [130].

Proteins were analyzed by matrix-assisted laser desorption/ionization, sodium dodecyl sulfate polyacrylamide gel electrophoresis and western blot to confirm the amelogenin production. Finally, recombinant amelogenin was quantified with a nanodrop and stored in aliquots at -20ºC until further use.

Protein purification has been performed by the ICTS “NANBIOSIS”, more specifically by the Protein Production Platform of CIBER in Bioengineering, Biomaterials & Nanomedicine (CIBER-BBN)/ IBB, at the UAB SePBioEs scientific-technical service (http://www.nanbiosis.es/portfolio/u1-protein-production-platform-ppp/).

3.2.6. *In vitro* remineralizing treatments

Bovine teeth are used as a model, given their similarity to human teeth [19,24,25]. Bovine tooth specimens were cleaned of gross debris before removing the root with a diamond saw (South Bay Technology, San Clemente, CA, USA). The resulting bovine tooth samples were embedded in Fastray acrylic resin (Harry J. Bosworth, Skokie, IL, USA) with pink color or Paladur clear autopolymerizing acrylic resin (Heraeus Kulzer, Hanau, Germany), closing the root aperture and leaving the front enamel surface exposed.

When using human teeth, the roots are preserved, but the teeth are embedded in the Paladur acrylic resin covering the roots and leaving the front enamel surface exposed.

The embedded teeth were then etched with hydrochloric acid 1 M for 30 seconds [131] to mimic the early stage of dental erosion and immediately afterwards cleaned by rinsing with MilliQ water while brushing for 20 seconds with an electric toothbrush. The surface of an acid-etched tooth can be seen in Figure 14.

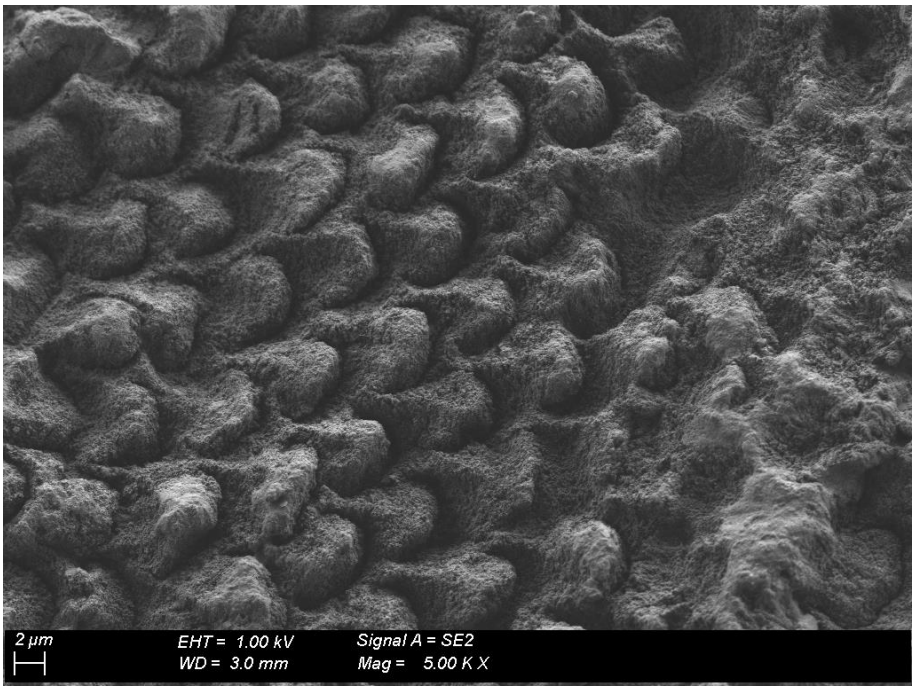

Figure 14. SEM image of the surface of an acid-etched human tooth.

To prepare blank samples acid-etched teeth were placed in artificial saliva solution at 37 ºC inside an incubator during the entire treatment period, which may vary from 4 to 20 days depending on the experiment, and cleaned with MilliQ water while brushing for 20 seconds with an electric toothbrush every 24 hours.

In order to perform the remineralizing treatments artificial saliva was added to NMTD until the optimal consistency of thick gel was reached for its application on the teeth. In the case of the treatment with NMTD and amelogenin, 100 µg/ml of human amelogenin was added to the saliva before mixing with NMTD. In both cases the mixture of NMTD with the corresponding saliva (with or without amelogenin) was distributed on the enamel surface of acid-etched teeth. Then, the samples were placed in a sealed vessel with the base filled with saliva to maintain the humidity of the environment (Figure 15). The recipient was placed inside an incubator at the normal temperature of the oral cavity (37 ºC). Every 24 hours for the whole period of treatment (between 4 and 20 days), each treatment was renewed by washing the samples carefully with MilliQ water and brushing for 20 seconds with an electric toothbrush before applying a fresh treatment portion.

Figure 15. Bovine teeth with NMTD treatment in the vessel before sealing.

Finally, all teeth were cleaned by brushing with MilliQ water for 20 seconds and stored in a 0.5% chloramine T solution until further preparation for analysis.

3.2.7. SEM-EDX tooth analysis

To study the evolution of the remineralized layer thickness, selected bovine samples embedded in Fastray acrylic resin and treated between 4 to 20 days (blank samples with only saliva, NMTD samples or NMTD and amelogenin samples) were longitudinally cut in two halves along the central lobe with a Struers Minitom precision diamond saw (Struers,

Copenhagen, Denmark). A sequence of silicon carbide paper was used to polish the longitudinal side with a Struers LaboPol-25 polishing machine (Struers, Copenhagen, Denmark), starting at grit size P1000 and sequentially increasing to P4000, under a constant water flow. A diamond paste with a mean particle size of 1 µm was used to finish the polishing. After each polishing, the samples were sonicated for one minute to clean the polishing residues.

In addition, to study the strength of the remineralization, some bovine samples treated during 15 days with NMTD were brushed continuously for 15 minutes with an electric toothbrush before proceeding to prepare the longitudinal sections.

Moreover, bovine tooth samples embedded in Fastray acrylic resin and treated during 4 or 15 days with saliva, NMTD or NMTD and amelogenin were selected for surface analysis.

In order to analyze dental samples by scanning electron microscopy, teeth were totally dried first. Thus, longitudinally cut tooth samples for lateral analysis and uncut tooth samples for surface analysis were rinsed thoroughly with MilliQ water, dried and placed for at least 24 hours in a desiccator. Bovine samples prepared for lateral and surface measurements can be seen in Figure 16.

Figure 16. Image of bovine dental specimens prepared for lateral (left) and surface (right) SEM-EDX analysis.

The structure and elemental composition of the samples were analyzed by SEM-EDX with a Zeiss Merlin FE-SEM equipped with an EDX Oxford INCA X-Max detector. Despite the equipment's charge compensation system, a conductive carbon tape, placed near the sample area of interest and extended to the metal holder, is used to prevent overcharging

of the teeth and to obtain higher resolution images. The images were taken on the longitudinal section and the surface of the teeth with the secondary electron detector with a low voltage of 1-3 kV and the EDX measurements were taken at 10 kV. All the measurements were performed at room temperature.

SEM image processing was performed using ImageJ [132,133], a public domain image processing and analysis program developed at the U.S. National Institutes of Health. GraphPad Prism 9 (GraphPad Software, San Diego, CA, USA) was used for statistical analysis through one-way analysis of variance (ANOVA).

3.2.8. Nanoindentation tooth measurements

To study the hardness of the remineralized layer, selected bovine samples after 15 days of NMTD treatment with or without amelogenin were entirely covered by the same Fastray acrylic resin in which they were initially embedded before treatment and longitudinally cut into two halves with a Struers Minitom precision diamond saw. The longitudinal side of the samples was polished as described in the previous section. A bovine sample prepared for lateral nanoindentation and an example of indentation can be seen in Figure 17.

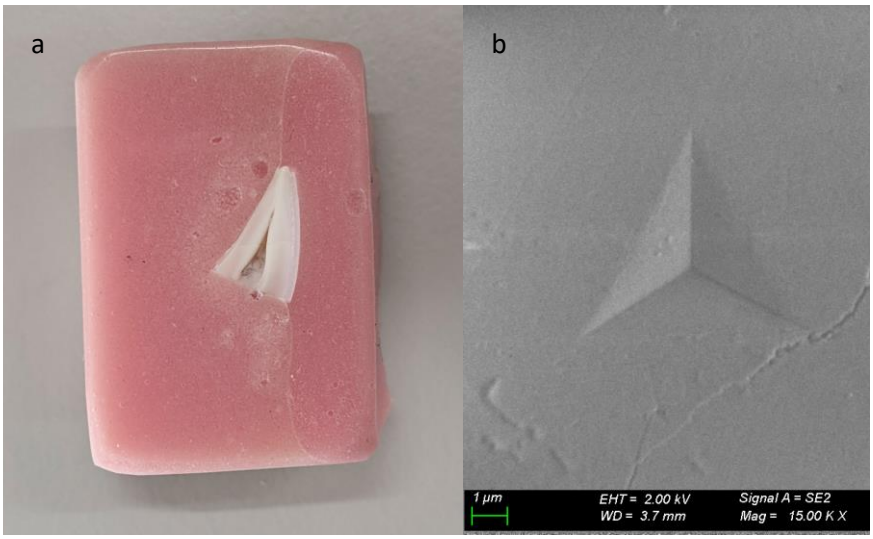

Figure 17. Image of a bovine dental specimen prepared for nanoindentation (a) and SEM image of a nanoindentation performed on the polished enamel of a bovine tooth longitudinal cut (b).

The hardness of the teeth was measured using an MTS Nano Indenter XP with a Berkovich tip that provides a fast and reliable way to acquire mechanical data on the submicron scale. The continuous stiffness measurements were performed in the longitudinal section of the tooth with a depth limit of 1000 nm and a Poisson's ratio of 0.25 [134,135]. CSM with depth,

in conjunction with the known indenter tip area function, allows continuous hardness monitoring [136]. Before every measurement, the Berkovich diamond indenter was calibrated on a standard fused silica specimen. All the measurements were performed at room temperature and with tooth samples still wet to avoid changes in the hardness due to drying.

3.2.9. Synchrotron tts-µXRD experiment

3.2.9.1. Sample preparation

A couple of bovine samples of each treatment (NMTD with or without amelogenin), which had been treated for 15 days, were released from the Paladur acrylic resin and embedded in Epofix resin (Struers, Copenhagen, Denmark). The tooth samples were longitudinally cut in half, fixed on a glass substrate of 1.5 mm thickness and polished to reduce the sample thickness down to 30 µm and achieve a flat surface. A tooth thin section image can be seen in Figure 18.

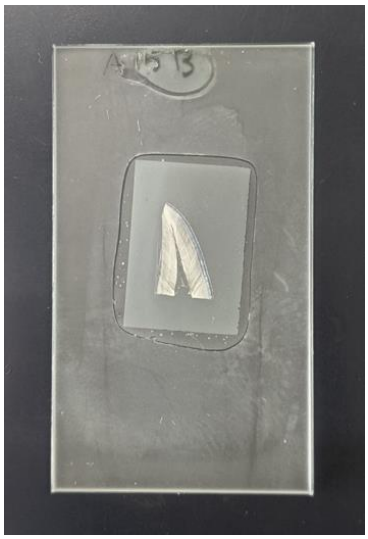

Figure 18. Image of a bovine dental specimen prepared for synchrotron through-the-substrate micro X-ray diffraction.

3.2.9.2. Data acquisition

Synchrotron tts-µXRD measurements were performed at the Materials Science and Powder Diffraction (MSPD) beamline of ALBA Synchrotron (Cerdanyola del Vallès, Spain) [137]. The MSPD beamline is equipped with Kirkpatrick-Baez mirrors, providing a monochromatic focused beam of 15x15 μm^2 size at full width at half maximum and with a Rayonix SX165 CCD detector (round active area of 165 mm diameter, frame size 2048x2048 pixels, 79 mm

pixel size and dynamic range 16 bit). The tooth sections were measured in transmission mode through the glass substrate (Figure 19) [138]. The energy employed was 29.2 keV (λ=0.4246 Å), as determined from the Sn absorption K-edge. Instrumental calibration was carried out with a LaB_6 standard (NIST SRM 660b). The final data consisted of a two dimensions (2D) diffraction pattern in a series of points from outside to inside the tooth in lines separated by 200 µm. Reference compounds (hydroxyapatite and fluorapatite) were measured using a Kapton polyimide film as support material. All the analyses were performed at room temperature.

Figure 19. Dental specimen (arrow) ready to be analyzed by tts-µXRD in the experimental hutch at MSPD beamline of ALBA Synchrotron.

3.2.9.3. Data treatment

The diffraction data of the samples were processed with the programs d1Dplot and d2Dplot [139], including the azimuthal plots, which consist of the evolution of pixel intensity along an ellipse specified by the Bragg angle 2θ and a given tolerance. This intensity was integrated over 360º in a narrow band containing the reflection with Miller indices (002) and then plotted versus the azimuthal angle Φ. The azimuthal plots of the reflection (002) were selected for this analysis since this reflection is normal to the c-axis of enamel crystallites [56,140].

Multivariate curve resolution (MCR) was performed using PLS_Toolbox (Eigenvector Research, Wenatchee, WA, USA) working under MATLAB (The MathWorks, Natick, MA, USA) to study the evolution of the different orientations along the azimuthal plots of the reflection (002) collected from each line measured from the surface to the inside of the samples and with baseline correction. MCR is a widespread and powerful chemometric methodology for data analysis that maximizes the explained variance in the data while imposing component profiles to follow significant physical or chemical constraints [141].

OriginLab software (OriginLab, Northampton, MA, USA) was used to perform baseline correction and maximum normalization to the diffractograms when observing peak shifts.

3.2.10. Specular reflectance SR-µFTIR experiment

3.2.10.1. Sample preparation

Two bovine samples and one human sample of each treatment (NMTD with or without amelogenin), which had been treated for 15 days, were completely covered by the same Paladur acrylic resin in which they were embedded before treatment and longitudinally cut in two halves with a Struers Minitom precision diamond saw to obtain a mesial view from the inside. Paladur acrylic resin is transparent and hence facilitates the sample cutting. A sequence of silicon carbide paper was used to polish the exposed tooth area with a Struers LaboPol-25 polisher, starting at grit size P2500 and increasing to P4000, under a constant flow of tap water. A sequence of diamond suspensions with a mean particle size of 3 and 1 µm was used to finish the polishing and obtain the appropriate reflection properties for the measurements. Afterwards, the specimens were sonicated for one minute to clean the polishing residues. Bovine and human samples can be observed in Figure 20.

Figure 20. Image of a bovine (left) and a human (right) dental specimen prepared for specular reflectance synchrotron radiation-based Fourier transform infrared microspectroscopy.

3.2.10.2. Data acquisition

µFTIR coupled to synchrotron radiation (SR-µFTIR) experiment in reflectance mode was carried out at MIRAS beamline of ALBA Synchrotron (Cerdanyola del Vallès, Spain) [142]. Specular reflectance spectra of the tooth samples (Figure 21) were acquired using a Hyperion 3000 microscope coupled to a Vertex 70 spectrometer (Bruker, Ettlingen, Germany) and equipped with a Mercury-Cadmium-Telluride (MCT) detector. The microscope uses a 36x Schwarzschild objective (NA=0.52) coupled to a 36x Schwarzschild condenser to focus the synchrotron IR light on the sample. Spectra were collected with OPUS 7.5 software (Bruker, Ettlingen, Germany) in the 700-4000 cm^{-1} range, at a spectral resolution of 4 cm^{-1}, with a masking aperture size of 6x6 μm^2, taking 256 co-added scans per spectrum to achieve a good signal-to-noise ratio and using and a step size of 5x5 μm^2. A gold mirror was used as the reference to collect the background. All the analyses were performed at room temperature.

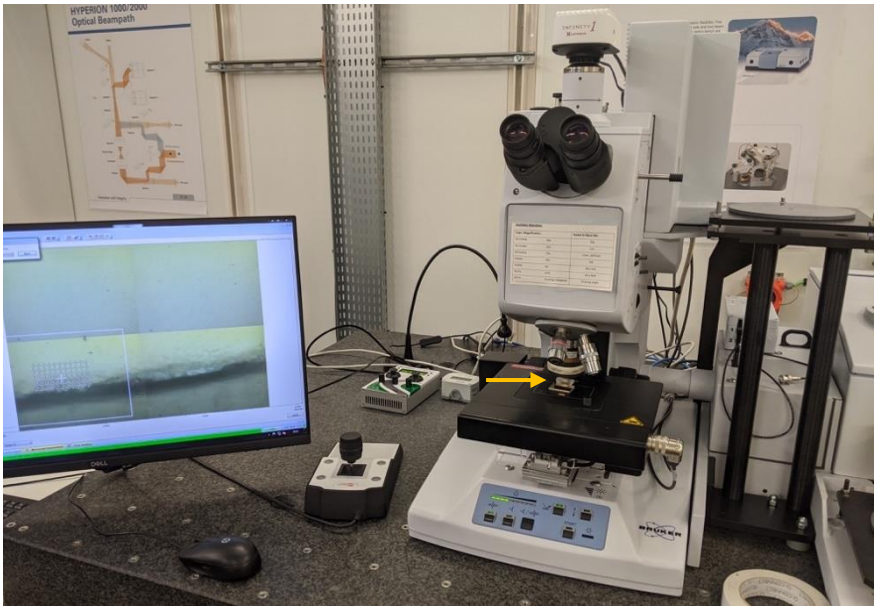

Figure 21. Dental specimen (arrow) being analyzed by specular reflectance µFTIR at MIRAS beamline of ALBA Synchrotron.

3.2.10.3. Data treatment

OriginLab software was employed to assign peak spectra numbers and perform maximum normalizations when comparing spectra. Savitsky-Golay algorithm for second derivative with a polynomial order of 3 was applied to the spectra on the region between 1660 and 700 cm^{-1} using the Unscrambler X 10.4 software (CAMO Software, Oslo, Norway).

Principal component analysis (PCA) was performed on the region between 1660 and 700 cm^{-1} of the mean centered spectra using PLS_Toolbox working under MATLAB. PCA is, arguably, the most frequently employed chemometric method. It is a variable reduction tool, which makes it possible to identify trends and patterns more easily [143]. This method generates a decomposition of the experimental data that maximizes the explained variance under the constraint of the orthonormality of the new components [141].

4. RESULTS AND DISCUSSION

4.1. Mineral growth in solution experiment

Prior to the growth of FA in solution, a theoretical species distribution diagram was performed. MEDUSA program (Stockholm, Sweden) [144] was used to create the theoretical chemical equilibrium diagram of the species formed in presence of the ions released from the NMTD. The basic parameters that are necessary for the calculation of distribution diagrams, including equilibrium constants, are included in the program database.

As shown in Figure 22, the predominant species formed in presence of the ions released from the NMTD at pH 7.1 of saliva would be calcium fluoride and fluorapatite.

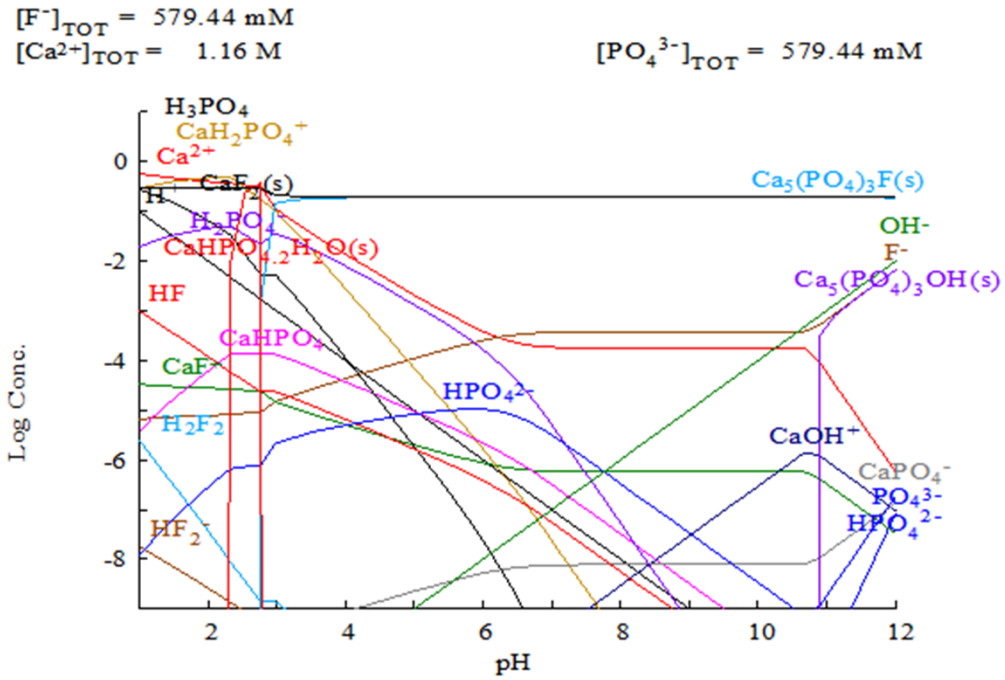

Figure 22. Theoretical distribution diagram of the species formed in presence of the ions released from NMTD as function of medium pH.

Regarding the mineral growth in solution, it can be seen in Figure 23a that crystals have grown on the resin after the incubation of NMTD in artificial saliva solution for 24 hours. The shape of these crystals obtained in the solution experiment resembles the first phase of the formation of fluorapatite spherulites [33,145–147].

Moreover, the EDX spectrum of the crystals matches the fluorapatite reference spectrum, as shows Figure 23 (b and c). Therefore, the results of the solution experiment confirm the expected formation of fluorapatite predicted by the theoretical species distribution diagram.

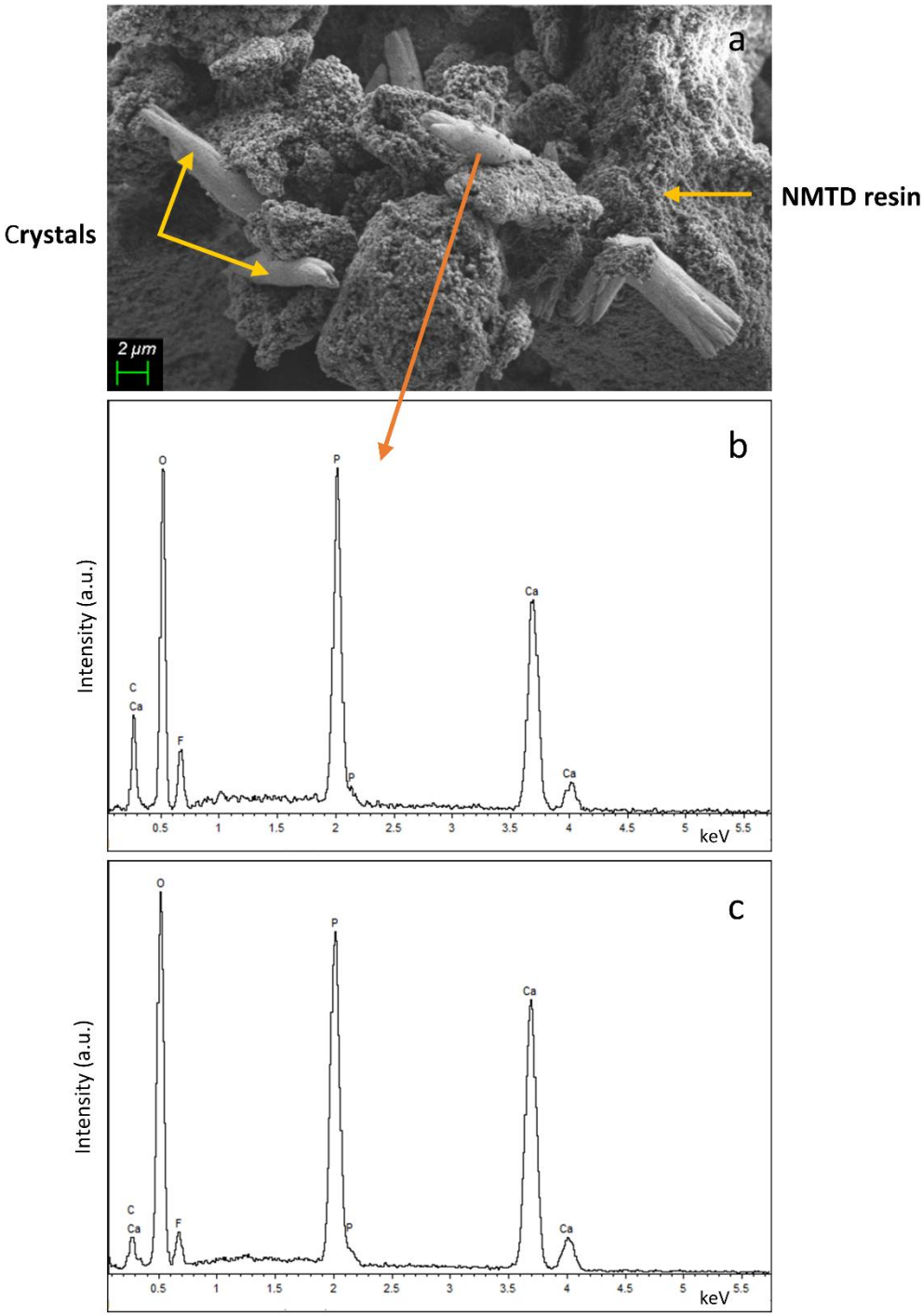

Figure 23. SEM image of the crystals obtained after the incubation of NMTD in artificial saliva solution during 24 hours with 5000X magnification (a), EDX spectrum of one of the crystals (b), EDX spectrum of the fluorapatite reference powder (c).

4.2. Determination of enamel remineralization by conventional techniques

4.2.1. SEM-EDX analysis of dental samples

Bovine teeth were lengthwise cut and the remineralized layer thickness after each NMTD treatment time was measured using ImageJ software. The remineralization of the tooth samples has been successful, as it can be seen in Figure 24, the thickness of the remineralized layer progressively increases until day 15, when it reaches a plateau around 23±1 µm.

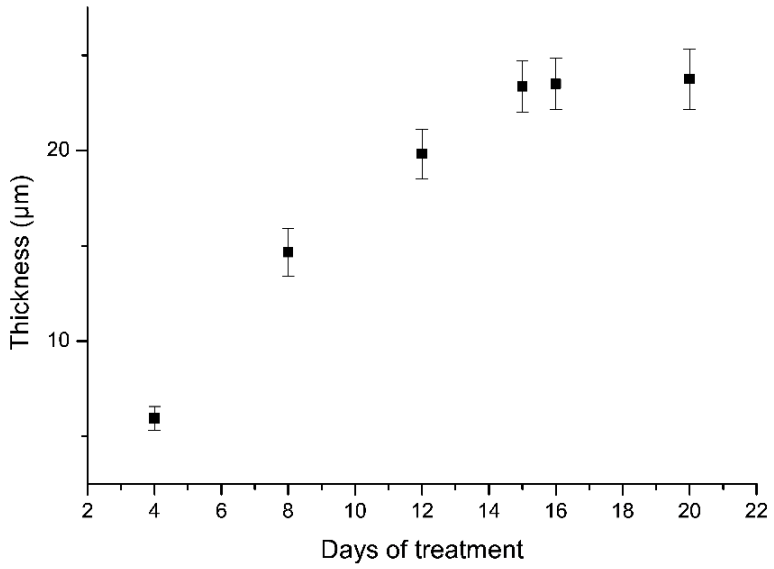

Figure 24. Evolution of the remineralized layer thickness with time of NMTD treatment in bovine tooth samples (n=24 for each point).

In order to study the formed layer bonding strength to the enamel surface, bovine teeth were brushed continuously for 15 minutes after 15 days of NMTD treatment when the layer has reached its maximum thickness. Figure 25 shows the remineralized layer of the 15-day treatment to remain intact after the long brushing, demonstrating that it is attached to the tooth surface strongly enough to resist the brushing of the daily hygiene.

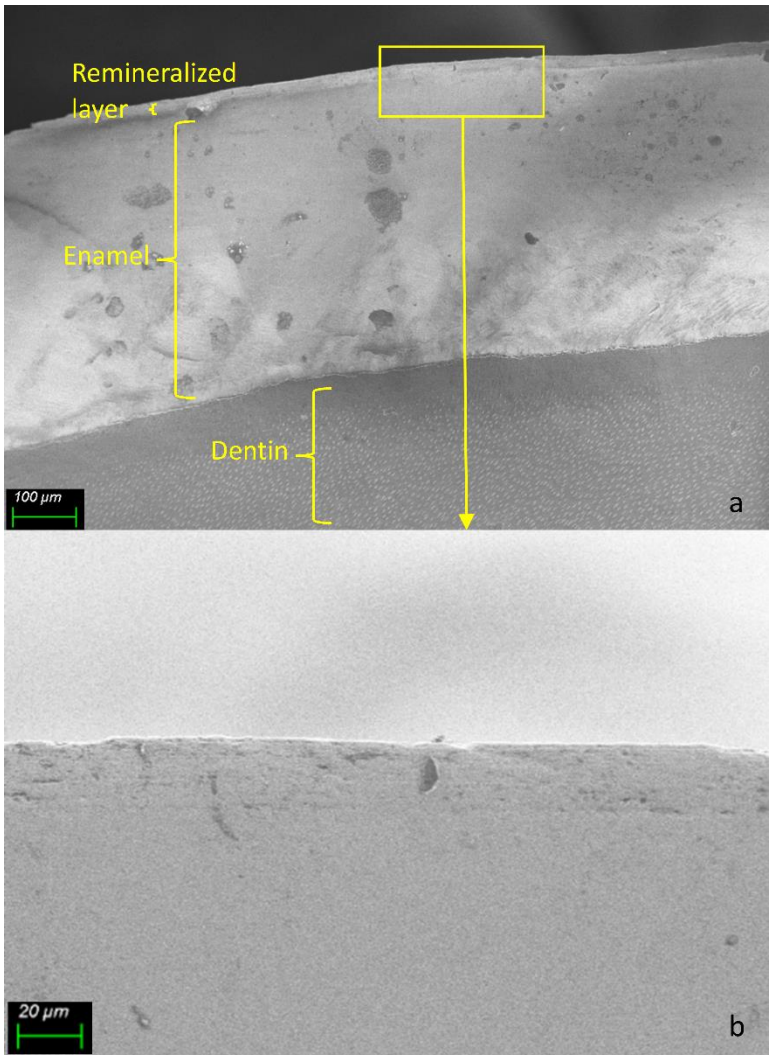

Figure 25. Longitudinal section SEM images of a bovine sample treated with NMTD for 15 days and brushed for 15 minutes with 250X magnification (a) and 1000X magnification of the square area (b).

The difference in crystal size between the treatment in presence and absence of amelogenin was studied, it can be appreciated in Figure 26 that the crystals are bigger in presence of amelogenin. The diameter of the crystals for the 4-day treatment is 0.11±0.02 µm for NMTD and 0.14±0.02 µm for NMTD in presence of amelogenin. In the case of the 15-day treatment, the diameter of the crystals is 0.13±0.02 µm for the treatment without protein and 0.17±0.03 µm with amelogenin. The increase in crystal size with amelogenin for both treatment times (4 and 15 days) suggests amelogenin protein to accelerate the crystallization rate [148]. Moreover, the 15-day treatment with protein shows significant differences in crystal size versus NMTD alone, according to the one-way ANOVA test performed with GraphPad Prism 9.

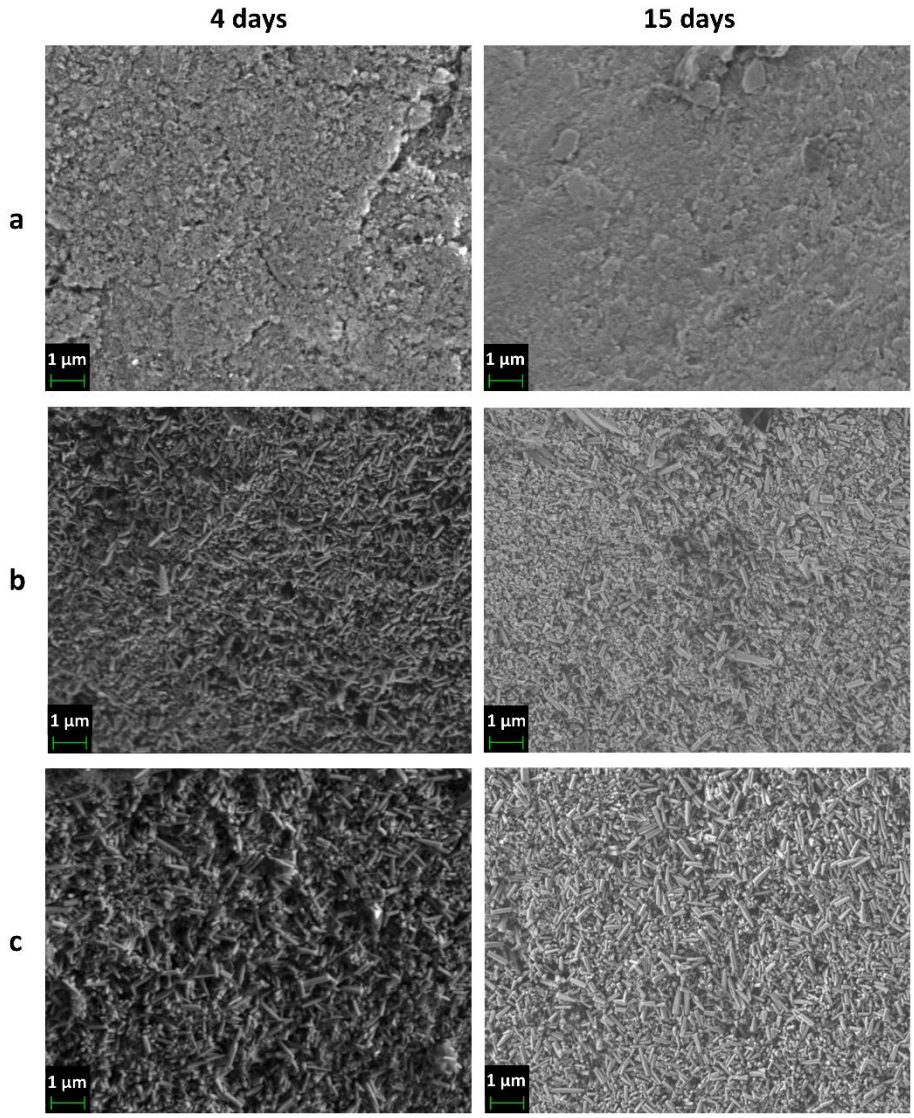

Figure 26. SEM images at 20000X magnification level of the bovine tooth surface after 4 and 15 days of treatment: blank (a), NMTD (b), NMTD and amelogenin (c).

To study the composition of the remineralized layer, an EDX study was performed by measuring blank and treated bovine samples (with and without amelogenin protein) and comparing them to the references of fluorapatite and hydroxyapatite powder. EDX results are shown in Table 3. We can observe that the presence of amelogenin during the remineralization process produces a layer more similar in composition to pure fluorapatite, with more calcium and phosphorus but less oxygen and fluorine than the layer formed only with NMTD that also shows the formation of other minerals like calcium fluoride (CaF_2). This calcium fluoride is a precursor that will derive in fluorapatite in the presence of phosphate [46,149]. The composition of the blank samples treated with saliva alone is similar to that of hydroxyapatite, as expected. The results obtained from the 4-day and 15-day treatments

are similar, which means that extending the treatment time increases the thickness of the layer, as observed previously, but does not alter its composition.

Table 3. Surface EDX measurements of the different treatments in bovine teeth at different times: blank sample after 4 days (B4), NMTD treated sample after 4 days (N4), NMTD and amelogenin treated sample after 4 days (N+A4), blank sample after 15 days (B15), NMTD treated sample after 15 days (N15), NMTD and amelogenin treated sample after 15 days (N+A15), fluorapatite powder reference (FA), hydroxyapatite powder reference (HA).

Atomic %	*B4*	*N4*	*N+A4*	*B15*	*N15*	*N+A15*	*FA*	*HA*
Ca	18±5	14±1	20.7±0.1	20±4	14.78±0.01	20.6±0.1	25±4	21±3
P	15±3	10.5±0.5	14.68±0.08	19±2	10.9±0.1	14.53±0.04	14.3±0.8	14.7±0.9
O	66±8	64.8±1.0	56.5±0.4	61±5	63.3±0.5	56.4±0.5	56±2	65±3
F	0.3±0.1	10.8±0.5	8.1±0.2	0.1±0.1	11.0±0.4	8.5±0.4	4.9±0.7	0.00±0.01

To study the evolution of the formed layer across its outer part to the enamel, different EDX measurements were taken in longitudinally cut bovine samples of 15 days through the formed layer until the enamel. Figure 27 shows the variations of each element when moving across the new layer to the natural enamel. Comparing the remineralized layer (first 23 µm) to natural enamel (beneath this 23 µm), fluorine concentration is higher and oxygen concentration is lower due to the expected production of fluorapatite in the remineralized layer, instead of the enamel hydroxyapatite. In the presence of amelogenin, calcium and phosphorus remain largely similar along the new layer to the original enamel since fluorapatite and hydroxyapatite contain the same amount of calcium and phosphorus, thus supporting our expected mineral formation. On the contrary, in absence of amelogenin, the observed decrease of oxygen, calcium and phosphorus in the formed layer against the original enamel may be interpreted by the formation of a considerable proportion of CaF_2 together with the fluorapatite. In the blank samples, these changes are not observed due to the absence of the remineralized layer.

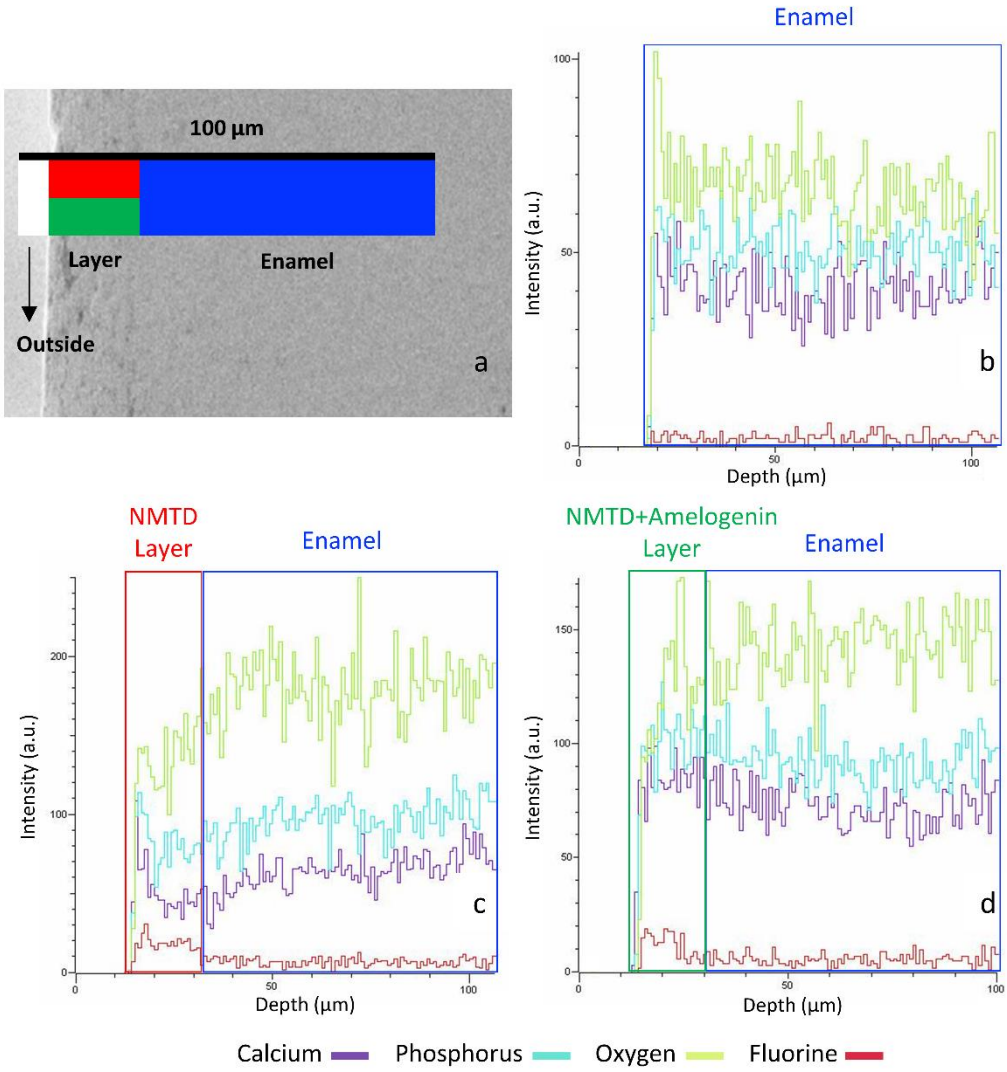

Figure 27. Longitudinal section SEM-EDX analysis of bovine teeth: representation of measurements (a), blank sample after 15 days (b), NMTD treated sample after 15 days (c), NMTD and amelogenin treated sample after 15 days (d).

4.2.2. Nanoindentation of treated teeth

To assess the hardness of both kinds of remineralized layer (NMTD and NMTD with amelogenin) with respect to the enamel, CSM measurements were taken in the layer and the enamel of longitudinally cut bovine samples, the measurements are shown in Figure 28. We can observe the remineralized layer without protein to be slightly harder than enamel during the first 500 nm although it loses hardness from there unlike enamel. However, in the presence of amelogenin, the hardness of the remineralized layer is maintained at values similar to the enamel. These results may be due to the role of amelogenin in guiding the morphology and alignment of crystals formation [17,84].

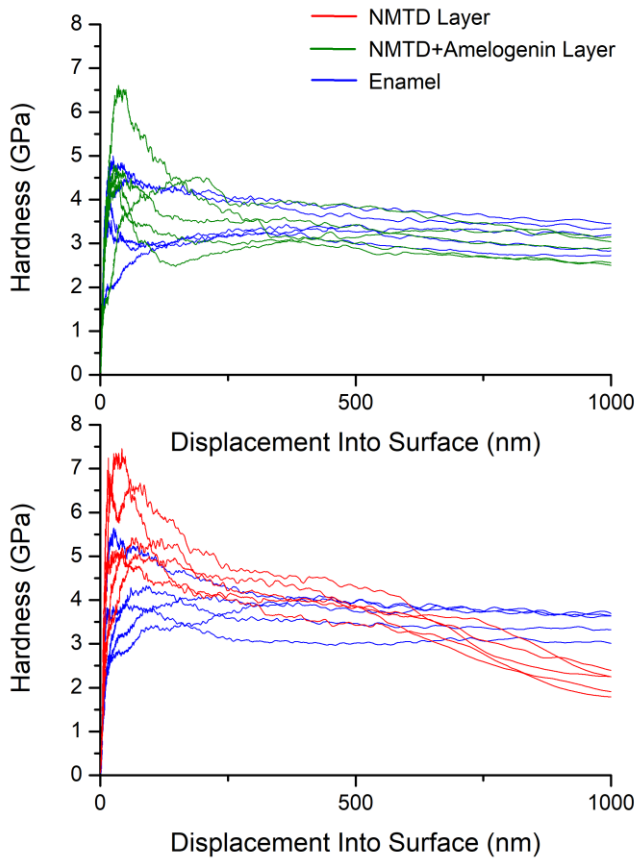

Figure 28. Longitudinal section continuous stiffness measurements of a bovine sample treated 15 days with NMTD and amelogenin (top) and a bovine sample treated 15 days with NMTD (bottom).

4.3. Synchrotron radiation-based multi-analytical approach to study dental remineralization

4.3.1. Synchrotron tts-µXRD

A typical diffraction pattern of HA was found inside the bovine enamel, the main (*hkl*) Miller indices (002), (211), (112), (300), (202), (222), (213) and (004) [26,150] are indicated in Figure 29. A shift to a slightly higher angle was observed in the (211), (112) and (300) reflections of the external layer and the FA reference, compared to the enamel and the HA reference, as expected from the slight reduction in a,b-axis dimension when F^- ions replaces OH^- ions [151,152]. This shift confirmed the substitution of fluoride ions into the apatite lattice, therefore the remineralized layer formed is composed of FA, more resistant than enamel HA.

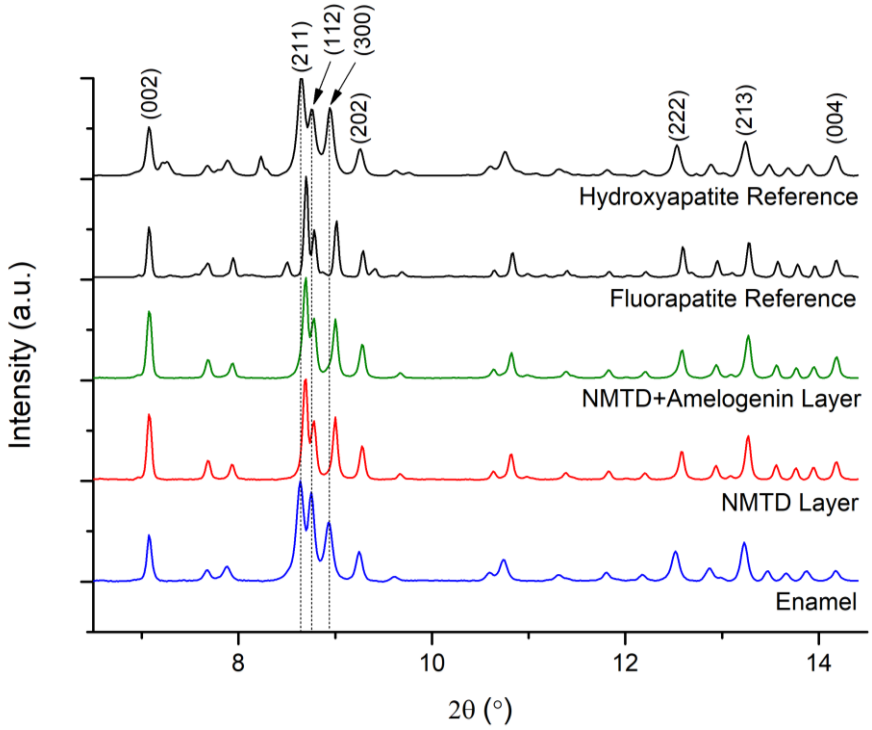

Figure 29. Diffractograms obtained by synchrotron tts-µXRD for HA reference, FA reference, bovine enamel, NMTD layer with amelogenin and NMTD layer without amelogenin, normalized to maximum and showing reflections.

Synchrotron tts-µXRD was also used to investigate the texture (or preferred orientation) of enamel crystallites in the tooth sections. The preferred orientation refers to the degree of alignment of the crystallites. The intensities of different XRD peaks can be employed to estimate the macroscopic level-specific orientation of crystals. Sharp and intense (002) and (004) peaks in the apatite, as can be seen for the new layers in Figure 29, indicate that crystals prefer to be aligned along the c-crystallographic axis as in real enamel [14,90]. The

lattice planes (002) and (004) along the c-axis of the enamel crystals are oriented perpendicular to the tooth surface, following the direction of the enamel prism arrangement [50,153]. Perpendicularity to the enamel surface maximizes the strength and bending capability and enhances the wear resistance capacity [154].

A high degree of crystalline anisotropy, as in dental enamel, produces a change in the intensity around the Debye ring of Bragg reflections in two dimensions that correlates with the degree of crystallite alignment or ordering [140]. The intensity variations around the diffraction rings are indicative of tooth enamel texture [153]. Diffraction spots in Figure 30 are concentrated in distinct arcs, both in the bovine enamel and in the layers, which means that the crystals are ordered [155]. The strongest texture (the most extreme intensity variation) for both kinds of samples (NMTD treatment with or without amelogenin) was found in the reflection (002), as can be appreciated in Figure 30. The lattice plane reflection (002) does not overlap with other reflections and has the greatest intensity variation with maxima normal to the c-axis [154]. Moreover, in the diffractograms shown in Figure 29, a shift was not observed in the (002) peak, since the contribution is due to the c-axis in this reflection and the c-axis dimension does not change from HA to FA [28].

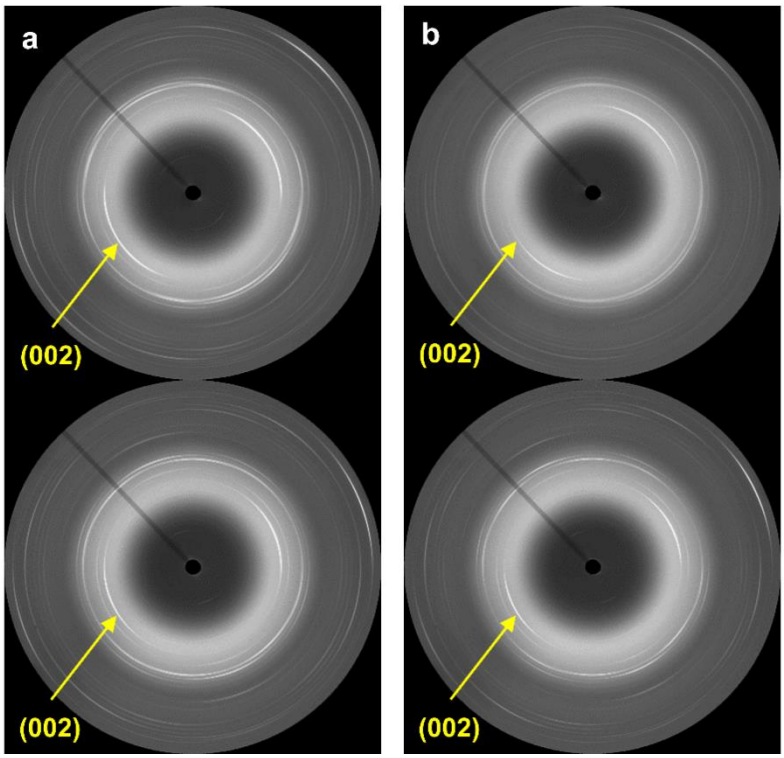

Figure 30. 2D µXRD images from a bovine sample with amelogenin (a) and a bovine sample without amelogenin (b). Enamel points on the top and layer points on the bottom.

To analyze the different behavior of crystal orientation along the lines of points that enter into the teeth, the evolution of the azimuthal intensity of the reflection (002) has been plotted. This gives a linear representation of the evolution of the pixel intensity along the ellipse specified by the angle 2θ (Debye ring) [139]. Figure 31 shows typical examples of the azimuthal plot for all the points of lines from both samples where two pronounced peaks separated by approximately 180º could be observed. These peaks represent the opposing (002) reflection maxima that can be seen in the 2D µXRD images of Figure 30. Sharp intense peaks are evidence of a strong preferred orientation, while broad peaks would indicate a more random orientation of the crystallites [56]. It can be seen in Figure 31 that both kinds of layers have a strong preferred orientation with intense peaks, even exceeding the intensity of the underlying bovine enamel.

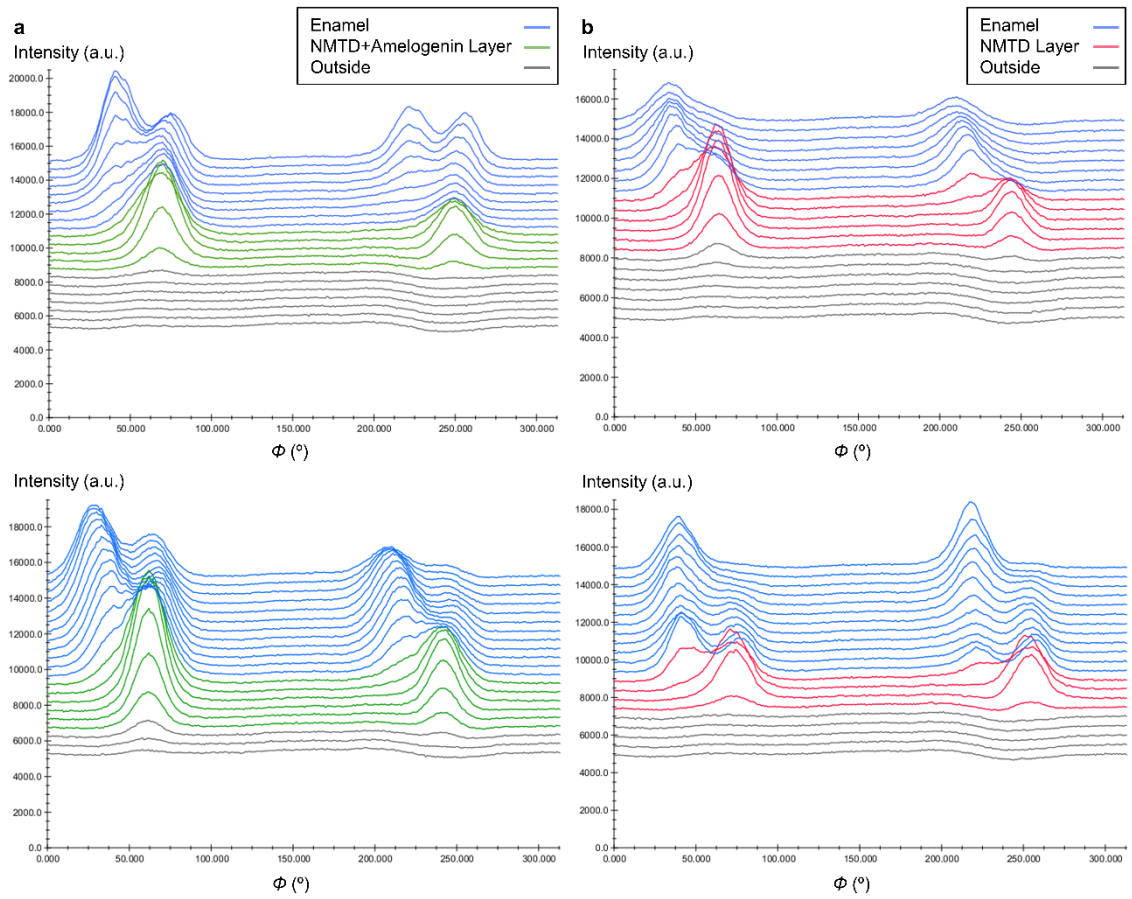

Figure 31. Representation of the azimuthal plots from lines of a bovine sample with amelogenin (a) and a bovine sample without amelogenin (b).

Moreover, the treatment with NMTD and amelogenin (Figure 30a and Figure 31a) produces a layer that follows the preferred orientation of the surface enamel better than the treatment with only NMTD (Figure 30b and Figure 31b), since the positions of the arcs and the peaks for the reflection (002) match better with enamel ones.

The presence of another population of crystallites with distinct preferred orientation can be appreciated deeper in the enamel of lines for both sample types in Figure 31, where there are two additional peaks in the azimuthal plots, also separated by approximately 180º. This effect of four peaks due to two crystal populations with different preferred orientation is due to the natural structure of the enamel.

MCR analysis of the azimuthal plots of the reflection (002) from both treatments (NMTD with amelogenin and NMTD alone) is shown in Figure 32. MCR was developed by imposing non-negativity in both the intensities and azimuthal profiles. The orientation of component 1 (blue) is mostly present in the layer, while component 2 (orange) appears in the outer enamel and component 3 (yellow) becomes more important in the deeper enamel where new preferred orientations appear. Component 4 (purple) belongs to the points outside before reaching the samples. The evolution of the different components confirms that the orientation of the layer with NMTD and amelogenin (Figure 32a) follows the enamel underneath better than the layer with only NMTD (Figure 32b). In the NMTD layer with amelogenin the change of the components 1 and 2 between the layer and the enamel is more gradual than in the one with NMTD alone, which is consistent with the movement of the peaks in Figure 31. The changes in the intensities of the components as they enter deeper into the tooth (Figure 32) can also be correlated with the intensities of the peaks in the azimuthal plots at different depths (Figure 31), the intensity in the layers of the azimuthal plots is also higher than in the bovine enamel.

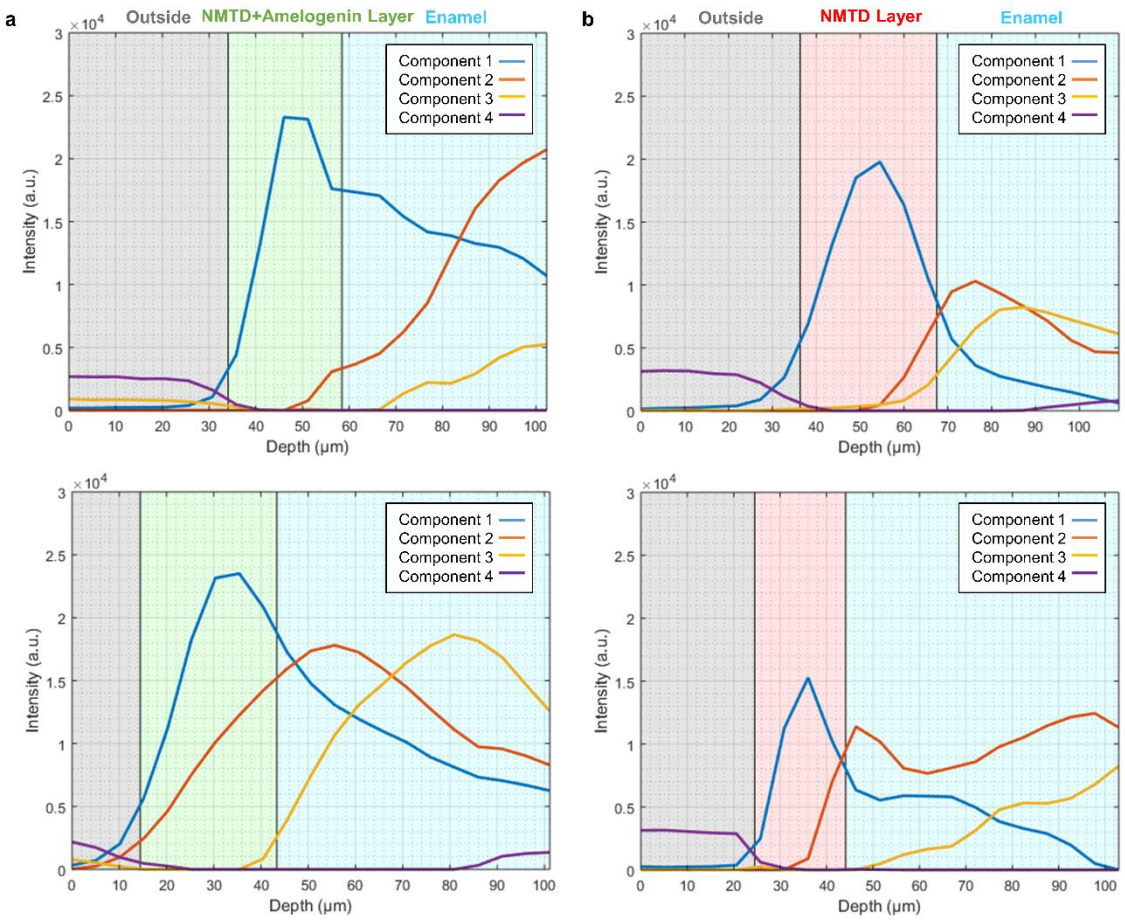

Figure 32. MCR analysis of the azimuthal plots from lines of the bovine sample with amelogenin (a) and the bovine sample without amelogenin (b).

The loadings in Figure 33 show peaks separated by 180º for both kinds of bovine samples (NMTD with or without amelogenin protein), as the peaks of the original azimuthal plots in Figure 31. The peaks of the loadings for components 1 and 2 are in similar positions, but component 3 has them shifted to lower angles. This fact is consistent with component 3 being predominant in the inner enamel (Figure 32), where azimuthal peaks appear at lower angles (Figure 31).

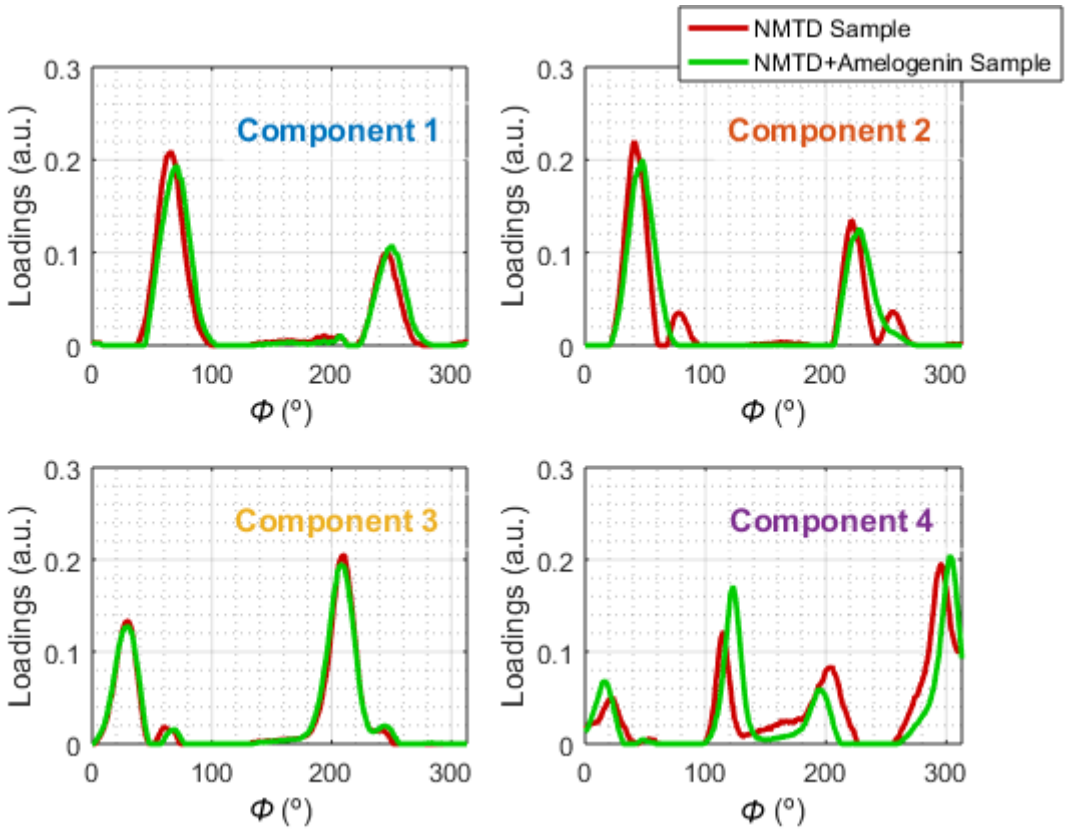

Figure 33. MCR loadings for each component of tooth bovine samples treated with NMTD: with amelogenin (green) and without amelogenin (red).

4.3.2. Specular reflectance SR-µFTIR

Measurements were taken on a selected frame on the tooth including points of the bovine enamel and of the new layer, to study the similarities and differences of the crystals of the newly formed layers for the different treatments (NMTD with amelogenin or NMTD alone) with the underlying enamel.

Bands corresponding to carbonates and phosphates in the bovine enamel HA are identified in Figure 34. The bands associated with the v_3PO_4 vibrations (antisymmetric stretching) are observed between 1170 and 965 cm^{-1} [156,157]. In the literature, the deconvolution of the v_3PO_4 bands in stoichiometric apatite is described as secondary phase vibrations of Ca-O-P at 1103 cm^{-1}, P-O at 1091 cm^{-1}, Ca-O at 1047 cm^{-1} and O-Ca-O at 1031 cm^{-1} [158]. The weak v_1PO_4 band (symmetric stretching) is present at 966 cm^{-1} [124]. The region between 1580-1320 cm^{-1} corresponds to v_3CO_3 antisymmetric stretching, where two maximums at 1442 and 1401 cm^{-1} can be appreciated [119]. An additional small band related to structural carbonates (v_2CO_3 symmetric angular deformation) is present at 867 cm^{-1} [119,124,157]. Carbonate can substitute two anionic sites of the HA structure: it could be located at

phosphate group sites in carbonated apatite type B, which is the predominant type in biological apatite, or at hydroxyl group sites in carbonated apatite type A [159]. According to the peak deconvolution from the literature, the v_3CO_3 vibration in carbonated apatite type A splits into two peaks at 1530 cm^{-1} and 1465 cm^{-1}. In contrast, type B can be characterized by peaks at 1456 and 1423 cm^{-1} in the IR spectrum [159,160]. In the case of the v_2CO_3 out-of-plane bending mode, a peak at 879 cm^{-1} is reported to belong to type A and another at 872 cm^{-1} to type B [159,161]. The combined presence of A and B carbonates affects the carbonate peak positions compared to apatite with only A type or only B type [159]. Thus, the carbonate peaks detected in the regions 1580-1320 cm^{-1} and 880-830 cm^{-1} of the enamel in reflection mode show a mixture of type A and B carbonates.

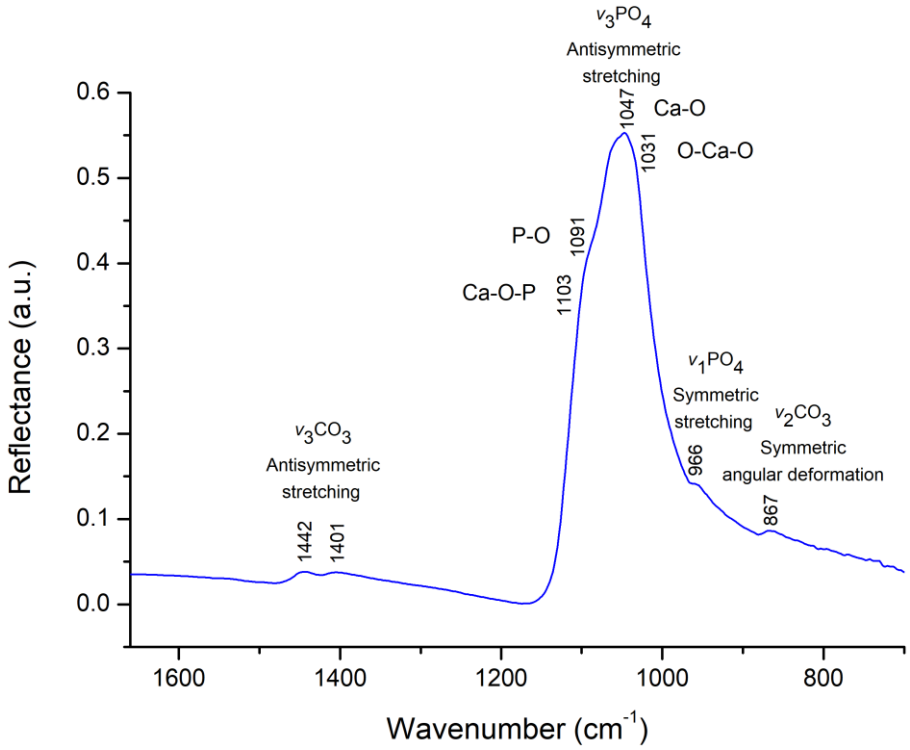

Figure 34. Average of the specular reflectance FTIR spectra of bovine enamel with band assignment numbers (n=11).

Specular reflectance FTIR spectra in Figure 35 show that both types of layers present the characteristic peak of apatites due to the phosphate group near 1050 cm^{-1}, indicating a high crystallinity [162]. In both layers, there is an absence of the two small peaks near 1400 cm^{-1} and the small peak at 867 cm^{-1} that are present in the bovine enamel due to the carbonate group [163]. The lack of the carbonate substitution group with high solubility and the

narrowing of the phosphate peak in both layers indicate conversion to a more highly crystalline apatite compared to enamel.

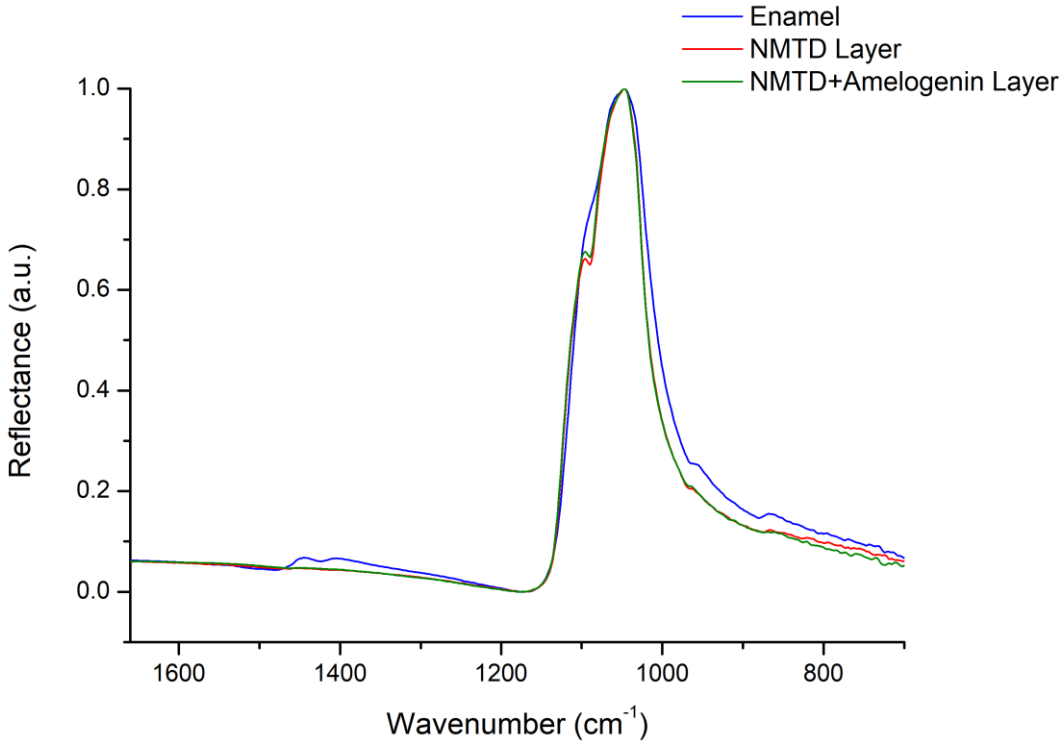

Figure 35. Average of specular reflectance FTIR spectra normalized to maximum corresponding to bovine enamel (blue), NMTD layer with amelogenin (green) and NMTD layer without amelogenin (red) (n=11).

In addition, layers appear to have a more evident vibration at 1103 cm^{-1} than the bovine enamel, corresponding to the Ca-O-P secondary phase vibration. This could be due to a higher amount of calcium interacting with phosphate than in enamel since there are no carbonates in the layer, and therefore there is no calcium bound to carbonate as in enamel. Further evidence of this behavior can be appreciated in the second derivative spectra of the layers and enamel in Figure 36.

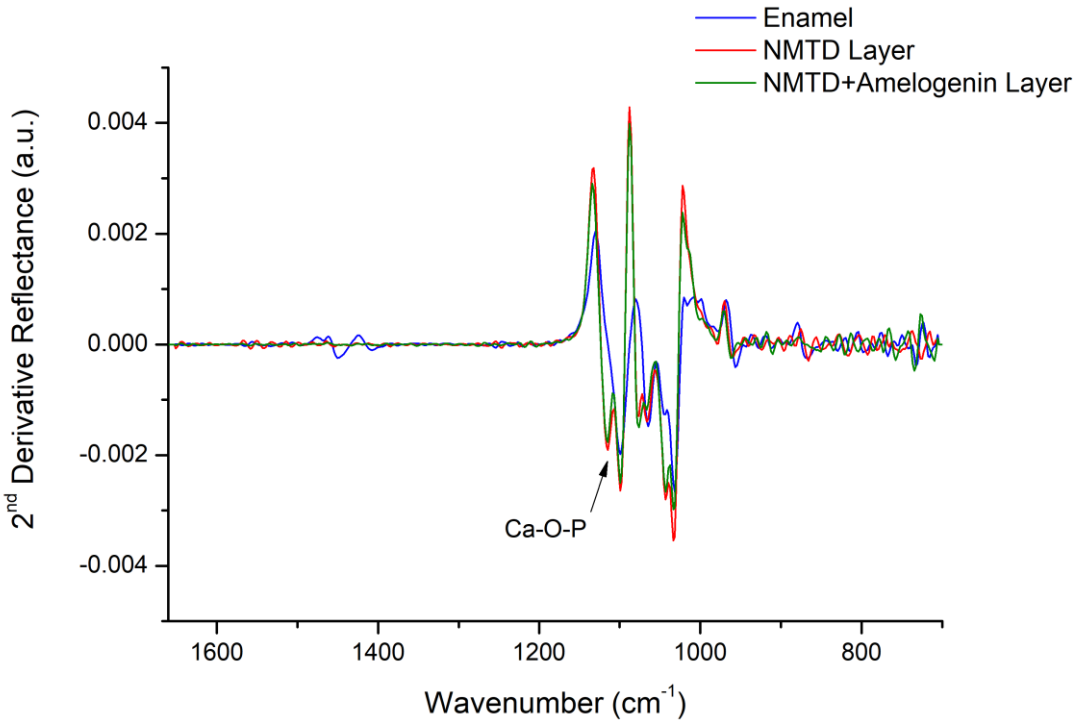

Figure 36. Savitzky-Golay second derivative average spectra of the bovine enamel and the different layers performed with a polynomial order 3 (n=11).

The PCA of spectra corresponding to enamel and both layers (Figure 37) shows that principal component 1 (PC 1) separates the two treatments (NMTD with and without amelogenin) from each other and principal component 2 (PC 2) separates the bovine enamel from the treatment layers as it separates according to the depth of the measurement. PC 1 represents 59.95% of the variation, while PC 2 accounts for the 33.10%. The points in the PCA belonging to the layer with protein are statistically closer to the enamel points than those belonging to the layer with NMTD alone, which may be due to the 1103 cm^{-1} shoulder being more pronounced in the NMTD layer (Figure 35).

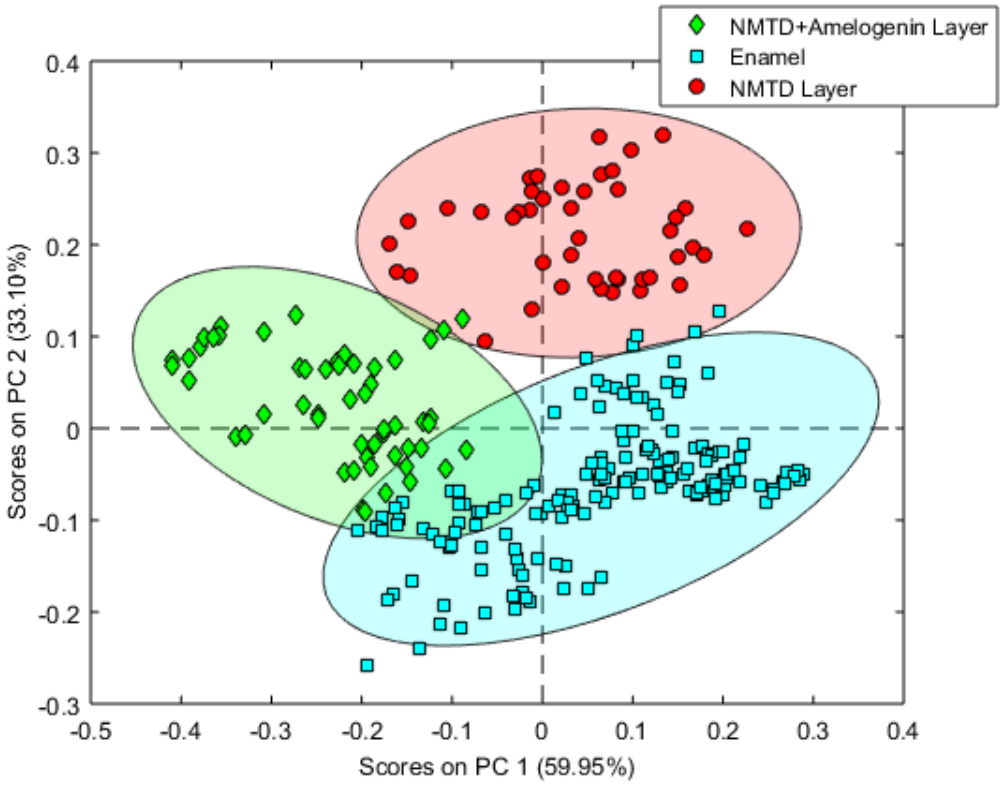

Figure 37. PCA scores graph of the FTIR spectra from the enamel and layer of two bovine samples with amelogenin and two bovine samples without amelogenin.

In Figure 38, the loadings for PC1 and PC2 show the main peaks in the regions 1580-1320 cm^{-1} and 1170 and 965 cm^{-1}, corresponding to the ν_3CO_3 and the ν_3PO_4 vibrations. Therefore, these vibrations are responsible for the separation of the scores in Figure 37.

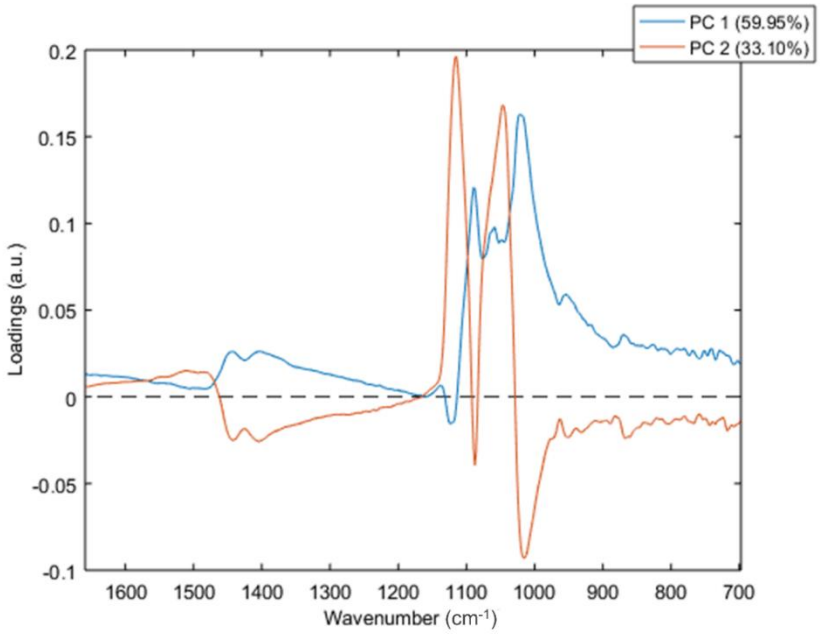

Figure 38. PC 1 and PC 2 loadings of the FTIR spectra PCA from bovine samples.

The same specular reflectance SR-µFTIR analysis was performed on human samples, in order to assess the similarities and differences of the crystals of the layers for the different treatments applied to human teeth (NMTD with or without amelogenin) with the underlying human enamel.

Both types of layers in Figure 39, with and without amelogenin protein, present the characteristic peak of apatites due to the phosphate group near 1050 cm^{-1} that indicates a high crystallinity and was also present in the treatments with bovine teeth of Figure 35. Moreover, there is also an absence in both layers of the two small peaks near 1400 cm^{-1} and the small peak at 867 cm^{-1} belonging to the carbonate group that are present in the human enamel. The absence of the high solubility carbonate substitution group and the narrowing of the phosphate peak in the layers indicate a conversion to a more crystalline apatite in comparison to human enamel, as happened in the bovine samples.

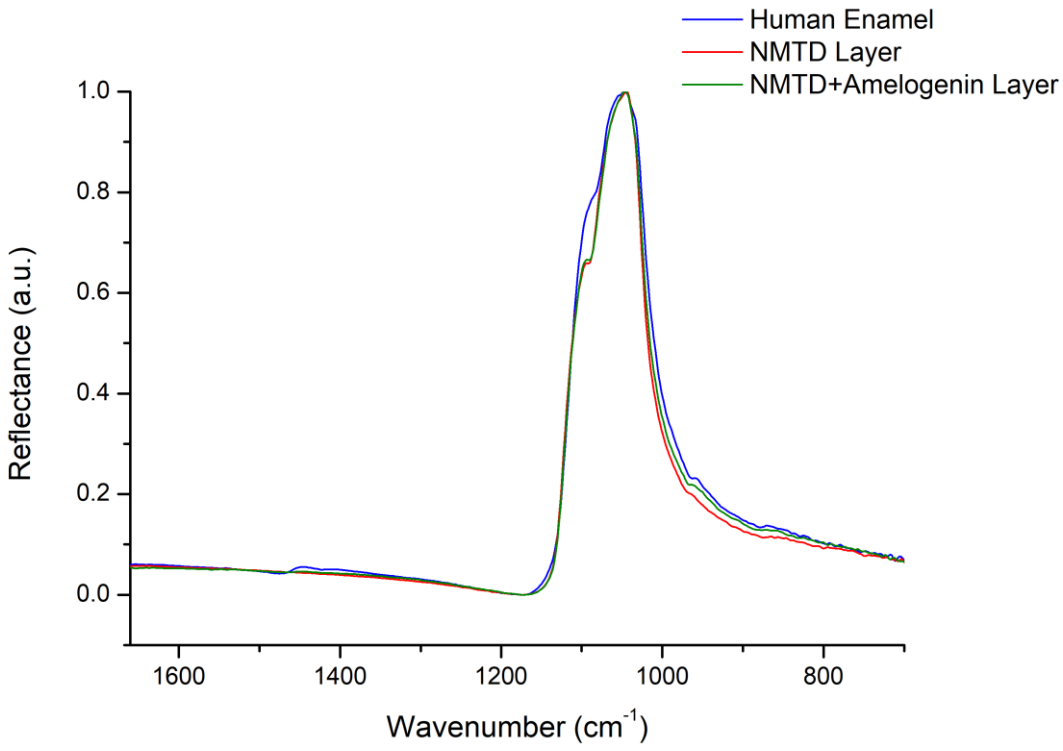

Figure 39. Average of specular reflectance FTIR spectra normalized to maximum corresponding to human enamel (blue), NMTD layer with amelogenin (green) and NMTD layer without amelogenin (red) (n=11).

Furthermore, the layers in Figure 39 seem to have a more evident Ca-O-P secondary phase vibration at 1103 cm^{-1} than the human enamel, such as bovine samples. The second derivative spectra of the layers and human enamel (Figure 40) appears to confirm this event

which, as stated for the bovine teeth, could be due to the fact that there are no carbonates in the layer, so there is no calcium bound to the carbonate as in the enamel and, as a result, there is a greater amount of calcium interacting with the phosphate.

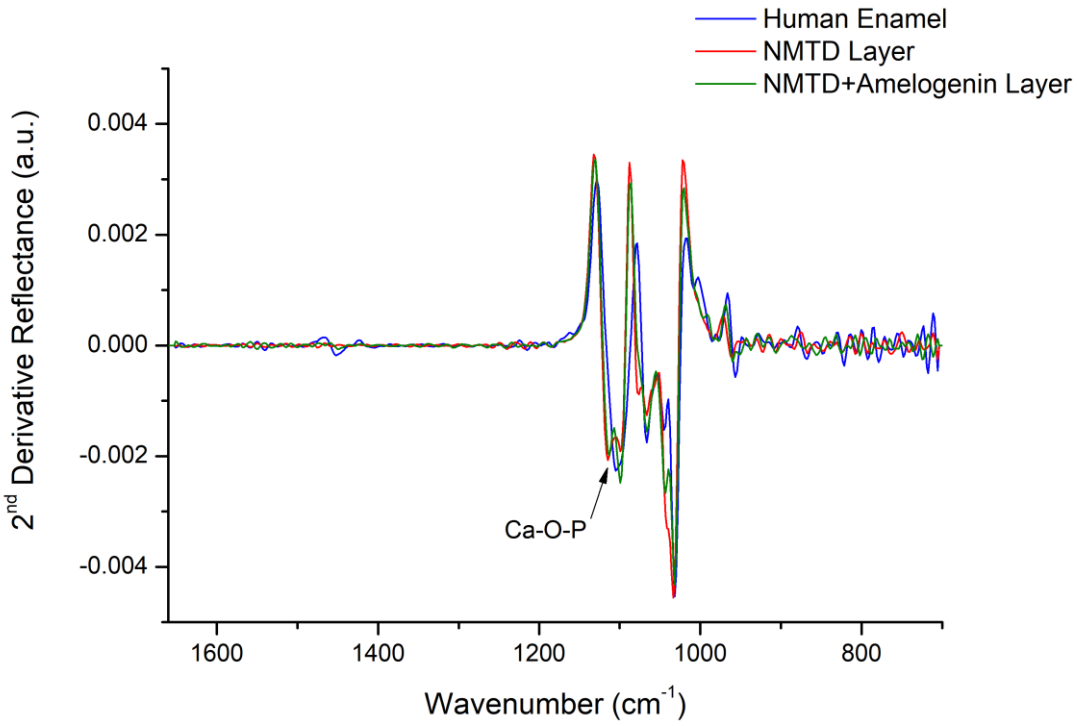

Figure 40. Savitzky-Golay second derivative average spectra of the human enamel and the different layers performed with a polynomial order 3 (n=11).

The PCA of spectra belonging to human enamel and both layers in Figure 41 shows that principal component 1 (PC 1) separates according to the depth of the measurement differentiating the human enamel from the treatments, and principal component 2 (PC 2) separates the two treatments (NMTD with and without amelogenin). PC 1 represents 85.53% of the variation and PC 2 the 8.59%. The points in the PCA from the layer with amelogenin are also statistically closer to the human enamel points than those from the layer with NMTD alone, probably because of the more pronounced 1103 cm^{-1} shoulder in the NMTD layer in Figure 39, as was the case with the bovine samples.

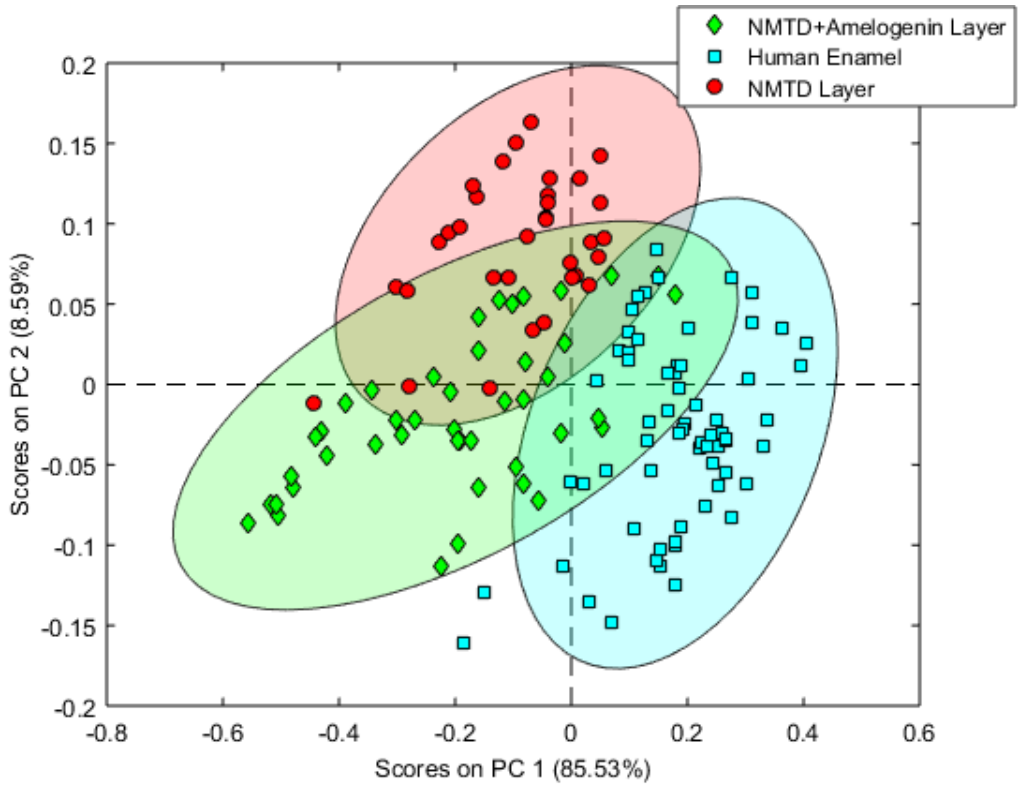

Figure 41. PCA scores graph of the FTIR spectra from the enamel and layer of a human sample with amelogenin and a human sample without amelogenin.

The loadings for PC1 and PC2 of Figure 42 show the main peaks in the regions of the v_3CO_3 and the v_3PO_4 vibrations (1580-1320 cm^{-1} and 1170 and 965 cm^{-1}). Thus, these vibrations are responsible for the score separation in Figure 41, as in the PCA of bovine samples.

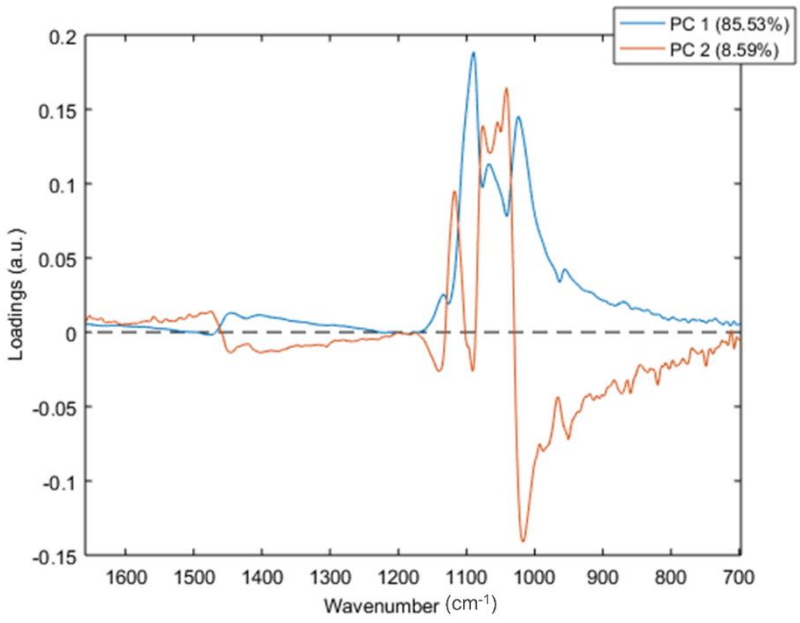

Figure 42. PC 1 and PC 2 loadings of the FTIR spectra PCA from human samples.

The application of these treatments on human samples has demonstrated their effectiveness for the treatment of human subjects, as was already predicted by the experiments with bovine teeth, and that the application of the amelogenin protein improves the result, making the remineralization more similar to natural human enamel.

5. CONCLUSIONS

- This thesis was focused on the development of a new dental remineralizing product. The NMTD ion-exchange material combined with human amelogenin protein has been applied and its effects on dental bovine and human samples have been studied, providing new knowledge in the field of dental remineralization and a possible new product for the market.
- The combination of conventional techniques with two synchrotron radiation-based techniques: infrared microspectroscopy and micro X-ray diffraction, with the help of specific data mining, has shown to conform a useful methodology to analyze the structure of apatites in samples of hard dental tissues and their allocation after the remineralization process. Infrared microspectroscopy provides information on chemical structural properties such as carbonate substitution, while micro X-ray diffraction allows the study of crystal structure and texture distribution on dental specimens. Synchrotron radiation allows to detect small changes with better resolution and to analyze microzones with high signal intensity.
- The NMTD product induces the remineralization after an acid attack creating a fluorapatite layer of around 23 µm on the enamel surface after 15 days of treatment. This carbonate free fluorapatite has higher physicochemical stability than tooth enamel hydroxyapatite and the formed layer can overcome the brushing process of the daily hygiene.
- The presence of amelogenin protein during the remineralization process with NMTD improves the layer hardness and the crystal orientation to mimic natural enamel, also accelerating the crystallization rate. Furthermore, amelogenin seems to induce the composition of the layer closer to that of pure fluorapatite without precipitation of other compounds. Amelogenin protein is a crucial component of this remineralizing product since it plays a critical role in controlling the preferred orientation of the growing crystal to resemble natural dental enamel.
- The novel product of NMTD with amelogenin induces complete remineralization with a hardness that reaches the levels observed in healthy enamel and an orientation of the fluorapatite crystals similar to that of natural enamel. Therefore, this is a promising product to inhibit demineralization and provide long-term remineralization to inhibit caries and protect tooth structures.

- Nevertheless, further studies would be convenient to evaluate the clinical applicability of this biomimetic treatment in humans. Although being a combination of food grade resins and human protein ensures easy approval for clinical trials.

6. BIBLIOGRAPHY

1. Mansoor A, Moeen F, Hussain A, Din SU, Khan MT, Said F: **Age related changes in physiology of normal human tooth enamel: A review**. *Pakistan J Physiol* 2020, **16**:35–40.

2. Lamont RJ, Egland PG: **Dental caries**. In *Molecular medical microbiology*. Edited by Tang Y-W, Sussman M, Liu D, Poxton I, Schwartzman J. Academic Press; 2015:945–955.

3. Gil-Bona A, Bidlack FB: **Tooth enamel and its dynamic protein matrix**. *Int J Mol Sci* 2020, **21**:4458.

4. Kis VK, Sulyok A, Hegedűs M, Kovács I, Rózsa N, Kovács Z: **Magnesium incorporation into primary dental enamel and its effect on mechanical properties**. *Acta Biomater* 2021, **120**:104–115.

5. Fattibene P, Callens F: **EPR dosimetry with tooth enamel: A review**. *Appl Radiat Isot* 2010, **68**:2033–2116.

6. Welborn VV: **Enamel synthesis explained**. *Proc Natl Acad Sci U S A* 2020, **117**:21847–21848.

7. Martinez-Avila O, Wu S, Kim SJ, Cheng Y, Khan F, Samudrala R, Sali A, Horst JA, Habelitz S: **Self-assembly of filamentous amelogenin requires calcium and phosphate: From dimers via nanoribbons to fibrils**. *Biomacromolecules* 2012, **13**:3494–3502.

8. Elsharkawy S, Mata A: **Hierarchical biomineralization: from nature's designs to synthetic materials for regenerative medicine and dentistry**. *Adv Healthc Mater* 2018, **7**:1800178.

9. Featherstone JD: **Prevention and reversal of dental caries: role of low level fluoride**. *Community Dent Oral Epidemiol* 1999, **27**:31–40.

10. Derceli J dos R, Faraoni JJ, Pereira–da–silva MA, Palma-Dibb RG: **Analysis of the early stages and evolution of dental enamel erosion**. *Braz Dent J* 2016, **27**:313–317.

11. Margolis HC, Beniash E, Fowler CE: **Role of macromolecular assembly of enamel matrix proteins in enamel formation**. *J Dent Res* 2006, **85**:775–793.

12. Lacruz RS, Habelitz S, Wright JT, Paine ML: **Dental enamel formation and implications for oral health and disease**. *Physiol Rev* 2017, **97**:939–993.

13. Ruan Q, Moradian-Oldak J: **Amelogenin and enamel biomimetics**. *J Mater Chem B* 2015, **3**:3112–3129.

14. Li L, Mao C, Wang J, Xu X, Pan H, Deng Y, Gu X, Tang R: **Bio-inspired enamel repair via glu-directed assembly of apatite nanoparticles: An approach to biomaterials with optimal characteristics**. *Adv Mater* 2011, **23**:4695–4701.

15. Jágr M, Ergang P, Pataridis S, Kolrosová M, Bartoš M, Mikšík I: **Proteomic analysis of dentin–enamel junction and adjacent protein-containing enamel matrix layer of healthy human molar teeth**. *Eur J Oral Sci* 2019, **127**:112–121.

16. Alkilzy M, Tarabaih A, Santamaria RM, Splieth CH: **Self-assembling peptide P11-4 and fluoride for regenerating enamel**. *J Dent Res* 2018, **97**:148–154.

17. Bai Y, Yu Z, Ackerman L, Zhang Y, Bonde J, Li W, Cheng Y, Habelitz S: **Protein nanoribbons template enamel mineralization**. *Proc Natl Acad Sci U S A* 2020, **117**:19201–19208.

18. Wang D, Deng J, Deng X, Fang C, Zhang X, Yang P: **Controlling enamel remineralization by amyloid-like amelogenin mimics**. *Adv Mater* 2020, **32**:200208.

19. Posada MC, Sánches CF, Gallego GJ, Vargas AP, Restrepo LF, López JD: **Dientes de bovino como sustituto de dientes humanos para su uso en la odontología. Revisión de**

literatura. *CES odontol* 2006, **19**:63–68.

20. Kim IH, Son JS, Min BK, Kim YK, Kim KH, Kwon TY: **A simple, sensitive and non-destructive technique for characterizing bovine dental enamel erosion: attenuated total reflection Fourier transform infrared spectroscopy**. *Int J Oral Sci* 2016, **8**:54–60.

21. Nakamichi I, Iwaku M, Fusayama T: **Bovine teeth as possible substitutes in the adhesion test**. *J Dent Res* 1983, **62**:1076–1081.

22. Yassen GH, Platt JA, Hara AT: **Bovine teeth as substitute for human teeth in dental research: a review of literature**. *J Oral Sci* 2011, **53**:273–282.

23. Olek A, Klimek L, Bottacz-Rzepkowska E: **Comparative scanning electron microscope analysis of the enamel of permanent human, bovine and porcine teeth**. *J Vet Sci* 2020, **21**:e83.

24. Fonseca RB, Haiter-Neto F, Carlo HL, Soares CJ, Sinhoreti MAC, Puppin-Rontani RM, Correr-Sobrinho L: **Radiodensity and hardness of enamel and dentin of human and bovine teeth, varying bovine teeth age**. *Arch Oral Biol* 2008, **53**:1023–1029.

25. Fonseca RB, Haiter-Neto F, Fernandes-Neto AJ, Barbosa GAS, Soares CJ: **Radiodensity of enamel and dentin of human, bovine and swine teeth**. *Arch Oral Biol* 2004, **49**:919–922.

26. Reyes-Gasga J, Martínez-Piñeiro EL, Rodríguez-Álvarez G, Tiznado-Orozco GE, García-García R, Brès EF: **XRD and FTIR crystallinity indices in sound human tooth enamel and synthetic hydroxyapatite**. *Mater Sci Eng C* 2013, **33**:4568–4574.

27. Rulis P, Ouyang L, Ching WY: **Electronic structure and bonding in calcium apatite crystals: Hydroxyapatite, fluorapatite, chlorapatite, and bromapatite**. *Phys Rev B - Condens Matter Mater Phys* 2004, **70**:155104.

28. Wei M, Evans JH, Bostrom T, Grondahl L: **Synthesis and characterization of hydroxyapatite, fluoride-substituted hydroxyapatite and fluorapatite**. *J Mater Sci Mater Med* 2003, **14**:311–320.

29. Gross KA, Rodríguez-Lorenzo LM: **Sintered hydroxyfluorapatites. Part II: Mechanical properties of solid solutions determined by microindentation**. *Biomaterials* 2004, **25**:1385–1394.

30. Oliveira M, Mansur HS: **Synthetic tooth enamel: SEM characterization of a fluoride hydroxyapatite coating for dentistry applications**. *Mater Res* 2007, **10**:115–118.

31. Aoba T, Shimazu Y, Taya Y, Soeno Y, Sato K, Miake Y: **Fluoride and apatite formation *in vivo* and *in vitro***. *J Electron Microsc (Tokyo)* 2003, **52**:615–625.

32. Campillo M, Lacharmoise PD, Reparaz JS, Goñi AR, Valiente M: **On the assessment of hydroxyapatite fluoridation by means of Raman scattering**. *J Chem Phys* 2010, **132**:244501.

33. Wu YJ, Tseng YH, Chan JCC: **Morphology control of fluorapatite crystallites by citrate ions**. *Cryst Growth Des* 2010, **10**:4240–4242.

34. Cochrane NJ, Cai F, Huq NL, Burrow MF, Reynolds EC: **New approaches to enhanced remineralization of tooth enamel**. *J Dent Res* 2010, **89**:1187–1197.

35. Perioli L, Nocchetti M, Giannelli P, Pagano C, Bastianini M: **Hydrotalcite composites for an effective fluoride buccal administration: A new technological approach**. *Int J Pharm* 2013, **454**:259–268.

36. Taha AA, Fleming PS, Hill RG, Patel MP: **Enamel remineralization with novel bioactive glass air abrasion**. *J Dent Res* 2018, **97**:1438–1444.

37. Rodríguez-Martínez J, Valiente M, Sánchez-Martín M: **Tooth whitening: From the established treatments to novel approaches to prevent side effects**. *J Esthet Restor Dent* 2019, **31**:431–440.

38. Marquillas CB, Procaccini R, Malmagro MV: **Breaking the rules: tooth whitening by means of a reducing agent**. *Clin Oral Investig* 2019, **24**:2773–2779.

39. Babot-Marquillas C, Sánchez-Martín MJ, Rodríguez-Martínez J, Estelrich J, Busquets MA, Valiente M: **Flash tooth whitening: A friendly formulation based on a nanoencapsulated reductant**. *Colloids Surfaces B Biointerfaces* 2020, **195**:111241.

40. Saads Carvalho T, Lussi A: **Chapter 9: Acidic beverages and foods associated with dental erosion and erosive tooth wear**. *Monogr Oral Sci* 2020, **28**:91–98.

41. Kwon SR, Kurti SR, Oyoyo U, Li Y: **Effect of various tooth whitening modalities on microhardness, surface roughness and surface morphology of the enamel**. *Odontology* 2015, **103**:274–279.

42. Srinivasan N, Kavitha M, Loganathan SC: **Comparison of the remineralization potential of CPP-ACP and CPP-ACP with 900 ppm fluoride on eroded human enamel: An *in situ* study**. *Arch Oral Biol* 2010, **55**:541–544.

43. Hannig C, Hamkens A, Becker K, Attin R, Attin T: **Erosive effects of different acids on bovine enamel: release of calcium and phosphate *in vitro***. *Arch Oral Biol* 2005, **50**:541–552.

44. Bijle MN, Abdalla MM, Ashraf U, Ekambaram M, Yiu CKY: **Enamel remineralization potential of arginine-fluoride varnish in a multi-species bacterial pH-cycling model**. *J Dent* 2021, **104**:103528.

45. Hicks J, Catherine FG: **Biological factors in dental caries: role of saliva and dental plaque in the dynamic process of demineralization and remineralization (part 1)**. *J Clin Pediatr Dent* 2003, **28**:47–52.

46. Hicks J, Garcia-Godoy F, Flaitz C: **Biological factors in dental caries: enamel structure and the caries process in the dynamic process of demineralization and remineralization (part 2)**. *J Clin Pediatr Dent* 2004, **28**:119–124.

47. Hicks J, Catherine FG: **Biological factors in dental caries: role of remineralization and fluoride in the dynamic process of demineralization and remineralization (part 3)**. *J Clin Pediatr Dent* 2004, **28**:203–214.

48. Reynolds EC: **Calcium phosphate-based remineralization systems: scientific evidence?** *Aust Dent J* 2008, **53**:268–273.

49. Widyarman AS, Udawatte NS, Theodorea CF, Apriani A, Richi M, Astoeti TE, Seneviratne CJ: **Casein phosphopeptide-amorphous calcium phosphate fluoride treatment enriches the symbiotic dental plaque microbiome in children**. *J Dent* 2021, **106**:103582.

50. Fujisaki K, Todoh M, Niida A, Shibuya R, Kitami S, Tadano S: **Orientation and deformation of mineral crystals in tooth surfaces**. *J Mech Behav Biomed Mater* 2012, **10**:176–182.

51. Nelson K, Hesse B, Addison O, Morrell AP, Gross C, Lagrange A, Suárez VI, Kohal R, Fretwurst T: **Distribution and chemical speciation of exogenous micro- and nanoparticles in inflamed soft tissue adjacent to titanium and ceramic dental implants**. *Anal Chem* 2020, **92**:14432–14443.

52. Guentsch A, Fahmy MD, Wehrle C, Nietzsche S, Popp J, Watts DC, Kranz S, Krafft C, Sigusch BW: **Effect of biomimetic mineralization on enamel and dentin: A Raman and EDX analysis**. *Dent Mater* 2019, **35**:1300–1307.

53. Gibson CW: **The amelogenin proteins and enamel development in humans and mice**. *J Oral Biosci* 2011, **53**:248–256.

54. Yao S, Jin B, Liu Z, Shao C, Zhao R, Wang X, Tang R: **Biomineralization: From material tactics to biological strategy**. *Adv Mater* 2017, **29**:1605903.

55. Wei Y, Liu S, Xiao Z, Zhao H, Luo J, Deng X, Guo L: **Enamel repair with amorphous ceramics**. *Adv Mater* 2020, **32**:1907067.

56. Siddiqui S, Anderson P, Al-Jawad M: **Recovery of crystallographic texture in remineralized dental enamel**. *PLoS One* 2014, **9**:1–9.

57. Yoshihara K, Nagaoka N, Nakamura A, Hara T, Hayakawa S, Yoshida Y, Van Meerbeek B: **Three-dimensional observation and analysis of remineralization in dentinal caries lesions**. *Sci Rep* 2020, **10**:4387.

58. Carrouel F, Viennot S, Ottolenghi L, Gaillard C, Bourgeois D: **Nanoparticles as anti-microbial, anti-inflammatory, and remineralizing agents in oral care cosmetics: A review of the current situation**. *Nanomaterials* 2020, **10**:140.

59. Sandomierski M, Buchwald Z, Koczorowski W, Voelkel A: **Calcium forms of zeolites A and X as fillers in dental restorative materials with remineralizing potential**. *Microporous Mesoporous Mater* 2020, **294**:109899.

60. Bapat RA, Chaubal T V., Dharmadhikari S, Abdulla AM, Bapat P, Alexander A, Dubey SK, Kesharwani P: **Recent advances of gold nanoparticles as biomaterial in dentistry**. *Int J Pharm* 2020, **586**:119596.

61. Owens TS, Dansereau RJ, Sakr A: **Development and evaluation of extended release bioadhesive sodium fluoride tablets**. *Int J Pharm* 2005, **288**:109–122.

62. Xiao Z, Que K, Wang H, An R, Chen Z, Qiu Z, Lin M, Song J, Yang J, Lu D, *et al.*: **Rapid biomimetic remineralization of the demineralized enamel surface using nano-particles of amorphous calcium phosphate guided by chimaeric peptides**. *Dent Mater* 2017, **33**:1217–1228.

63. Bröseler F, Tietmann C, Bommer C, Drechsel T, Heinzel-Gutenbrunner M, Jepsen S: **Randomised clinical trial investigating self-assembling peptide P11-4 in the treatment of early caries**. *Clin Oral Investig* 2020, **24**:123–132.

64. Örtengren U, Lehrkinder A, Safarloo A, Axelsson J, Lingström P: **Opportunities for caries prevention using an ion-releasing coating material: a randomised clinical study**. *Odontology* 2021, **109**:358–367.

65. Cummins D: **The development and validation of a new technology, based upon 1.5% arginine, an insoluble calcium compound and fluoride, for everyday use in the prevention and treatment of dental caries**. *J Dent* 2013, **41**:S1–S11.

66. Fan M, Yang J, Xu HHK, Weir MD, Tao S, Yu Z, Liu Y, Li M, Zhou X, Liang K, *et al.*: **Remineralization effectiveness of adhesive containing amorphous calcium phosphate nanoparticles on artificial initial enamel caries in a biofilm-challenged environment**. *Clin Oral Investig* 2021, **25**:5375–5390.

67. Olivan SRG, Sfalcin RA, Fernandes KPS, Ferrari RAM, Horliana ACRT, Motta LJ, Ortega SM, Pinto MM, Deana AM, Bussadori SK: **Preventive effect of remineralizing materials on dental erosion lesions by speckle technique: An *in vitro* analysis**. *Photodiagnosis Photodyn Ther* 2020, **29**:101655.

68. Yagi N, Ohta N, Matsuo T, Tanaka T, Terada Y, Kamasaka H, To-O K, Kometani T, Kuriki T: **Evaluation of enamel crystallites in subsurface lesion by microbeam X-ray diffraction**. *J*

Synchrotron Radiat 2009, **16**:398–404.

69. Creeth JE, Karwal R, Hara AT, Zero DT: **A randomized *in situ* clinical study of fluoride dentifrices on enamel remineralization and resistance to demineralization: Effects of zinc**. *Caries Res* 2018, **52**:129–138.

70. Ratanaporncharoen C, Tabata M, Kitasako Y, Ikeda M, Goda T, Matsumoto A, Tagami J, Miyahara Y: **pH mapping on tooth surfaces for quantitative caries diagnosis using micro Ir/IrOx pH sensor**. *Anal Chem* 2018, **90**:4925–4931.

71. Tammaro L, Vittoria V, Calarco A, Petillo O, Riccitiello F, Peluso G: **Effect of layered double hydroxide intercalated with fluoride ions on the physical, biological and release properties of a dental composite resin**. *J Dent* 2014, **42**:60–67.

72. Hoxha A, Gillam DG, Agha A, Karpukhina N, Bushby AJ, Patel MP: **Novel fluoride rechargeable dental composites containing MgAl and CaAl layered double hydroxide (LDH)**. *Dent Mater* 2020, **36**:973–986.

73. Wei Su L, Lin DJ, Yen Uan J: **Novel dental resin composites containing LiAl-F layered double hydroxide (LDH) filler: Fluoride release/recharge, mechanical properties, color change, and cytotoxicity**. *Dent Mater* 2019, **35**:663–672.

74. Taha AA, Patel MP, Hill RG, Fleming PS: **The effect of bioactive glasses on enamel remineralization: A systematic review**. *J Dent* 2017, **67**:9–17.

75. Aoba T: **The effect of fluoride on apatite structure and growth**. *Crit Rev Oral Biol Med* 1997, **8**:136–153.

76. Reis DP, Filho JDN, Rossi AL, de Almeida Neves A, Portela MB, da Silva EM: **Remineralizing potential of dental composites containing silanized silica-hydroxyapatite (Si-HAp) nanoporous particles charged with sodium fluoride (NaF)**. *J Dent* 2019, **90**:103211.

77. Torrado A, Valiente M, Zhang W, Li Y, Muñoz CA: **Remineralization potential of a new toothpaste formulation: An *in-vitro* study**. *J Contemp Dent Pract* 2004, **5**:18–30.

78. Wierichs RJ, Zelck H, Doerfer CE, Appel P, Paris S, Esteves-Oliveira M, Meyer-Lueckel H: **Effects of dentifrices differing in fluoride compounds on artificial enamel caries lesions *in vitro***. *Odontology* 2017, **105**:36–45.

79. Hussain I, Ahamad KU, Nath P: **Low-cost, robust, and field portable smartphone platform photometric sensor for fluoride level detection in drinking water**. *Anal Chem* 2017, **89**:767–775.

80. Seredin P, Goloshchapov D, Ippolitov Y, Vongsvivut J: **Development of a new approach to diagnosis of the early fluorosis forms by means of FTIR and Raman microspectroscopy**. *Sci Rep* 2020, **10**:20891.

81. Pendrys DG: **Risk of fluorosis in a fluoridated population. Implications for the dentist and hygienist.** *J Am Dent Assoc* 1995, **126**:1617–1624.

82. Walker G, Cai F, Shen P, Reynolds C, Ward B, Fone C, Honda S, Koganei M, Oda M, Reynolds E: **Increased remineralization of tooth enamel by milk containing added casein phosphopeptide-amorphous calcium phosphate**. *J Dairy Res* 2006, **73**:74–78.

83. Navarro M, Serra T: **Biomimetic mineralization of ceramics and glasses**. In *Biomineralization and biomaterials: Fundamentals and applications*. Edited by Aparicio C, Ginebra M-P. Woodhead Publishing; 2016:315–338.

84. Carneiro KMM, Zhai H, Zhu L, Horst JA, Sitlin M, Nguyen M, Wagner M, Simpliciano C, Milder M, Chen CL, *et al.*: **Amyloid-like ribbons of amelogenins in enamel mineralization**. *Sci Rep* 2016, **6**:23105.

85. Sharma V, Srinivasan A, Roychoudhury A, Rani K, Tyagi M, Dev K, Nikolajeff F, Kumar S: **Characterization of protein extracts from different types of human teeth and insight in biomineralization**. *Sci Rep* 2019, **9**:9314.

86. Cao Y, Liu W, Ning T, Mei ML, Li QL, Lo ECM, Chu CH: **A novel oligopeptide simulating dentine matrix protein 1 for biomimetic mineralization of dentine**. *Clin Oral Investig* 2014, **18**:873–881.

87. Fan M, Zhang M, Xu HHK, Tao S, Yu Z, Yang J, Yuan H, Zhou X, Liang K, Li J: **Remineralization effectiveness of the PAMAM dendrimer with different terminal groups on artificial initial enamel caries *in vitro***. *Dent Mater* 2020, **36**:210–220.

88. Li D, Lv X, Tu H, Zhou X, Yu H, Zhang L: **Remineralization of initial enamel caries *in vitro* using a novel peptide based on amelogenin**. *Front Mater Sci* 2015, **9**:293–302.

89. Fan YW, Sun Z, Wang R, Abbott C, Moradian-Oldak J: **Enamel inspired nanocomposite fabrication through amelogenin supramolecular assembly**. *Biomaterials* 2007, **28**:3034–3042.

90. Fan Y, Sun Z, Moradian-Oldak J: **Controlled remineralization of enamel in the presence of amelogenin and fluoride**. *Biomaterials* 2009, **30**:478–483.

91. Fan Y, Nelson JR, Alvarez JR, Hagan J, Berrier A, Xu X: **Amelogenin-assisted *ex vivo* remineralization of human enamel: Effects of supersaturation degree and fluoride concentration**. *Acta Biomater* 2011, **7**:2293–2302.

92. Fan Y, Wen ZT, Liao S, Lallier T, Hagan JL, Twomley JT, Zhang JF, Sun Z, Xu X: **Novel amelogenin-releasing hydrogel for remineralization of enamel artificial caries**. *J Bioact Compat Polym* 2012, **27**:585–603.

93. Kwak SY, Litman A, Margolis HC, Yamakoshi Y, Simmer JP: **Biomimetic enamel regeneration mediated by leucine-rich amelogenin peptide**. *J Dent Res* 2017, **96**:524–530.

94. Iijima M, Moradian-Oldak J: **Control of apatite crystal growth in a fluoride containing amelogenin-rich matrix**. *Biomaterials* 2005, **26**:1595–1603.

95. Helfferich F: *Ion exchange*. Dover Publications; 1995.

96. Dorfner K: **Introduction to ion exchange and ion exchangers**. In *Ion exchangers*. Edited by Dorfner K. Walter de Gruyter; 2011:7–188.

97. Torrado A, Valiente M: **Kinetics characterization of ion release under dynamic and batch conditions. I. Weak acid and weak base ion exchange resins**. *J Solution Chem* 2008, **37**:581–594.

98. Muraviev D, Torrado A, Valiente M: **Kinetics of release of calcium and fluoride ions from ion-exchange resins in artificial saliva**. *Solvent Extr Ion Exch* 2000, **18**:345–374.

99. Valiente M: **Remineralizing material for organomineral tissues. USA patent US 6,413,498 B1**. 1999.

100. Matsunaga T, Ishizaki H, Tanabe S, Hayashi Y: **Synchrotron radiation microbeam X-ray fluorescence analysis of zinc concentration in remineralized enamel *in situ***. *Arch Oral Biol* 2009, **54**:420–423.

101. Rochow TG, Rochow EG: **Scanning electron microscopy**. In *An introduction to microscopy by means of light, electrons, X-rays, or ultrasound*. Edited by Rochow TG, Rochow EG. Plenum Press; 1978:273–298.

102. Goldstein JI, Newbury DE, Michael JR, Ritchie NWM, Scott JHJ, Joy DC: *Scanning electron*

microscopy and X-ray microanalysis. Springer; 2018.

103. Brodusch N, Demers H, Gauvin R: *Field emission scanning electron microscopy: New perspectives for materials characterization*. Springer; 2018.

104. Deerinck TJ, Shone TM, Bushong EA, Ramachandra R, Peltier ST, Ellisman MH: **High-performance serial block-face SEM of non-conductive biological samples enabled by focal gas injection-based charge compensation**. *J Microsc* 2018, **270**:142–149.

105. Sutton MA, Li N, Joy DC, Reynolds AP, Li X: **Scanning electron microscopy for quantitative small and large deformation measurements Part I: SEM imaging at magnifications from 200 to 10,000**. *Exp Mech* 2007, **47**:775–787.

106. Willems G, Celis JP, Lambrechts P, Braem M, Vanherle G: **Hardness and Young's modulus determined by nanoindentation technique of filler particles of dental restorative materials compared with human enamel**. *J Biomed Mater Res* 1993, **27**:747–755.

107. Giráldez de Luis I, Garrido MA, Gómez-del Río T, Ceballos L, Rodríguez J: **Comparison of the mechanical properties of dentin and enamel determined by different nanoindentation techniques: Conventional method and continuous stiffness measurement**. *Bol la Soc Esp Ceram y Vidr* 2010, **49**:177–182.

108. Li X, Bhushan B: **A review of nanoindentation continuous stiffness measurement technique and its applications**. *Mater Charact* 2002, **48**:11–36.

109. White AJ, Yorath C, Ten Hengel V, Leary SD, Huysmans MCDNJM, Barbour ME: **Human and bovine enamel erosion under "single-drink" conditions**. *Eur J Oral Sci* 2010, **118**:604–609.

110. Cuy JL, Mann AB, Livi KJ, Teaford MF, Weihs TP: **Nanoindentation mapping of the mechanical properties of human molar tooth enamel**. *Arch Oral Biol* 2002, **47**:281–291.

111. Zhang YF, Li DY, Yu JX, He HT: **On the thickness and nanomechanical properties of salivary pellicle formed on tooth enamel**. *J Dent* 2016, **55**:99–104.

112. Ge J, Cui FZ, Wang XM, Feng HL: **Property variations in the prism and the organic sheath within enamel by nanoindentation**. *Biomaterials* 2005, **26**:3333–3339.

113. Ziller JW, Rheingold AL: **X-ray crystallography**. In *Physical methods for chemists*. Edited by Drago RS. Surfside Scientific Publishers; 1992:689–711.

114. Stan C, Beavers C, Kunz M, Tamura N: **X-ray diffraction under extreme conditions at the advanced light source**. *Quantum Beam Sci* 2018, **2**:4.

115. Deng Y, Hsu CYS: **Combined effect of fluoride and laser on the crystalline structure of human enamel: A pilot study**. *Lasers Dent XI* 2005, **5687**:42.

116. Xue J, Zhang L, Zou L, Liao Y, Li J, Xiao L, Li W: **High-resolution X-ray microdiffraction analysis of natural teeth**. *J Synchrotron Radiat* 2008, **15**:235–238.

117. Stuart BH: *Infrared spectroscopy: Fundamentals and applications*. John Wiley & Sons; 2004.

118. Khoshhesab ZM: **Reflectance IR spectroscopy**. In *Infrared spectroscopy - Materials science, engineering and technology*. Edited by Theophile T. InTech; 2012:233–244.

119. Lopes C de CA, Limirio PHJO, Novais VR, Dechichi P: **Fourier transform infrared spectroscopy (FTIR) application chemical characterization of enamel, dentin and bone**. *Appl Spectrosc Rev* 2018, **53**:747–769.

120. Mukherjee S, Gowen A: **A review of recent trends in polymer characterization using non-destructive vibrational spectroscopic modalities and chemical imaging**. *Anal Chim*

Acta 2015, **895**:12–34.

121. Acerbo AS, Carr GL, Judex S, Miller LM: **Imaging the material properties of bone specimens using reflection-based infrared microspectroscopy**. *Anal Chem* 2012, **84**:3607–3613.

122. Goloshchapov DL, Kashkarov VM, Seredin P V., Ippolitov YA, Plotnikova YA, Bambery K: **The study of efficiency of endogenous and exogenous preventive methods of tooth enamel remineralisation by FTIR microscopy using synchrotron radiation**. *J Phys Conf Ser* 2016, **741**:012054.

123. Dumas P, Sockalingum GD, Sulé-Suso J: **Adding synchrotron radiation to infrared microspectroscopy: what's new in biomedical applications?** *Trends Biotechnol* 2007, **25**:40–44.

124. Aufort J, Ségalen L, Gervais C, Brouder C, Balan E: **Modeling the attenuated total reflectance infrared (ATR-FTIR) spectrum of apatite**. *Phys Chem Miner* 2016, **43**:615–626.

125. Martínez Prieto AB, Biscari C, García López G: **The ALBA Synchrotron light source**. *Contrib to Sci* 2016, **12**:13–21.

126. Willmott P: *An introduction to synchrotron radiation*. John Wiley & Sons; 2019.

127. Duncan DA: **Synchrotron-based spectroscopy in on-surface polymerization of covalent networks**. In *Encyclopedia of interfacial chemistry: Surface science and electrochemistry*. Edited by Wandelt K. Elsevier; 2018:436–445.

128. van de Kamp T, Ershov A, dos Santos Rolo T, Riedel A, Baumbach T: **Insect imaging at the ANKA synchrotron radiation facility**. *Entomol heute* 2013, **25**:147–160.

129. Maritan L, Casas L, Crespi A, Gravagna E, Rius J, Vallcorba O, Usai D: **Synchrotron tts-μXRD identification of secondary phases in ancient ceramics**. *Herit Sci* 2018, **6**:74.

130. Svensson Bonde J, Bulow L: **One-step purification of recombinant human amelogenin and use of amelogenin as a fusion partner**. *PLoS One* 2012, **7**:e33269.

131. Groenhuis RAJ, Jongebloed WL, ten Bosch JJ: **Surface roughness of acid-etched and demineralized bovine enamel measured by a laser speckle method**. *Caries Res* 1980, **14**:333–340.

132. Abràmoff MD, Magalhães PJ, Ram SJ: **Image processing with ImageJ**. *Biophotonics Int* 2004, **11**:36–41.

133. Collins T: **ImageJ for microscopy**. *Biotechniques* 2007, **43**:25–30.

134. Braly A, Darnell LA, Mann AB, Teaford MF, Weihs TP: **The effect of prism orientation on the indentation testing of human molar enamel**. *Arch Oral Biol* 2007, **52**:856–860.

135. Xu HHK, Smith DT, Jahanmir S, Romberg E, Kelly JR, Thompson VP, Rekow ED: **Indentation damage and mechanical properties of human enamel and dentin**. *J Dent Res* 1998, **77**:472–480.

136. Ma Y, Cohen SR, Addadi L, Weiner S: **Sea urchin tooth design: An "all-calcite" polycrystalline reinforced fiber composite for grinding rocks**. *Adv Mater* 2008, **20**:1555–1559.

137. Fauth F, Peral I, Popescu C, Knapp M: **The new Material Science Powder Diffraction beamline at ALBA Synchrotron**. *Powder Diffr* 2013, **28**:360–370.

138. Rius J, Vallcorba O, Frontera C, Peral I, Crespi A, Miravitlles C: **Application of synchrotron through-the-substrate microdiffraction to crystals in polished thin sections**. *IUCrJ* 2015,

2:452–463.

139. Vallcorba O, Rius J: **d2Dplot: 2D X-ray diffraction data processing and analysis for through-the-substrate microdiffraction**. *J Appl Crystallogr* 2019, **52**:478–484.

140. Al-Jawad M, Addison O, Khan MA, James A, Hendriksz CJ: **Disruption of enamel crystal formation quantified by synchrotron microdiffraction**. *J Dent* 2012, **40**:1074–1080.

141. Ruckebusch C, Blanchet L: **Multivariate curve resolution: A review of advanced and tailored applications and challenges**. *Anal Chim Acta* 2013, **765**:28–36.

142. Ribó L, Sics I, Gevorgyan A, Nicolas J, Crisol A, Colldelram C, Nikitina L, Monge R, Quispe M, Yousef I, *et al.*: **Mechanical design of MIRAS, infrared microspectroscopy beam line at ALBA Synchrotron**. *JACoW, Geneva, Switz* 2017, 403–408.

143. Chatterjee S, Singh B, Diwan A, Lee ZR, Engelhard MH, Terry J, Tolley HD, Gallagher NB, Linford MR: **A perspective on two chemometrics tools: PCA and MCR, and introduction of a new one: Pattern recognition entropy (PRE), as applied to XPS and ToF-SIMS depth profiles of organic and inorganic materials**. *Appl Surf Sci* 2018, **433**:994–1017.

144. Puigdomenech I: **Program MEDUSA (Make equilibrium diagrams using sophisticated algorithms)**. *R Inst Technol Inorg Chem* 2010.

145. Simon P, Schwarz U, Kniep R: **Hierarchical architecture and real structure in a biomimetic nano-composite of fluorapatite with gelatine: a model system for steps in dentino- and osteogenesis?** *J Mater Chem* 2005, **15**:4992–4996.

146. Busch S, Schwarz U, Kniep R: **Morphogenesis and structure of human teeth in relation to biomimetically grown fluorapatite-gelatine composites**. *Chem Mater* 2001, **13**:3260–3271.

147. Busch S, Dolhaine H, DuChesne A, Heinz S, Hochrein O, Laeri F, Podebrad O, Vietze U, Weiland T, Kniep R: **Biomimetic morphogenesis of fluorapatite-gelatin composites: Fractal growth, the question of intrinsic electric fields, core/shell assemblies, hollow spheres and reorganization of denatured collagen**. *Eur J Inorg Chem* 1999, **1999**:1643–1653.

148. Habelitz S, Kullar A, Marshall SJ, DenBesten PK, Balooch M, Marshall GW, Li W: **Amelogenin-guided crystal growth on fluoroapatite glass-ceramics**. *J Dent Res* 2004, **83**:698–702.

149. Jardim JJ, Pagot MA, Maltz M: **Artificial enamel dental caries treated with different topical fluoride regimes: An *in situ* study**. *J Dent* 2008, **36**:396–401.

150. Brundavanam RK, Eddy G, Poinern J, Fawcett D: **Modelling the crystal structure of a 30 nm sized particle based hydroxyapatite powder synthesised under the influence of ultrasound irradiation from X-ray powder diffraction data**. *Am J M aterials Sci* 2013, **3**:84–90.

151. Okazaki M, Hirata I, Matsumoto T, Takahashi J: **Advantages of TOF-SIMS analysis of hydroxyapatite and fluorapatite in comparison with XRD, HR-TEM and FT-IR**. *Dent Mater J* 2005, **24**:508–514.

152. Zheo J, Dong X, Bian M, Zhao J, Zhang Y, Sun Y, Chen J, Wang X: **Solution combustion method for synthesis of nanostructured hydroxyapatite, fluorapatite and chlorapatite**. *Appl Surf Sci* 2014, **314**:1026–1033.

153. Al-Jawad M, Steuwer A, Kilcoyne SH, Shore RC, Cywinski R, Wood DJ: **2D mapping of texture and lattice parameters of dental enamel**. *Biomaterials* 2007, **28**:2908–2914.

154. Al-Mosawi M, Davis GR, Bushby A, Montgomery J, Beaumont J, Al-Jawad M:

Crystallographic texture and mineral concentration quantification of developing and mature human incisal enamel. *Sci Rep* 2018, **8**:1–18.

155. Free R, Derocher K, Xu R, Joester D, Stock SR: **A method for mapping submicron-scale crystallographic order/disorder applied to human tooth enamel**. *Powder Diffr* 2020, **35**:117–123.

156. Bachmann L, Diebolder R, Hibst R, Zezell DM: **Infrared absorption bands of enamel and dentin tissues from human and bovine teeth**. *Appl Spectrosc Rev* 2003, **38**:1–14.

157. Garskaite E, Gross KA, Yang SW, Yang TCK, Yang JC, Kareiva A: **Effect of processing conditions on the crystallinity and structure of carbonated calcium hydroxyapatite (CHAp)**. *CrystEngComm* 2014, **16**:3950–3959.

158. Arboleda A, Franco M, Caicedo J, Tirado L, Goyes C: **Synthesis and chemical and structural characterization of hydroxyapatite obtained from eggshell and tricalcium phosphate**. *Ing y Compet* 2016, **18**:69–71.

159. Madupalli H, Pavan B, Tecklenburg MMJ: **Carbonate substitution in the mineral component of bone: Discriminating the structural changes, simultaneously imposed by carbonate in A and B sites of apatite**. *J Solid State Chem* 2017, **255**:27–35.

160. Brangule A, Gross KA: **Importance of FTIR spectra deconvolution for the analysis of amorphous calcium phosphates**. *IOP Conf Ser Mater Sci Eng* 2015, **77**:012027.

161. Chen KH, Cheng WT, Li MJ, Yang DM, Lin SY: **Calcification of senile cataractous lens determined by Fourier transform infrared (FTIR) and Raman microspectroscopies**. *J Microsc* 2005, **219**:36–41.

162. Fan K, Bell P, Fried D: **Rapid and conservative ablation and modification of enamel, dentin, and alveolar bone using a high repetition rate transverse excited atmospheric pressure CO_2 laser operating at λ=9.3 μm**. *J Biomed Opt* 2006, **11**:064008.

163. Jones RS, Darling CL, Featherstone JDB, Fried D: **Remineralization of *in vitro* dental caries assessed with polarization-sensitive optical coherence tomography**. *J Biomed Opt* 2006, **11**:014016.

ANNEXES

ANNEX I. Pending paper: The power of weak ion-exchange resins assisted by amelogenin for natural remineralization of dental enamel. An *in vitro* study.

Sandra Diez-García[1(¥)], María-Jesús Sánchez-Martín[1*(¥)] and Manuel Valiente[1]

[1] GTS Research Group, Department of Chemistry, Faculty of Science, Universitat Autònoma de Barcelona, 08193 Bellaterra, Spain

[(¥)] Shared co-first authorship

[*] Author for correspondence e-mail address: mariajesus.sanchez@uab.cat

Abstract

This study aims to develop an innovative dental material to remineralize dental enamel by a proper combination of ion-exchange resins as controlled release of mineral ions forming dental enamel, in presence of amelogenin to guide the appropriate crystal growth. The novel product proposed consists of a combination of ion-exchange resins (weak acid and weak base) individually loaded with the remineralizing ions: Ca^{2+}, PO_4^{3-} and F^-, also including Zn^{2+} in a minor amount as antibacterial, together with the protein amelogenin. Such cocktail provides onsite controlled release of the ions necessary for enamel remineralization and at the same time, a guiding tool for related crystal growth by the indicated protein. Amelogenin protein is involved in the structural development of natural enamel and takes a key role in controlling the crystal growth morphology and alignment at the enamel surface. Treated teeth were evaluated with nanoindentation, scanning electron microscopy (SEM) and energy dispersive X-ray spectroscopy (EDX). The innovative material induces the dental remineralization creating a fluorapatite layer with a hardness equivalent to sound enamel, with the appropriate alignment of corresponding nanocrystals, being the fluorapatite more acid-resistant than the original mineral. Our results suggest that the new product shows potential for inhibiting demineralization and promoting long-term remineralization leading to the inhibition of caries and protection of dental structures.

Keywords

Controlled release system, Amelogenin, Enamel remineralization, Dental caries, Fluorapatite.

1. Introduction

Dental caries is a complex disease process that afflicts a large proportion of the world's population, regardless of gender, age and ethnicity, although it is more likely to be present in individuals with a low socioeconomic status [1–4]. Despite the fact that the prevalence of dental caries has descended over the last decades, the disease is still a major problem for adults and children, and an improved approach to prevention and therapy is currently needed [5]. Dental caries progresses when organic acids, produced by bacterial action from biofilms of dental plaque on dietary fermentable carbohydrates, diffuse into the tooth and dissolve the mineral [6–13]. Dental caries is a process, which can be stopped and reversed in its initial stages. If left untreated, the early reversible lesion can progress to the point of being irreversible [14,15]. Another factor that puts oral health at risk and makes it necessary to find a solution, is the popularity of the whitening systems and their side effects [16–19]. The mature enamel has no residual cellular components that can carry out the repair when it is damaged, so the restoration depends on physicochemical events at the tooth surface [1,2]; here are protective factors that can prevent or reverse it, such as salivary proteins, calcium, phosphate, salivary flow and fluoride in saliva [5,20,21].

Enamel is the outer layer of the teeth and is the hardest and most mineralized tissue in vertebrates [22–25]. It is an acellular mineralized tissue comprised of highly oriented crystallites of calcium hydroxyapatite organized into rod and interrod structures. These crystals are unique in shape, organization and orientation. Tooth enamel rods seem to extend from the dentino-enamel junction to the tooth surface and they are remarkably longer than wide [26].

During tooth germination, the enamel mineral is a highly substituted carbonated apatite, not pure hydroxyapatite (HA). The mineral is related to hydroxyapatite but is much more soluble in acid, as well as calcium deficient (calcium is replaced by sodium, magnesium and zinc) and contains between 3 to 6% of carbonate ions replacing phosphate ions in the crystal lattice. Demineralization and remineralization can be contemplated as a dynamic process. The carbonate is preferentially lost during the demineralization process, and it is excluded during remineralization. Thus, the calcium-deficient and carbonate-rich regions of the crystal are markedly susceptible to be attacked during demineralization [5]. When the OH^- groups in pure hydroxyapatite ($Ca_{10}(PO_4)_6(OH)_2$) are completely replaced by fluoride ions (F^-), it results in mineral fluorapatite (FA) ($Ca_{10}(PO_4)_6F_2$), which is really resistant to

dissolution by acid. Mature enamel is mostly a mixture of hydroxyapatite and fluorapatite and for this reason, it is much less soluble than the original mineral [5,21,27].

Fluoride is widely used in dental products because primarily via topical mechanisms it has a cariostatic effect inhibiting the demineralization at the crystal surfaces, enhancing the remineralization, interfering with plaque formation and inhibiting bacterial metabolism [5,10,21,28–32]. The presence of fluoride ions restricts the formation of acidic, more soluble calcium phosphates as dicalcium phosphate dihydrate or octacalcium phosphate, and facilitates the creation of more acid-resistant fluorapatite or fluorhydroxyapatite (partial substitution of fluoride by hydroxyl groups). Fluorapatite or fluorhydroxyapatite are formed when low levels of fluoride ions are present, and calcium fluoride will be created with high levels of fluoride ions. This calcium fluoride will hydrolyze to fluorhydroxyapatite in the presence of acid phosphate or phosphate ions. Moreover, fluoride is more effective in inhibiting hydroxyapatite dissolution when calcium and phosphate ions are also present in the solution [2]. With fluoride availability, demineralization is reduced because part of the calcium and phosphate lost by the dissolution of hydroxyapatite returns to the enamel as more acid-resistant fluorapatite [33].

Even though systemic fluoride by means of water fluoridation has been promoted in the past for the decline in dental caries, it has been found that the systemic benefits of fluoride are minimal and the primary reduction in dental caries is due to the topical effect of water fluoridation and the availability of fluoridated toothpastes. In several European countries without water fluoridation, a caries reduction has been seen after the introduction of fluoridated toothpastes [3]. Toothpastes are probably the most widespread products in health care and are one of the most effective ways to deliver free or soluble fluoride [34]. Nevertheless, high concentrations of fluoride can cause numerous side effects and due to the short oral application time of many fluoride products, fluoride ions are released rapidly producing high concentrations in a short time [21]. There has been an increase in the exposure to fluoride ingestion in children increasing the risk of toxicity and dental fluorosis due to the high levels of fluoride released into biological fluids [35].

A different approach to induce remineralization is used in the present study to avoid high concentrations of fluoride with its side effects and prolong the contact time between fluoride ions and teeth. The fluorapatite formation could be guided controlling the release speed of fluoride in the oral environment, in conjunction with the release of calcium and

phosphate ions in order to induce the remineralization. For this purpose, a product (called NMTD [36], new dental treatment material or *Nuevo Material de Tratamiento Dental* in Spanish) that provides a controlled release system for the anticaries treatment of dental tissues is used. NMTD is a combination of ion-exchange resins of weak acid and weak base ion-exchangers composition, loaded with calcium, fluoride, phosphate and zinc. The molar ratio of the ions has to be close to that of the organomineral tissue to be remineralized; in the case of the teeth, the approximate molar ratio between Ca^{2+}, F^- and PO_4^{3-}, is 2:1:1, respectively. In contact with NMTD, the organomineral tissues are remineralized in a fast and effective way, especially in the presence of Zn^{2+} ions. Zinc has two effects: it helps to combat the micro-organisms which cause caries due to its bactericidal properties against oral bacteria [37], and it is an initiator of the ionic release of the other structural ions. A toothpaste containing NMTD was proven to be effective in limiting *in vitro* enamel demineralization and in enhancing remineralization [38]. The application of ion-exchange materials has advantages compared to conventional chemical reagents, since the release of ions is only due to the ion-exchange mechanism and they do not introduce undesirable ions into the solution, they are characterized by practically neutral pH values and they can also adsorb bacteria on their surfaces. Most of these resins are non-toxic and are used in the pharmaceutical industry, in medical applications and also in the food industry [39].

On the other hand, the organic matrix composed of proteins secreted by the ameloblasts provides a scaffold for the enamel minerals to grow. But following this stage of development, the enamel enters a maturation phase in which most of the organic matter is degraded [23,24,40–42]. The protein amelogenin, that constitutes the 90% of the protein matrix, plays a central role in guiding the hierarchical organization of apatite crystals observed in mature enamel [22,43–46]. It is known that the crystal morphology and alignment of enamel, as well as the correct enamel thickness, are the result of a protein-guided uniaxial growth process. The exact mechanism guiding this process remains undetermined due to the rapid degradation of the underlying protein matrix during tissue maturation. However, the role of self-assembly of enamel matrix proteins, particularly amelogenin, has been widely recognized as a key factor in controlling enamel structural development [22,43,47]. Therefore, there is considerable interest in the use of amelogenin and other similar self-assembling peptides for dental remineralization [48–54]. The aim of this study is to assess the NMTD remineralization capacity in presence and absence of

amelogenin in order to understand the influence of this protein on the crystal morphology and alignment during the remineralization process.

2. Materials and methods

2.1. Materials

Hydrochloric acid (37%) and potassium hydroxide pellets (85%) were purchased from Panreac (Barcelona, Spain). Chloramine T trihydrate (98-103%), HEPES (4-(2-hydroxyethyl)-1-piperazine-ethanesulfonic acid, 99.5%), magnesium chloride hexahydrate (99%) and calcium fluoride (95%) were purchased from Sigma Aldrich (Steinheim, Germany); calcium chloride dihydrate (74-78%), potassium dihydrogen phosphate (99.5%) and tricalcium phosphate (35-40% (Ca)) from Panreac (Barcelona, Spain); potassium chloride (99-100.5%) from J. T. Baker (Deventer, Holland), all in powder form. Deionized water was purified through a Millipore purification system from Millipore (Milford, MA, USA). Reference sample of the hydroxyapatite was of analytical grade and was used as received without any further purification (>90%, Fluka, Sigma-Aldrich, Steinheim, Germany).

The base of the weak acid ion-exchange resins is a copolymer from acrylic acid, divinylbenzene and aliphatic diene with carboxylic acid functional groups (Lewatit S 8528, Lanxess, Leverkusen, Germany); and the base of the weak base ion-exchange resins is a styrene-divinylbenzene-copolymer with tertiary amine functional groups (Lewatit S 4528, Lanxess, Leverkusen, Germany). These food grade ion-exchange resins charged with different ions (Zn^{2+}, Ca^{2+}, F^{-} and PO_4^{3-}) were purchased from MionTec (Leverkusen, Germany). They were ground to below 50 μm particle size and mixed to form the NMTD product, in which the corresponding molar ratio between Ca^{2+}, F^{-} and PO_4^{3-}, is 2:1:1, respectively. Moreover, Zn^{2+} ions-charged resin is added, representing the 0.2% of the dry weight of the related resin.

2.2. Methods

2.2.1. Reference fluorapatite sample

The fluorapatite reference powder was synthetized following a solid phase reaction [55] mixing in the agate miller calcium fluoride (95%) and tricalcium phosphate (35-40% (Ca)) at the ratio of 1.67 Ca/P. Subsequently, the reagents were placed in the muffle furnace (Selecta 366 PE, Barcelona, Spain) and heated to 1200 ºC for 2 hours. The solid FA was then grounded during 15 minutes into powder.

2.2.2. Mineral growth in solution

In order to form FA in solution, 0.6 g of NMTD were mixed with 1 ml of artificial saliva (KCl 0.24 g/l, $CaCl_2 \cdot 2H_2O$ 0.078 g/l, KH_2PO_4 0.544 g/l, $MgCl_2 \cdot 6H_2O$ 0.041 g/l, HEPES 4.77 g/l; adjusted to pH 7.1±0.4 with KOH pellets) and placed in a closed container inside an incubator at 37 ºC during 24 hours. The resultant paste is filtered with the aid of a funnel and a Kitasato flask under vacuum and dried at room temperature.

2.2.3. Amelogenin production

A human 175 amino acid amelogenin (Swissprot Q99217, isoform 1, excluding the signal peptide) was expressed in the *Escherichia coli* strain BL21 (DE3) and purified with an acid/heat treatment as described previously Svensson Bonde and Bulow [56]. The proteins were analysed by matrix-assisted laser desorption/ionization, sodium dodecyl sulfate polyacrylamide gel electrophoresis and western blot to confirm the obtainment of amelogenin. The recombinant amelogenin was quantified with a nanodrop.

Protein purification has been performed by the ICTS "NANBIOSIS", more specifically by the Protein Production Platform of CIBER in Bioengineering, Biomaterials & Nanomedicine (CIBER-BBN)/ IBB, at the UAB SePBioEs scientific-technical service (http://www.nanbiosis.es/portfolio/u1-protein-production-platform-ppp/).

2.2.4. Specimen preparation

Bovine teeth are used as a model due to their resemblance to human teeth [57]. Specimens of bovine teeth were cleaned of gross debris and the root was sectioned using a diamond saw (South Bay Technology, San Clemente, CA, USA). Samples were embedded in a Fastray acrylic resin (Harry J. Bosworth, Skokie, IL, USA) to close the root hole. Then, teeth were etched with 1 M HCl for 30 seconds [58] to simulate the early stage of dental erosion and cleaned by rinsing with MilliQ water while brushing for 20 seconds with an electric toothbrush.

2.2.5. *In vitro* remineralizing treatment

Groups of six teeth were prepared as explained in section 2.2.4 for each time and treatment: NMTD, NMTD with human amelogenin and blank samples.

Blank samples were placed in the saliva solution at 37 ºC during the different times of the experiment and cleaned with MilliQ water while brushing for 20 seconds every 24 hours.

For both remineralizing treatments, artificial saliva (in presence or absence of 100 µg/ml of human amelogenin) was added to NMTD until obtaining the optimal consistence of thick gel for its application onto the tooth. The mixture was applied directly on the enamel surface of the etched teeth. The samples were placed in a closed container with saliva on the bottom and inside an incubator in order to maintain the humidity and the natural temperature of the oral cavity (37 ºC). Every 24 hours, each treatment was renewed by carefully washing the specimens with MilliQ water and brushing for 20 seconds before applying a fresh portion of treatment.

The different groups of samples were treated between 4 and 20 days. Finally, teeth were cleaned by brushing with MilliQ water for 20 seconds and stored in a 0.5% chloramine T solution until their analysis.

Moreover, some samples that were treated during 15 days with NMTD were brushed continuously for 15 minutes with the electric toothbrush to study the strength of the remineralization.

To study the remineralized layer, selected samples were longitudinally cut in two halves along the central lobe with a Struers Minitom precision diamond saw (Copenhagen, Denmark) and polished with a Struers LaboPol-25 polisher (Copenhagen, Denmark). A sequence of silicon carbide paper was used to polish the longitudinal side, starting at grit size P1000 and sequentially increasing to P4000, under a constant flow of water. Then, a diamond paste with a mean particle size of 1 µm was used to finish the polishing.

2.2.6. SEM-EDX measurements

The structure and elemental composition of the samples were analyzed by scanning electron microscopy (SEM) and energy dispersive X-ray spectroscopy (EDX) with a Zeiss Merlin field emission SEM equipped with an EDX Oxford INCA X-Max detector. This microscope has a unique charge compensation system that allows the high-resolution imaging of non-conductive samples, electrons which accumulate on the sample surface are swept away by a fine jet of nitrogen. The images were taken on the surface and the longitudinal section of the teeth with the secondary electron detector with a low voltage of 1-3 kV and the EDX measurements were taken at 10 kV. The powder from the mineral growth experiment and the HA and FA references were characterized under the same conditions as described above. All the experiments were performed at room temperature.

2.2.7. Nanoindentation

The hardness of the teeth was measured using an MTS Nano Indenter XP with a Berkovich tip that provides a fast and reliable way to acquire mechanical data on the submicron scale. The continuous stiffness measurements (CSM) were performed in the longitudinal section of the tooth with a depth limit of 1000 nm and a Poisson's ratio of 0.25 [59,60]. Continuous stiffness measurement with depth, in conjunction with the known indenter tip area function, allows continuous hardness monitoring [61]. All the experiments were performed at room temperature. Before every measurement, the Berkovich diamond indenter was calibrated on a standard fused silica specimen.

2.2.8. Sotfware

MEDUSA program (Stockholm, Sweden) [62] was used to create the chemical equilibrium diagram of the species formed in presence of the ions released from the NMTD. The basic parameters that are necessary for the calculation of distribution diagrams, including equilibrium constants, are included in the program database.

SEM images treatment was done using ImageJ [63,64], a public domain image processing and analysis program developed at the U.S. National Institutes of Health.

GraphPad Prism 9 (GraphPad Software, San Diego, CA, USA) was used for statistical analysis.

3. Results

3.1. Mineral growth in solution

Theoretically, the predominant species formed in presence of the ions released from the NMTD at pH 7.1 would be calcium fluoride and fluorapatite, as it can be seen in the species distribution diagram of Fig. 1.

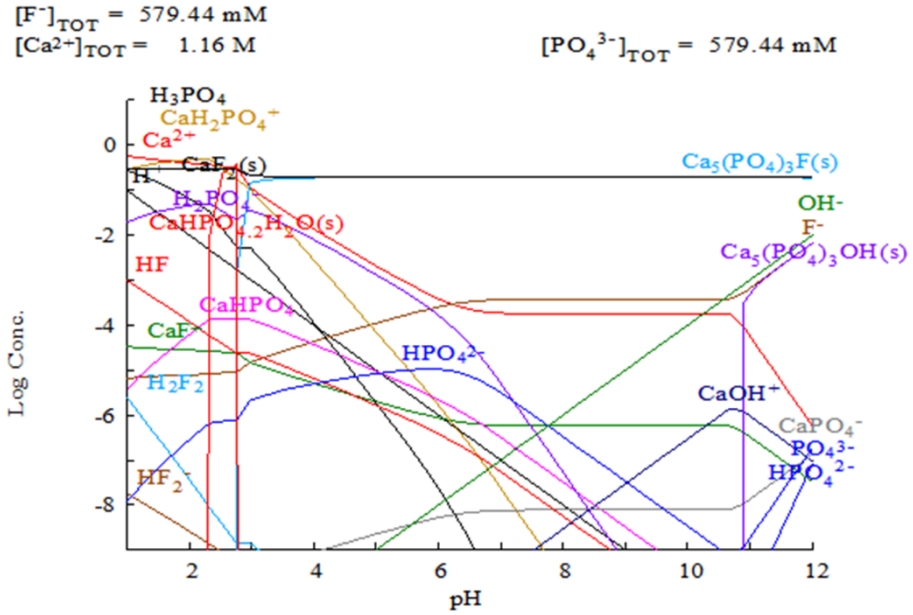

Fig. 1 Theoretical distribution diagram of the species formed in presence of the released ions from NMTD as function of medium pH (saliva solution in our case).

Fig. 2 shows the SEM image of the elongated crystals obtained after the incubation of NMTD in artificial saliva solution for 24 hours and the EDX results of one crystal and the fluorapatite reference powder.

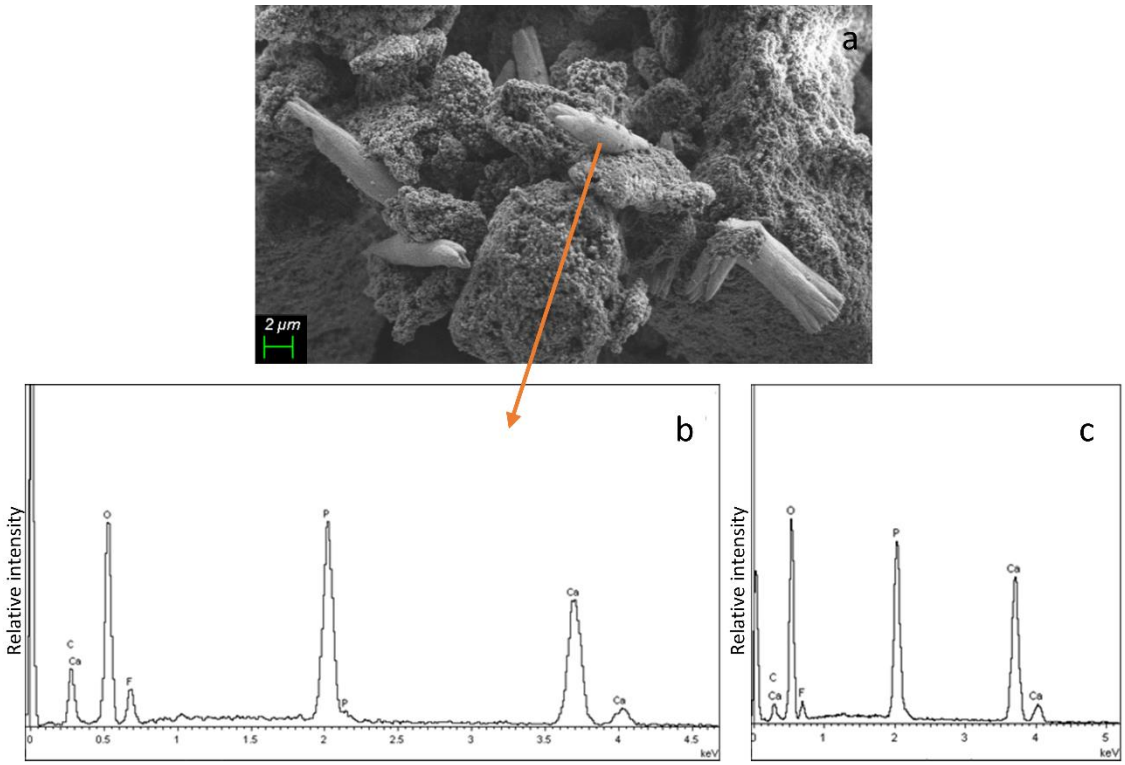

Fig. 2 SEM image of the crystals obtained after the incubation of NMTD in artificial saliva solution during 24 hours with 5000X magnification (a), EDX spectrum of one of the crystals (b), EDX spectrum of the fluorapatite reference powder (c).

3.2. *In vitro* experiment

3.2.1. SEM-EDX measurements

Teeth were lengthwise cut and the remineralized layer thickness after each treatment time was measured using ImageJ software. Fig. 3 shows that the layer grows gradually until day 15, when it reaches a plateau around 23±1 µm.

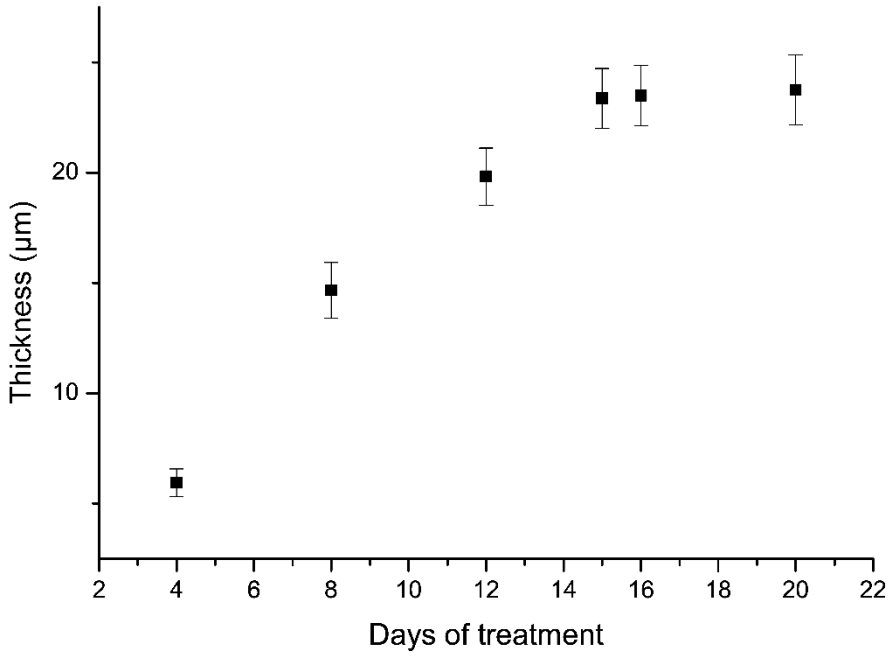

Fig. 3 Evolution of the remineralized layer thickness with the time of NMTD treatment.

In order to study the formed layer bonding strength to the enamel surface, teeth were brushed continuously for 15 minutes after 15 days of treatment. Fig. 4 represents a longitudinal section of a tooth showing the remineralized layer after brushing.

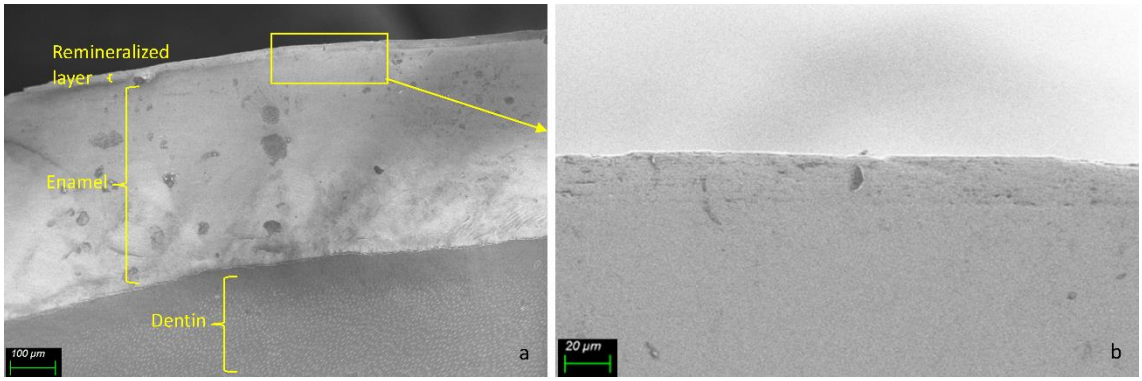

Fig. 4 Longitudinal section SEM images of a sample treated with NMTD for 15 days and brushed for 15 minutes with 250X magnification (a) and 1000X magnification of the square area (b).

The difference between the treatment in presence and absence of amelogenin was studied. In Fig. 5 it can be appreciated that the crystals are bigger in presence of amelogenin. The diameter of the crystals for the 4-day treatment is 0.11±0.02 µm for NMTD and 0.14±0.02 µm for NMTD in presence of amelogenin. In the case of the 15-day treatment, the diameter of the crystals is 0.13±0.02 µm for the treatment without protein and 0.17±0.03 µm with amelogenin. The 15-day treatment with protein shows significant differences in crystal size versus NMTD alone, according to the one-way ANOVA (analysis of variance) test performed with GraphPad Prism 9.

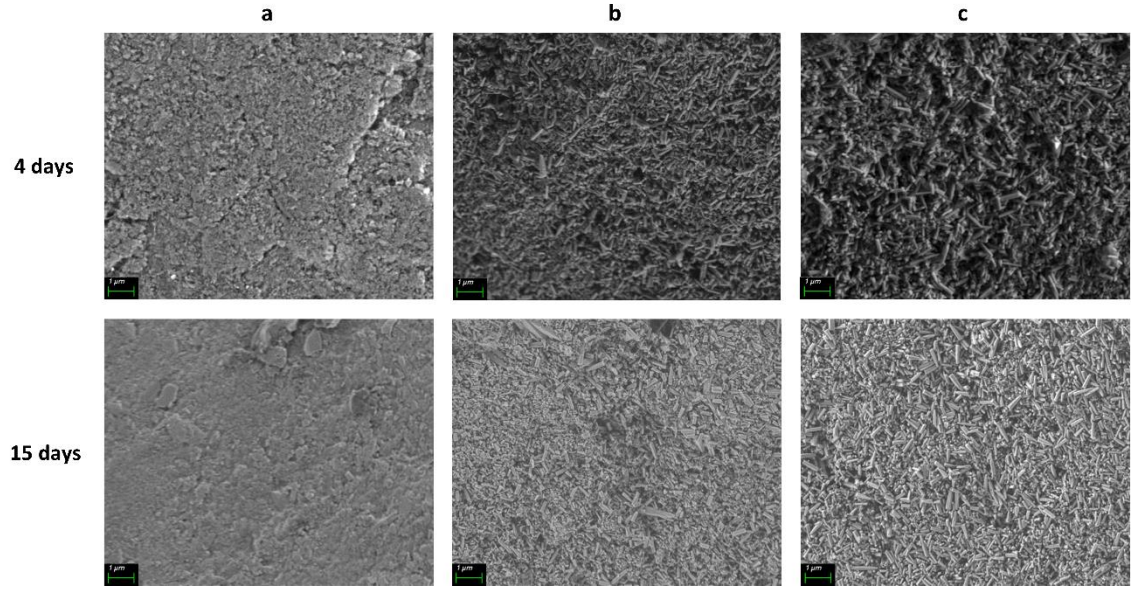

Fig. 5 SEM images at 20000X magnification level of the tooth surface after 4 and 15 days of treatment: blank (a), NMTD (b), NMTD and amelogenin (c).

To study the composition of the remineralized layer, an EDX study was performed by measuring blank and treated samples after 4 and 15 days of treatment and comparing them to the references of fluorapatite and hydroxyapatite powder. EDX results are shown in Table 1.

Table 1 Surface EDX measurements of the different treatments at different times: blank sample after 4 days (BL4), NMTD treated sample after 4 days (NMTD4), NMTD and amelogenin treated sample after 4 days (AH4), blank sample after 15 days (BL15), NMTD treated sample after 15 days (NMTD15), NMTD and amelogenin treated sample after 15 days (AH15), fluorapatite powder reference (FA), hydroxyapatite powder reference (HA).

	BL4	*NMTD4*	*AH4*	*BL15*	*NMTD15*	*AH15*	*FA*	*HA*
Ca (Atomic %)	18±5	14±1	20.7±0.1	20±4	14.78±0.01	20.6±0.1	25±4	21±3
P (Atomic %)	15±3	10.5±0.5	14.68±0.08	19±2	10.9±0.1	14.53±0.04	14.3±0.8	14.7±0.9
O (Atomic %)	66±8	64.8±1.0	56.5±0.4	61±5	63.3±0.5	56.4±0.5	56±2	65±3
F (Atomic %)	0.3±0.1	10.8±0.5	8.1±0.2	0.1±0.1	11.0±0.4	8.5±0.4	4.9±0.7	0.00±0.01

To study the evolution of the formed layer across its outer part to the enamel, different EDX measurements were taken in longitudinally cut samples of 15 days through the formed layer until the enamel. Fig. 6 shows the variations of each element when moving across the new layer to the natural enamel.

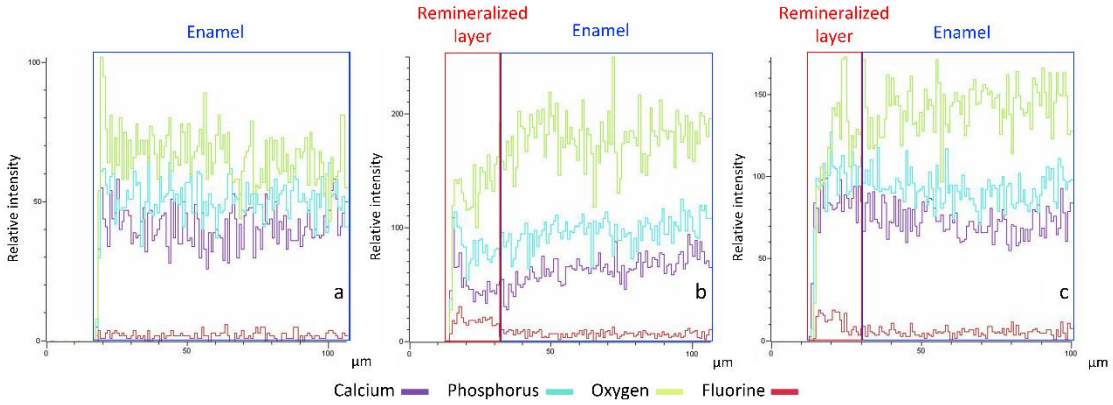

Fig. 6 Longitudinal section SEM-EDX analysis of blank sample after 15 days (a), NMTD treated sample after 15 days (b), NMTD and amelogenin treated sample after 15 days (c).

3.2.2. Nanoindentation

To assess the hardness of both kinds of remineralized layer with respect to the enamel, CSM measurements were taken in the layer and the enamel of longitudinally cut samples, the measurements are shown in Fig. 7.

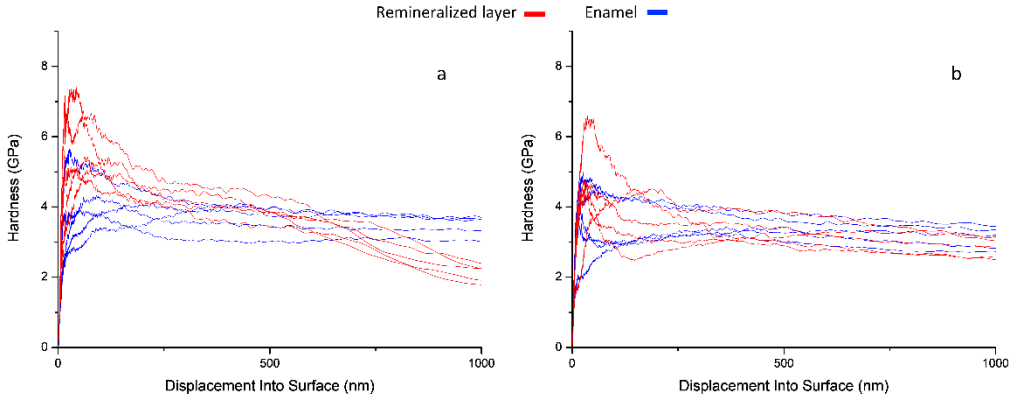

Fig. 7 Longitudinal section continuous stiffness measurements of a 15 days NMTD treated sample (a) and a 15 days NMTD and amelogenin treated sample (b).

4. Discussion

The results of the solution experiment confirm the expected formation of fluorapatite. It can be observed in Fig. 2 that the shape of the crystals formed with the NMTD in saliva solution after 24 hours resembles the first phase of the formation of fluorapatite spherulites

[65–68]. Moreover, the EDX spectrum of the crystals matches the fluorapatite reference spectrum.

The remineralization of the tooth samples has been successful, as it can be seen in Fig. 3, the thickness of the remineralized layer progressively increases until day 15, when it reaches its maximum at around 23±1 µm.

Fig. 4 shows the remineralized layer of the 15 days treatment to remain intact after brushing for 15 minutes, demonstrating that it is attached to the tooth surface strongly enough to resist the brushing of the daily hygiene.

The increase in crystal size with amelogenin for both treatment times (4 and 15 days) seen in Fig. 5 suggests amelogenin protein to accelerate the crystallization rate [69].

We can observe in Table 1 that the presence of amelogenin during the remineralization process produces a layer more similar in composition to pure fluorapatite, with more Ca and P but less O and F than the layer formed only with NMTD that also shows the formation of other minerals like calcium fluoride. This calcium fluoride is a precursor that will derive in fluorapatite in the presence of phosphate [2,70]. The composition of the blank samples treated with saliva alone is similar to that of hydroxyapatite as expected. The results obtained from the 4-day and 15-day treatments are similar, which means that extending the treatment time increases the thickness of the layer, as observed previously, but does not alter its composition.

In Fig. 6, comparing the remineralized layer (first 23 µm) to natural enamel (beneath this 23 µm), fluorine concentration is higher and the oxygen concentration is lower due to the expected production of fluorapatite in the layer (increase of fluoride content) replacing corresponding hydroxyapatite (decrease of the OH^- content). In the presence of amelogenin, calcium and phosphorus remain largely similar along the new layer to the original enamel since fluorapatite and hydroxyapatite contain the same amount of calcium and phosphorus, thus supporting our expected mineral formation. On the contrary and in absence of amelogenin, the observed decrease of oxygen, calcium and phosphorus in the formed layer against the original enamel may be interpreted by the formation of a considerable proportion of CaF_2 instead of just fluorapatite. In the blank samples, these changes are not observed due to the absence of the remineralized layer.

We can observe in Fig. 7 the remineralized layer without protein to be slightly harder than enamel during the first 500 nm although it loses hardness from there unlike enamel. However, in the presence of amelogenin, the hardness of the remineralized layer is maintained at values similar to the enamel. These results may be due to the role of amelogenin in guiding the morphology and alignment of crystals formation [22,43].

The development of technologies to rebuild tooth enamel and preserve tooth structure is of great interest due to the inability of the mature tooth enamel to regenerate itself after substantial mineral loss [1,2,25,40,47,71–73].

In conclusion, the NMTD product is effective and induces the remineralization after an acid attack creating a fluorapatite layer of around 23 µm after 15 days of treatment, overcoming the brushing process of the daily hygiene. The presence of amelogenin protein during the remineralization process improves the layer hardness and the crystal morphology, also accelerating the crystallization rate. Furthermore, amelogenin seems to induce the composition of the layer closer to that of pure fluorapatite. The novel product of NMTD with amelogenin induces complete remineralization with a hardness that reaches the levels observed in natural healthy enamel. Therefore, the novel product is promising to inhibit demineralization and provide long-term remineralization to inhibit caries and protect tooth structures. Nevertheless, further studies would be convenient to evaluate the clinical applicability of this biomimetic material.

Acknowledgements

The Spanish *Ministerio de Economía y Competitividad*, is acknowledged for the financial support provided (Project: CTM2015-65414-C2-1-R). Sandra Diez-García acknowledges the FI-2017 fellowship from *Agència de Gestió d'Ajuts Universitaris i de Recerca (Generalitat de Catalunya)*.

Funding

This work was supported by the *Agència de Gestió d'Ajuts Universitaris i de Recerca (Generalitat de Catalunya)* [grant number FI-2017]; and the Spanish *Ministerio de Economía y Competitividad* [grant number CTM2015- 65414-C2-1-R]. The funders had no role in study design, data collection and analysis, decision to publish, or preparation of the manuscript.

Compliance with ethical standards

Conflict of interest The authors declare that they have no conflicts of interest.

Ethical approval This article does not contain any studies with human participants or animals performed by any of the authors.

References

1. Hicks J, Catherine FG. Biological factors in dental caries: role of saliva and dental plaque in the dynamic process of demineralization and remineralization (part 1). J Clin Pediatr Dent. 2003;28:47–52.

2. Hicks J, Garcia-Godoy F, Flaitz C. Biological factors in dental caries: enamel structure and the caries process in the dynamic process of demineralization and remineralization (part 2). J Clin Pediatr Dent. 2004;28:119–24.

3. Hicks J, Catherine FG. Biological factors in dental caries: role of remineralization and fluoride in the dynamic process of demineralization and remineralization (part 3). J Clin Pediatr Dent. 2004;28:203–14.

4. Wang D, Deng J, Deng X, Fang C, Zhang X, Yang P. Controlling enamel remineralization by amyloid-like amelogenin mimics. Adv Mater. 2020;32:200208.

5. Featherstone JD. Prevention and reversal of dental caries: role of low level fluoride. Community Dent Oral Epidemiol. 1999;27:31–40.

6. Yoshihara K, Nagaoka N, Nakamura A, Hara T, Hayakawa S, Yoshida Y, *et al.* Three-dimensional observation and analysis of remineralization in dentinal caries lesions. Sci Rep. 2020;10:4387.

7. Carrouel F, Viennot S, Ottolenghi L, Gaillard C, Bourgeois D. Nanoparticles as anti-microbial, anti-inflammatory, and remineralizing agents in oral care cosmetics: A review of the current situation. Nanomaterials. 2020;10:140.

8. Sandomierski M, Buchwald Z, Koczorowski W, Voelkel A. Calcium forms of zeolites A and X as fillers in dental restorative materials with remineralizing potential. Microporous Mesoporous Mater. 2020;294:109899.

9. Bapat RA, Chaubal T V., Dharmadhikari S, Abdulla AM, Bapat P, Alexander A, *et al.* Recent advances of gold nanoparticles as biomaterial in dentistry. Int J Pharm. 2020;586:119596.

10. Owens TS, Dansereau RJ, Sakr A. Development and evaluation of extended release bioadhesive sodium fluoride tablets. Int J Pharm. 2005;288:109–22.

11. Xiao Z, Que K, Wang H, An R, Chen Z, Qiu Z, *et al.* Rapid biomimetic remineralization of the demineralized enamel surface using nano-particles of amorphous calcium phosphate guided by chimaeric peptides. Dent Mater. 2017;33:1217–28.

12. Bröseler F, Tietmann C, Bommer C, Drechsel T, Heinzel-Gutenbrunner M, Jepsen S. Randomised clinical trial investigating self-assembling peptide P11-4 in the treatment of early caries. Clin Oral Investig. 2020;24:123–32.

13. Örtengren U, Lehrkinder A, Safarloo A, Axelsson J, Lingström P. Opportunities for caries prevention using an ion-releasing coating material: a randomised clinical study. Odontology. 2021;109:358–67.

14. Cummins D. The development and validation of a new technology, based upon 1.5% arginine, an insoluble calcium compound and fluoride, for everyday use in the prevention and treatment of dental caries. J Dent. 2013;41:S1–11.

15. Fan M, Yang J, Xu HHK, Weir MD, Tao S, Yu Z, *et al.* Remineralization effectiveness of adhesive containing amorphous calcium phosphate nanoparticles on artificial initial enamel caries in a biofilm-challenged environment. Clin Oral Investig. 2021;25:5375–90.

16. Rodríguez-Martínez J, Valiente M, Sánchez-Martín M. Tooth whitening: From the established treatments to novel approaches to prevent side effects. J Esthet Restor Dent. 2019;31:431–40.

17. Marquillas CB, Procaccini R, Malmagro MV. Breaking the rules: tooth whitening by means of a reducing agent. Clin Oral Investig. 2019;24:2773–9.

18. Babot-Marquillas C, Sánchez-Martín MJ, Rodríguez-Martínez J, Estelrich J, Busquets MA, Valiente M. Flash tooth whitening: A friendly formulation based on a nanoencapsulated reductant. Colloids Surfaces B Biointerfaces. 2020;195:111241.

19. Kwon SR, Kurti SR, Oyoyo U, Li Y. Effect of various tooth whitening modalities on microhardness, surface roughness and surface morphology of the enamel. Odontology. 2015;103:274–9.

20. Olivan SRG, Sfalcin RA, Fernandes KPS, Ferrari RAM, Horliana ACRT, Motta LJ, *et al.* Preventive effect of remineralizing materials on dental erosion lesions by speckle technique: An *in vitro* analysis. Photodiagnosis Photodyn Ther. 2020;29:101655.

21. Perioli L, Nocchetti M, Giannelli P, Pagano C, Bastianini M. Hydrotalcite composites for an effective fluoride buccal administration: A new technological approach. Int J Pharm. 2013;454:259–68.

22. Carneiro KMM, Zhai H, Zhu L, Horst JA, Sitlin M, Nguyen M, *et al.* Amyloid-like ribbons of amelogenins in enamel mineralization. Sci Rep. 2016;6:23105.

23. Welborn VV. Enamel synthesis explained. Proc Natl Acad Sci U S A. 2020;117:21847–8.

24. Gil-Bona A, Bidlack FB. Tooth enamel and its dynamic protein matrix. Int J Mol Sci. 2020;21:4458.

25. Guentsch A, Fahmy MD, Wehrle C, Nietzsche S, Popp J, Watts DC, *et al.* Effect of biomimetic mineralization on enamel and dentin: A Raman and EDX analysis. Dent Mater. 2019;35:1300–7.

26. Simmer JP, Fincham AG. Molecular mechanisms of dental enamel formation. Crit Rev Oral Biol Med. 1995;6:84–108.

27. Taha AA, Fleming PS, Hill RG, Patel MP. Enamel remineralization with novel bioactive glass air abrasion. J Dent Res. 2018;97:1438–44.

28. Widyarman AS, Udawatte NS, Theodorea CF, Apriani A, Richi M, Astoeti TE, *et al.* Casein phosphopeptide-amorphous calcium phosphate fluoride treatment enriches the symbiotic dental plaque microbiome in children. J Dent. 2021;106:103582.

29. Tammaro L, Vittoria V, Calarco A, Petillo O, Riccitiello F, Peluso G. Effect of layered double hydroxide intercalated with fluoride ions on the physical, biological and release properties of a dental composite resin. J Dent. 2014;42:60–7.

30. Bijle MN, Abdalla MM, Ashraf U, Ekambaram M, Yiu CKY. Enamel remineralization potential of arginine-fluoride varnish in a multi-species bacterial pH-cycling model. J Dent. 2021;104:103528.

31. Hoxha A, Gillam DG, Agha A, Karpukhina N, Bushby AJ, Patel MP. Novel fluoride rechargeable dental composites containing MgAl and CaAl layered double hydroxide (LDH). Dent Mater. 2020;36:973–86.

32. Wei Su L, Lin DJ, Yen Uan J. Novel dental resin composites containing LiAl-F layered double hydroxide (LDH) filler: Fluoride release/recharge, mechanical properties, color change, and cytotoxicity. Dent Mater. 2019;35:663–72.

33. Reis DP, Filho JDN, Rossi AL, de Almeida Neves A, Portela MB, da Silva EM. Remineralizing potential of dental composites containing silanized silica-hydroxyapatite (Si-HAp) nanoporous particles charged with sodium fluoride (NaF). J Dent. 2019;90:103211.

34. Wierichs RJ, Zelck H, Doerfer CE, Appel P, Paris S, Esteves-Oliveira M, *et al.* Effects of dentifrices differing in fluoride compounds on artificial enamel caries lesions *in vitro*. Odontology. 2017;105:36–45.

35. Pendrys DG. Risk of fluorosis in a fluoridated population. Implications for the dentist and hygienist. J Am Dent Assoc. 1995;126:1617–24.

36. Valiente M. Remineralizing material for organomineral tissues. USA patent US 6,413,498 B1. 1999.

37. Imazato S, Kohno T, Tsuboi R, Thongthai P, Xu HHK, Kitagawa H. Cutting-edge filler technologies to release bio-active components for restorative and preventive dentistry. Dent Mater J. 2020;39:69–79.

38. Torrado A, Valiente M, Zhang W, Li Y, Muñoz CA. Remineralization potential of a new toothpaste formulation: An *in-vitro* study. J Contemp Dent Pract. 2004;5:18–30.

39. Torrado A, Valiente M. Kinetics characterization of ion release under dynamic and batch conditions. I. Weak acid and weak base ion exchange resins. J Solution Chem. 2008;37:581–94.

40. Li L, Mao C, Wang J, Xu X, Pan H, Deng Y, *et al.* Bio-inspired enamel repair via glu-directed assembly of apatite nanoparticles: An approach to biomaterials with optimal characteristics. Adv Mater. 2011;23:4695–701.

41. Jágr M, Ergang P, Pataridis S, Kolrosová M, Bartoš M, Mikšík I. Proteomic analysis of dentin–enamel junction and adjacent protein-containing enamel matrix layer of healthy human molar teeth. Eur J Oral Sci. 2019;127:112–21.

42. Alkilzy M, Tarabaih A, Santamaria RM, Splieth CH. Self-assembling peptide P11-4 and fluoride for regenerating enamel. J Dent Res. 2018;97:148–54.

43. Bai Y, Yu Z, Ackerman L, Zhang Y, Bonde J, Li W, *et al.* Protein nanoribbons template enamel mineralization. Proc Natl Acad Sci U S A. 2020;117:19201–8.

44. Sharma V, Srinivasan A, Roychoudhury A, Rani K, Tyagi M, Dev K, *et al.* Characterization of protein extracts from different types of human teeth and insight in biomineralization. Sci Rep. 2019;9:9314.

45. Cao Y, Liu W, Ning T, Mei ML, Li QL, Lo ECM, *et al.* A novel oligopeptide simulating dentine matrix protein 1 for biomimetic mineralization of dentine. Clin Oral Investig. 2014;18:873–81.

46. Fan M, Zhang M, Xu HHK, Tao S, Yu Z, Yang J, *et al.* Remineralization effectiveness of the PAMAM dendrimer with different terminal groups on artificial initial enamel caries *in vitro*. Dent Mater. 2020;36:210–20.

47. Gibson CW. The amelogenin proteins and enamel development in humans and mice. J Oral Biosci. 2011;53:248–56.

48. Li D, Lv X, Tu H, Zhou X, Yu H, Zhang L. Remineralization of initial enamel caries *in vitro* using a novel peptide based on amelogenin. Front Mater Sci. 2015;9:293–302.

49. Fan YW, Sun Z, Wang R, Abbott C, Moradian-Oldak J. Enamel inspired nanocomposite fabrication through amelogenin supramolecular assembly. Biomaterials. 2007;28:3034–42.

50. Fan Y, Sun Z, Moradian-Oldak J. Controlled remineralization of enamel in the presence of amelogenin and fluoride. Biomaterials. 2009;30:478–83.

51. Fan Y, Nelson JR, Alvarez JR, Hagan J, Berrier A, Xu X. Amelogenin-assisted *ex vivo* remineralization of human enamel: Effects of supersaturation degree and fluoride concentration. Acta Biomater. 2011;7:2293–302.

52. Fan Y, Wen ZT, Liao S, Lallier T, Hagan JL, Twomley JT, *et al.* Novel amelogenin-releasing hydrogel for remineralization of enamel artificial caries. J Bioact Compat Polym. 2012;27:585–603.

53. Kwak SY, Litman A, Margolis HC, Yamakoshi Y, Simmer JP. Biomimetic enamel regeneration mediated by leucine-rich amelogenin peptide. J Dent Res. 2017;96:524–30.

54. Iijima M, Moradian-Oldak J. Control of apatite crystal growth in a fluoride containing amelogenin-rich matrix. Biomaterials. 2005;26:1595–603.

55. Wei M, Evans JH, Bostrom T, Grondahl L. Synthesis and characterization of hydroxyapatite, fluoride-substituted hydroxyapatite and fluorapatite. J Mater Sci Mater Med. 2003;14:311–20.

56. Svensson Bonde J, Bulow L. One-step purification of recombinant human amelogenin and use of amelogenin as a fusion partner. PLoS One. 2012;7:e33269.

57. Posada MC, Sánches CF, Gallego GJ, Vargas AP, Restrepo LF, López JD. Dientes de bovino como sustituto de dientes humanos para su uso en la odontología. Revisión de literatura. CES odontol. 2006;19:63–8.

58. Groenhuis RAJ, Jongebloed WL, ten Bosch JJ. Surface roughness of acid-etched and demineralized bovine enamel measured by a laser speckle method. Caries Res. 1980;14:333–40.

59. Braly A, Darnell LA, Mann AB, Teaford MF, Weihs TP. The effect of prism orientation on the indentation testing of human molar enamel. Arch Oral Biol. 2007;52:856–60.

60. Xu HHK, Smith DT, Jahanmir S, Romberg E, Kelly JR, Thompson VP, *et al.* Indentation damage and mechanical properties of human enamel and dentin. J Dent Res. 1998;77:472–80.

61. Ma Y, Cohen SR, Addadi L, Weiner S. Sea urchin tooth design: An “all-calcite” polycrystalline reinforced fiber composite for grinding rocks. Adv Mater. 2008;20:1555–9.

62. Puigdomenech I. Program MEDUSA (Make equilibrium diagrams using sophisticated algorithms). R. Inst. Technol. Inorg. Chem. 2010. p. 10644.

63. Abràmoff MD, Magalhães PJ, Ram SJ. Image processing with ImageJ. Biophotonics Int. 2004;11:36–41.

64. Collins T. ImageJ for microscopy. Biotechniques. 2007;43:25–30.

65. Wu YJ, Tseng YH, Chan JCC. Morphology control of fluorapatite crystallites by citrate ions. Cryst Growth Des. 2010;10:4240–2.

66. Simon P, Schwarz U, Kniep R. Hierarchical architecture and real structure in a biomimetic nano-composite of fluorapatite with gelatine: a model system for steps in dentino- and osteogenesis? J Mater Chem. 2005;15:4992–6.

67. Busch S, Schwarz U, Kniep R. Morphogenesis and structure of human teeth in relation to biomimetically grown fluorapatite-gelatine composites. Chem Mater. 2001;13:3260–71.

68. Busch S, Dolhaine H, DuChesne A, Heinz S, Hochrein O, Laeri F, *et al.* Biomimetic morphogenesis of fluorapatite-gelatin composites: Fractal growth, the question of intrinsic electric fields, core/shell assemblies, hollow spheres and reorganization of denatured collagen. Eur J Inorg Chem. 1999;1999:1643–53.

69. Habelitz S, Kullar A, Marshall SJ, DenBesten PK, Balooch M, Marshall GW, *et al.* Amelogenin-guided crystal growth on fluoroapatite glass-ceramics. J Dent Res. 2004;83:698–702.

70. Jardim JJ, Pagot MA, Maltz M. Artificial enamel dental caries treated with different topical fluoride regimes: An *in situ* study. J Dent. 2008;36:396–401.

71. Ruan Q, Moradian-Oldak J. Amelogenin and enamel biomimetics. J Mater Chem B. 2015;3:3112–29.

72. Yao S, Jin B, Liu Z, Shao C, Zhao R, Wang X, *et al.* Biomineralization: From material tactics to biological strategy. Adv Mater. 2017;29:1605903.

73. Wei Y, Liu S, Xiao Z, Zhao H, Luo J, Deng X, *et al.* Enamel repair with amorphous ceramics. Adv Mater. 2020;32:1907067.

ANNEX II. Pending paper: A combination of two synchrotron radiation-based techniques and chemometrics to study an enhanced natural remineralization of enamel.

Sandra Diez-García[1(¥)], María-Jesús Sánchez-Martín[1*(¥)], José Manuel Amigo[2] and Manuel Valiente[1]

[1] GTS Research Group, Department of Chemistry, Faculty of Science, Universitat Autònoma de Barcelona, 08193 Bellaterra, Spain

[2] Chemical and Environmental Engineering Department, School of Engineering, University of the Basque Country, Alameda de Urquijo s/n, E-48013 Bilbao, Spain

[(¥)] Shared co-first authorship

[*] Author for correspondence e-mail address: mariajesus.sanchez@uab.cat

ABSTRACT

The limitations to assess dental enamel remineralization have been overcome by a methodology resulting from the appropriate combination of synchrotron radiation-based techniques on both, infrared microspectroscopy and micro X-ray diffraction, with the help of specific data mining. Since amelogenin plays a key role in modulating the mineralization of tooth enamel, we propose a controlled ion release for fluorapatite structural ions (Ca^{2+}, PO_4^{3-} and F^-, also including Zn^{2+}) by using weak acid and weak base ion-exchange resins in presence of amelogenin to remineralize the surface of etched teeth. This combination provides the necessary ions for enamel remineralization and a guide for crystal growth due to the protein. Remineralized tooth samples were analyzed by applying the indicated methodology. The synchrotron data were treated using principal component analysis and multivariate curve resolution to analyze the mineral layer formed in the presence and absence of amelogenin. The remineralizing treatment created a fluorapatite layer free of carbonate impurities and with a similar orientation to that of the natural enamel thanks to amelogenin contribution.

TABLE OF CONTENTS

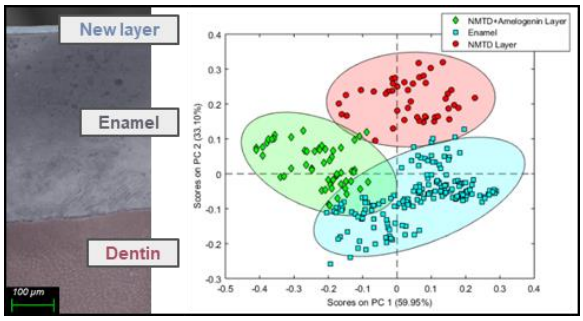

1. INTRODUCTION

Teeth have a layered structure composed of dental enamel that covers the dentin containing the tooth pulp. Tooth enamel is the most mineralized and hardest tissue in the human body. The enamel is constituted by multiple rod-like apatite crystals, which are arranged in ordered prisms.[1,2] Mineral composition of mature enamel is a mixture of compounds, primarily hydroxyapatite (HA), which is crystalline calcium phosphate ($Ca_{10}(PO_4)_6(OH)_2$) that has a hexagonal crystal system with the $P6_3/m$ space group.[3,4] This enamel HA is not stable and suffers changes due to chemical interactions. The major change is produced when phosphate is substituted by carbonate because this substitution increases the solubility of the enamel. However, if the hydroxyl ions of HA are replaced by fluoride ions, fluorapatite (FA), a more acid-resistant compound, is generated.[5] As the fluoride ion is smaller than the hydroxyl ion, the triangle formed by the three coordinating calcium ions shrinks, resulting in a symmetry-conserving contraction of the unit cell in the a,b-plane with no change in the c-axis dimension (long axis of apatite crystal). This reduction in the volume of about 1% is responsible for the greater mechanical strength of FA compared to HA and the enhanced chemical stability by the electrostatic bond between fluoride and the adjacent ions.[6–9]

In vitro models are established methods in dental research as a powerful instrument to evaluate the anticaries efficiency of remineralizing agents. Several techniques have been used to assess tooth remineralization, such as scanning electron microscopy, atomic force microscopy or indentation. However, these techniques have certain limitations regarding the analysis of the composition of enamel remineralization and crystal orientation.[10,11] Therefore, synchrotron radiation-based infrared microspectroscopy and microdiffraction were used for this study to overcome these constraints.

Fourier transformed infrared (FTIR) spectroscopy is a well-recognized molecular vibrational technique that has been widely used to investigate the chemical structural properties of natural materials.[12,13] It has been extensively used for mapping the material properties of mineralized tissues such as dental enamel, including mineralization, crystallinity or carbonate substitution.[14] The incorporation of a microscope in FTIR microspectroscopy (μFTIR) has introduced the possibility of combining biochemical and spatial information. Coupling this technique to a synchrotron radiation light source, synchrotron radiation-based FTIR microspectroscopy (SR-μFTIR), allows a much better signal-to-noise ratio and the use

of a smaller beam size without losing signal efficiency, since one of the most outstanding properties of a synchrotron radiation source is its high brightness compared with a traditional globar source.[15]

On the other hand, as apatites have a well-defined hexagonal crystal structure, diffraction methods can be used to analyze the crystal structure in teeth.[1] The crystallographic properties of enamel and fluoridated enamel have been investigated using X-ray diffraction (XRD). Incorporating fluoride into the enamel structure may lead to crystallographic changes in enamel (contraction of a,b-axis, increase in apatite crystal size and reduction of crystal defects). Nevertheless, enamel crystallinity varies at different layers. If the enamel is ground into powder mixing them, it may affect the accuracy of the measurement.[16] The micro X-ray diffraction (μXRD) analysis overcomes the limitations of conventional powder XRD and can obtain site-specific data directly from the tooth allowing the study of the enamel crystallinity at different levels.[17] The synchrotron through-the-substrate micro X-ray diffraction (tts-μXRD) used in the present work allows performing punctual analysis in thin sections with a spot size of few micrometers. Therefore, this technique enables data collection directly on thin tooth sections preserving the textural context and allowing local identification of mineral phases.[18]

There are several factors that put oral health at risk, such as the popularity of whitening systems with their side effects or the excessive consumption of acidic foods and beverages.[19–22] Demineralization caused by regular exposure of the tooth enamel to acids, such as those produced within accumulations of bacterial plaque from dietary carbohydrates, removes mineral ions from HA crystals and may cause a caries lesion. Dental caries is a dynamic process, but if left unchecked, enamel demineralization can progress from a stage of an early reversible lesion to an irreversible collapse of the enamel surface, with the development of a dental cavity. Demineralization in early caries lesion can be reversed by calcium and phosphate in saliva.[23–26] However, mature tooth enamel is acellular and does not regenerate itself after substantial loss.[27,28] Mechanical properties of the macroscopic enamel tissue are highly dependent on the alignment and orientation of HA crystals. Tooth surfaces formed by dental enamel are required to have a high resistance to abrasion and corrosion. Therefore, changes in surface structure as a result of caries or microscopic damage can cause significant impairment of the dental function and, ultimately, tooth loss.[1] More than 12 million dental implants are needed annually worldwide as part of routine oral rehabilitation.[29]

Fluoride is the most popular agent for enhancing remineralization. Besides the antibacterial properties at low concentrations, fluoride stops the demineralization and favours the opposite process of remineralization on the tooth surface.[24] During remineralization processes, fluoride ions promote the formation of FA in the presence of calcium and phosphate ions. At higher concentrations, it creates a calcium fluoride layer that acts as a reservoir source for fluoride and protects the enamel from the formation of caries.[30] When early enamel lesions are fluoride-enhanced, the fluoride provides remineralization and acid resistance to enamel. The presence of fluoride in saliva has been associated with increased remineralization rates and decreased caries incidence. Therefore, fluoride is added to toothpastes, mouthwashes and drinking water as an anticaries agent.[24] Despite its benefits, high concentrations of fluoride can cause undesirable side effects and unfortunately, in many dental products, fluoride ions are released too rapidly, producing high concentrations in a brief period due to the short oral application time.[31,32]

This research employs an innovative approach against dental demineralization to avoid the side effects of high fluoride concentrations in the oral environment and extend the contact time between the fluoride ions and the tooth surface, enabling successful remineralization. The product called NMTD[33] (new dental treatment material or *Nuevo Material de Tratamiento Dental* in Spanish) provides a controlled release system for the anticaries treatment and it is composed of a combination of weak acid and weak base ion-exchange resins loaded with calcium, fluoride, phosphate and zinc. This agent allows the formation of FA by controlling the rate of fluoride release into the oral environment, in conjunction with the release of calcium and phosphate ions to induce remineralization. Thus, the remineralized layer made of FA shows lower mineral solubility, higher mechanical strength and greater resistance to caries diseases than enamel HA. The molar ratio of the calcium, fluoride and phosphate ions has to be close to that of the organomineral tissue to be remineralized. Zinc ions act as initiators of the ionic release of the structural ions. In addition, zinc incorporation into enamel may accelerate its remineralization and reduce the rate of enamel demineralization, zinc also has antibacterial and malodor control properties.[25,34] Ion-exchange materials have the advantage of releasing ions only due to the ion-exchange mechanism and therefore do not introduce undesirable ions into the solution. These resins are mostly non-toxic and used in medical applications, the pharmaceutical industry, and even in the food industry.[35] An NMTD containing toothpaste has

demonstrated efficacy in limiting enamel demineralization and enhancing remineralization *in vitro*.[36]

Furthermore, enamel matrix proteins play a vital part during the development of enamel in the regulation of mineralization and crystal organization. Then, the protein matrix is proteolytically degraded during the enamel maturation stage. Amelogenin constitutes more than 90% of the organic matrix, being the most abundant protein in the forming enamel. The importance of the amelogenin protein is well known because amelogenin self-assembly controls the morphology, size and orientation of the growing crystals.[27] For this reason, amelogenin in conjunction with NMTD is used in this research to achieve a remineralization similar to that of natural enamel.

Principal component analysis (PCA) and multivariate curve resolution (MCR) were used to study the obtained data deeply. PCA is, arguably, the most frequently employed chemometric method. PCA is a variable reduction tool, which makes it possible to identify trends and patterns more easily.[37] MCR was also used to analyze the differences of the mineral formed in the presence and absence of amelogenin. MCR is a widespread and powerful methodology for data analysis that maximizes the explained variance in the data, as PCA would, but imposing component profiles to follow significant physical or chemical constraints, instead of mathematical or statistical restrictions as for PCA.[38]

This study aims to evaluate the efficiency of the remineralization after the treatment with NMTD and amelogenin; and to determine the protein influence on the morphological changes of the remineralized enamel. Synchrotron infrared microspectroscopy and microdiffraction, joined with the proper chemometric method, allow us to study the evolution of the structure of apatites and their distribution after the remineralization process. Thus, we could achieve the spatial resolution required to determine the changes in the remineralization as a function of the depth thanks to the enhanced signal-to-noise ratio provided by the synchrotron source.

2. EXPERIMENTAL SECTION

2.1. Reagents

HEPES [4-(2-hydroxyethyl)-1-piperazine-ethanesulfonic acid] (99.5%), magnesium chloride hexahydrate (99%), calcium fluoride (95%) and chloramine T trihydrate (98-103%) were purchased from Sigma Aldrich (Steinheim, Germany); potassium dihydrogen phosphate

(99.5%), calcium chloride dihydrate (74-78%) and tricalcium phosphate (35-40% (Ca)) from Panreac (Barcelona, Spain); potassium chloride (99-100.5%) from J. T. Baker (Deventer, Holland), all in powder form. Potassium hydroxide pellets (85%) and hydrochloric acid (37%) were purchased from Panreac (Barcelona, Spain). Deionized water was purified using a Millipore purification system (Millipore, Milford, MA, USA). The hydroxyapatite reference powder was of analytical grade and was used as received without further purification (>90%, Fluka, Sigma-Aldrich, Steinheim, Germany).

Food grade ion-exchange resins charged with different ions (Zn^{2+}, Ca^{2+}, F^- and PO_4^{3-}) were purchased from MionTec (Leverkusen, Germany). The base of the weak acid ion-exchange resins is a copolymer from acrylic acid, divinylbenzene and aliphatic diene with carboxylic acid functional groups (Lewatit S 8528, Lanxess, Leverkusen, Germany). While the base of the weak base ion-exchange resins is a styrene-divinylbenzene-copolymer with tertiary amine functional groups (Lewatit S 4528, Lanxess, Leverkusen, Germany). The different resins, ground to a particle size below 50 μm, were mixed to form the NMTD product, with a molar ratio between Ca^{2+}, F^- and PO_4^{3-} of 2:1:1, respectively. In addition, resin charged with Zn^{2+} ions is added, representing 0.2% of the dry weight of the resulting product.

2.2. Fluorapatite Reference Synthesis

The fluorapatite sample was synthetized by a solid phase reaction[3] mixing calcium fluoride (95%) and tricalcium phosphate (35-40% (Ca)) in the agate miller at the ratio of 1.67 Ca/P. Afterwards, the reagents were placed in the muffle furnace Selecta 366 PE (Selecta, Barcelona, Spain) to heat them at 1200 ºC for 2 hours. The solid fluorapatite was then ground to powder for 15 minutes.

2.3. Amelogenin Protein Synthesis

A human 175 amino acid amelogenin (Swissprot Q99217, isoform 1, excluding the signal peptide) was expressed in *Escherichia coli* strain BL21 (DE3) and purified by an acid/heat treatment as described previously Svensson Bonde and Bulow[39]. Proteins were analyzed by matrix-assisted laser desorption/ionization, sodium dodecyl sulfate polyacrylamide gel electrophoresis and western blot to confirm the amelogenin production. Finally, recombinant amelogenin was quantified with a nanodrop.

Protein purification has been performed by the ICTS “NANBIOSIS”, more specifically by the Protein Production Platform of CIBER in Bioengineering, Biomaterials & Nanomedicine

(CIBER-BBN)/ IBB, at the UAB SePBioEs scientific-technical service (http://www.nanbiosis.es/portfolio/u1-protein-production-platform-ppp/).

2.4. *In Vitro* Dental Remineralization

Bovine teeth are used as a model, given their similarity to human teeth.[40,41] Bovine tooth specimens were cleaned of gross debris before removing the root with a diamond saw (South Bay Technology, San Clemente, CA, USA). The resulting tooth samples were embedded in a Paladur clear autopolymerizing acrylic resin (Heraeus Kulzer, Hanau, Germany), closing the root aperture and leaving the front surface exposed. The embedded teeth were then etched with hydrochloric acid 1 M for 30 seconds to mimic the early stage of dental erosion and immediately afterwards cleaned by rinsing with MilliQ water while brushing for 20 seconds with an electric toothbrush.

Artificial saliva was prepared by mixing the following compounds in the indicated concentrations: potassium chloride 0.24 g/l, calcium chloride dihydrate 0.078 g/l, potassium dihydrogen phosphate 0.544 g/l, magnesium chloride hexahydrate 0.041 g/l, HEPES 4.77 g/l. After complete dissolution of the saliva components, the pH was adjusted to 7.1±0.4 with potassium hydroxide pellets.

In order to perform the remineralizing treatments artificial saliva was added to NMTD until the consistency of dense gel was reached for its application to the teeth. In the case of the treatment with NMTD and amelogenin, 100 µg/ml of human amelogenin was added to the saliva before mixing with NMTD. In both cases the mixture of NMTD with the corresponding saliva (with or without amelogenin) was distributed on the enamel surface of acid-etched teeth, and then the samples were placed in a sealed vessel. The base of this container was filled with saliva to maintain the humidity of the environment and the recipient was placed inside an incubator at the normal temperature of the oral cavity (37 ºC). Every 24 hours for 15 days, each treatment was renewed by washing the samples carefully with MilliQ water and brushing for 20 seconds before applying a fresh treatment portion.

Finally, all teeth were cleaned by brushing with MilliQ water for 20 seconds and stored in a 0.5% chloramine T solution until the preparatation for the synchrotron experiments.

2.5. Specular Reflectance SR-µFTIR Experiment

2.5.1. Sample Preparation

Two samples of each treatment were completely embedded in the same Paladur acrylic resin and longitudinally cut in two halves with a Struers Minitom precision diamond saw (Copenhagen, Denmark) to obtain a mesial view from the inside. A sequence of silicon carbide paper was used to polish the exposed tooth area with a Struers LaboPol-25 polishing machine (Copenhagen, Denmark), starting at grit size P2500 and increasing to P4000, under a constant flow of tap water. A sequence of diamond suspensions with a mean particle size of 3 and 1 µm was used to finish the polishing and obtain the appropriate reflection properties for the measurements. A sample image can be observed in the **Supporting Information Figure S1a**.

2.5.2. Data Acquisition

µFTIR coupled to synchrotron radiation (SR-µFTIR) experiment in reflectance mode was carried out at MIRAS beamline of ALBA Synchrotron (Cerdanyola del Vallès, Spain)[42]. Specular reflectance spectra of the tooth samples were acquired using a Hyperion 3000 microscope coupled to a Vertex 70 spectrometer (Bruker, Ettlingen, Germany) and equipped with a Mercury-Cadmium-Telluride (MCT) detector. The microscope uses a 36x Schwarzschild objective (NA=0.52) coupled to a 36x Schwarzschild condenser to focus the synchrotron IR light on the sample. Spectra were collected with OPUS 7.5 software (Bruker, Ettlingen, Germany) in the 700-4000 cm^{-1} range, at a spectral resolution of 4 cm^{-1}, with a masking aperture size of 6x6 μm^2, taking 256 co-added scans per spectrum to achieve a good signal-to-noise ratio and using and a step size of 5x5 μm^2. A gold mirror was used as the reference to collect the background.

2.5.3. Data Treatment

OriginLab software (OriginLab, Northampton, MA, USA) was employed to assign peak spectra numbers and perform maximum normalizations when comparing spectra. PCA was performed on these data on the mean centered spectra using PLS_Toolbox (Eigenvector Research, Wenatchee, WA, USA) working under MATLAB (The MathWorks, Natick, MA, USA).

2.6. Synchrotron tts-µXRD Experiment

2.6.1. Sample Preparation

A couple of samples of each treatment were released from the Paladur acrylic resin and embedded in Epofix resin (Struers, Copenhagen, Denmark). The tooth samples were longitudinally cut in half, fixed on a glass substrate of 1.5 mm thickness and polished to reduce the sample thickness down to 30 µm and achieve a flat surface. A tooth thin section image can be seen in the **Supporting Information Figure S1b**.

2.6.2. Data Acquisition

Synchrotron tts-µXRD measurements were performed at the Materials Science and Powder Diffraction (MSPD) beamline of ALBA Synchrotron (Cerdanyola del Vallès, Spain)[43]. The MSPD beamline is equipped with Kirkpatrick-Baez mirrors, providing a monochromatic focused beam of 15x15 μm^2 size at full width at half maximum and with a Rayonix SX165 CCD detector (round active area of 165 mm diameter, frame size 2048x2048 pixels, 79 mm pixel size and dynamic range 16 bit). The tooth sections were measured in transmission mode through the glass substrate.[44] The energy employed was 29.2 keV (λ=0.4246 Å), as determined from the Sn absorption K-edge. Instrumental calibration was carried out with a LaB_6 standard (NIST SRM 660b). The final data consisted of a two dimensions (2D) diffraction pattern in a series of points from outside to inside the tooth in lines separated by 200 µm. Reference compounds (hydroxyapatite and fluorapatite) were measured using a Kapton polyimide film as support material.

2.6.3. Data Treatment

The diffraction data of the samples were processed with the programs d1Dplot and d2Dplot[45], including the azimuthal plots, which consist of the evolution of pixel intensity along an ellipse specified by the Bragg angle 2θ and a given tolerance. This intensity was integrated over 360º in a narrow band containing the reflection with Miller indices (002) and then plotted versus the azimuthal angle Φ. The azimuthal plots of the reflection (002) were selected for this analysis since this reflection is normal to the c-axis of enamel crystallites.[46,47] MCR was performed using the same toolbox as before to study the evolution of the different orientations along the azimuthal plots of the reflection (002) collected from each line measured from the surface to the inside of the samples and with baseline

correction. OriginLab was used to perform baseline correction and maximum normalization to the diffractograms when observing peak shifts.

3. RESULTS AND DISCUSSION

3.1. Specular Reflectance SR-µFTIR

After 15 days of the remineralizing treatments, teeth had a new mineral layer between 20 and 30 µm of thickness measurable with the microscope of MIRAS beamline. Measurements were taken on a frame including points of the enamel and of this new layer to study the similarities and differences of the crystals of the newly formed layers for the different treatments (NMTD with amelogenin or NMTD alone) with the underlying enamel.

Infrared spectroscopy of apatites generally provides two different kinds of information. The crystalline quality is evaluated from the width of the absorption bands due to the phosphate vibrational modes. The other type of information is based on the presence of molecular species, like carbonate groups, which are detected by specific vibrational bands.[48] Bands corresponding to carbonates and phosphates in the enamel HA are identified in **Figure 1a**. The bands associated with the v_3PO_4 vibrations (antisymmetric stretching) are observed between 1170 and 965 cm^{-1}.[49,50] In the literature, the deconvolution of the v_3PO_4 bands in stoichiometric apatite is described as secondary phase vibrations of Ca-O-P at 1103 cm^{-1}, P-O at 1091 cm^{-1}, Ca-O at 1047 cm^{-1} and O-Ca-O at 1031 cm^{-1}.[51] The weak v_1PO_4 band (symmetric stretching) is present at 966 cm^{-1}.[48] The region between 1580-1320 cm^{-1} corresponds to v_3CO_3 antisymmetric stretching, where two maximums at 1442 and 1401 cm^{-1} can be appreciated.[12] An additional small band related to structural carbonates (v_2CO_3 symmetric angular deformation) is present at 867 cm^{-1}.[12,48,50] Carbonate can substitute into two anionic sites of the HA structure. In carbonated apatite type B, which is the predominant type in biological apatite, it is located at phosphate group sites, while in carbonated apatite type A, it is found at hydroxyl group sites.[52] According to the peak deconvolution from the literature, the v_3CO_3 vibration in carbonated apatite type A splits into two peaks at 1530 cm^{-1} and 1465 cm^{-1}. In contrast, type B can be characterized by peaks at 1456 and 1423 cm^{-1} in the IR spectrum.[52,53] In the case of the v_2CO_3 out-of-plane bending mode, a peak at 879 cm^{-1} is reported to belong to type A and another at 872 cm^{-1} to type B.[52,54] The combined presence of A and B carbonates affects the carbonate peak positions compared to apatite with only A or only B type.[52] Meaning that the carbonate peaks detected in the regions 1580-

1320 cm^{-1} and 880-830 cm^{-1} of the enamel in reflection mode show a mixture of type A and B carbonates.

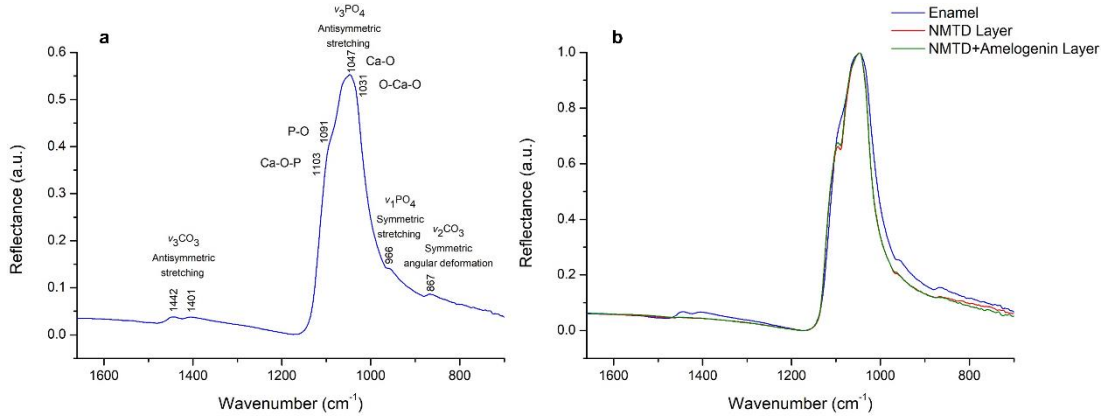

Figure 1. (a) Average of the specular reflectance FTIR spectra of enamel and band assignment numbers (n=11). (b) Average of spectra corresponding to enamel, NMTD layer with amelogenin and NMTD layer without amelogenin normalized to maximum (n=11).

Both types of layers (**Figure 1b**) present the characteristic peak of apatites due to the phosphate group near 1050 cm^{-1}, indicating a high crystallinity.[55] In both layers, there is an absence of the two small peaks near 1400 cm^{-1} and the small peak at 867 cm^{-1} that are present in the enamel due to the carbonate group.[56] The lack of the carbonate substitution group with high solubility and the narrowing of the phosphate peak in both layers indicate conversion to a more highly crystalline apatite compared to enamel. In addition, the layers appear to have a more evident vibration at 1103 cm^{-1} than the enamel, corresponding to the Ca-O-P secondary phase vibration. This could be due to a higher amount of calcium interacting with phosphate than in enamel since there are no carbonates in the layer, and therefore there is no calcium bound to carbonate as in enamel. Further evidence is included in the **Supporting Information Figure S2**.

In **Figure 2a**, the PCA of spectra corresponding to enamel and both layers shows that principal component 1 (PC 1) separates the two treatments (NMTD with and without amelogenin) from each other and principal component 2 (PC 2) separates the enamel from the treatments as it separates according to the depth of the measurement. PC 1 represents 59.95% of the variation, while PC 2 accounts for the 33.10%. In **Figure 2b**, the loadings for PC1 and PC2 show the main peaks in the regions 1580-1320 cm^{-1} and 1170 and 965 cm^{-1}, corresponding to the v_3CO_3 and the v_3PO_4 vibrations. Therefore, these vibrations are responsible for the scores separation in **Figure 2a**. The points in the PCA belonging to the layer with protein are statistically closer to the enamel points than those belonging to the

layer with NMTD alone, which may be due to the 1103 cm^{-1} shoulder being more pronounced in the NMTD layer (**Figure 1b**).

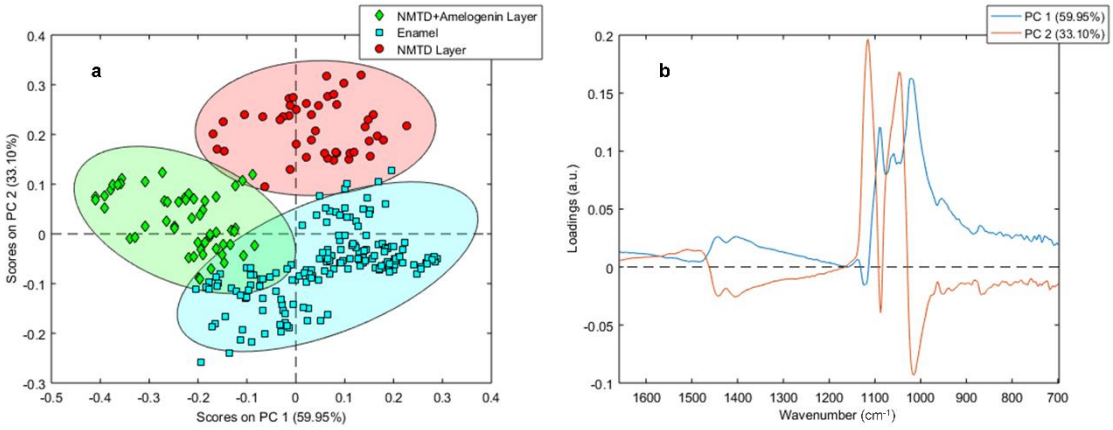

Figure 2. (a) PCA scores graph of the FTIR spectra from the enamel and layer of two samples with amelogenin and two samples without amelogenin. (b) PC 1 and PC 2 loadings of the PCA.

3.2. Synchrotron tts-µXRD

A typical diffraction pattern of HA was found inside the enamel, the main (*hkl*) Miller indices[4,57] (002), (211), (112), (300), (202), (222), (213) and (004) are indicated in **Figure 3**. A shift to a slightly higher angle was observed in the (211), (112) and (300) reflections of the external layer and the FA reference, compared to the enamel and the HA reference, as expected from the slight reduction in a,b-axis dimension when F^- ions replaces OH^- ions.[58,59] This shift confirmed the substitution of fluoride ions into the apatite lattice, therefore the remineralized layer formed is composed of FA, more resistant than enamel HA.

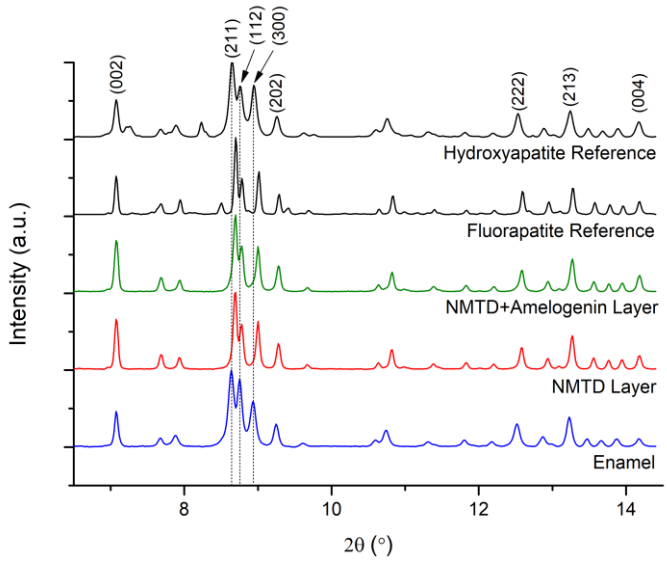

Figure 3. Diffractograms obtained by synchrotron tts-µXRD for HA reference, FA reference, enamel, NMTD layer with amelogenin and NMTD layer without amelogenin, normalized to maximum and showing reflections.

Synchrotron tts-µXRD was also used to investigate the texture (or preferred orientation) of enamel crystallites in the tooth sections. The preferred orientation refers to the degree of alignment of the crystallites. The intensities of different XRD peaks can be employed to estimate the macroscopic level-specific orientation of crystals. Sharp and intense (002) and (004) peaks in the apatite, as can be seen for the new layers in **Figure 3**, indicate that crystals prefer to be aligned along the c-crystallographic axis as in real enamel.[60,61] The lattice planes (002) and (004) along the c-axis of the enamel crystals are oriented perpendicular to the tooth surface, following the direction of the enamel prism arrangement.[1,62] Perpendicularity to the enamel surface maximizes the strength and bending capability and enhances the wear resistance capacity.[63]

A high degree of crystalline anisotropy, as in dental enamel, produces a change in the intensity around the Debye ring of Bragg reflections in two dimensions that correlates with the degree of crystallite alignment or ordering.[46] The intensity variations around the diffraction rings are indicative of tooth enamel texture.[62] Diffraction spots in **Figure 4 (a and b)** are concentrated in distinct arcs, both in the enamel and in the layers, which means that the crystals are ordered.[64] The strongest texture (the most extreme intensity variation) for both kinds of samples (NMTD treatment with or without amelogenin) was found in the reflection (002), as can be appreciated in **Figure 4 (a and b)**. The lattice plane reflection (002) does not overlap with other reflections and has the greatest intensity variation with maxima normal to the c-axis.[63] Moreover, in the diffractograms shown in **Figure 3** a shift was not observed in the (002) peak, since the contribution is due to the c-axis in this reflection and the c-axis dimension does not change from HA to FA.[3] To analyze the different behavior of crystal orientation along the lines of points that enter into the teeth, the evolution of the azimuthal intensity of the reflection (002) has been plotted. This gives a linear representation of the evolution of the pixel intensity along the ellipse specified by the angle 2θ (Debye ring).[45] **Figure 4 (c and d)** shows a typical example of the azimuthal plot for all the points of one line from both samples where there are two pronounced peaks separated by approximately 180º. The two pronounced peaks represent the opposing (002) reflection maxima that can be observed in the 2D µXRD images of **Figure 4 (a and b)**. Sharp intense peaks are evidence of a strong preferred orientation, while broad peaks would indicate a more random orientation of the crystallites.[47] It can be seen in **Figure 4 (c and d)** that both kinds of layers have a strong preferred orientation with intense peaks, even exceeding the intensity of the underlying enamel. Moreover, the treatment with NMTD and amelogenin

(**Figure 4a and 4c**) produces a layer that follows the preferred orientation of the surface enamel better than the treatment with only NMTD (**Figure 4b and 4d**), since the positions of the arcs and the peaks for the reflection (002) match better with enamel ones. The presence of another population of crystallites with distinct preferred orientation can be appreciated deeper in the enamel of the sample with protein where there are two additional peaks, also separated by approximately 180º (**Figure 4c**). This effect of four peaks due to two crystal populations with different preferred orientation is due to the natural structure of the enamel and can also be seen in the azimuthal plots of the enamel of both sample types in the **Supporting Information Figure S3 (a and b)**.

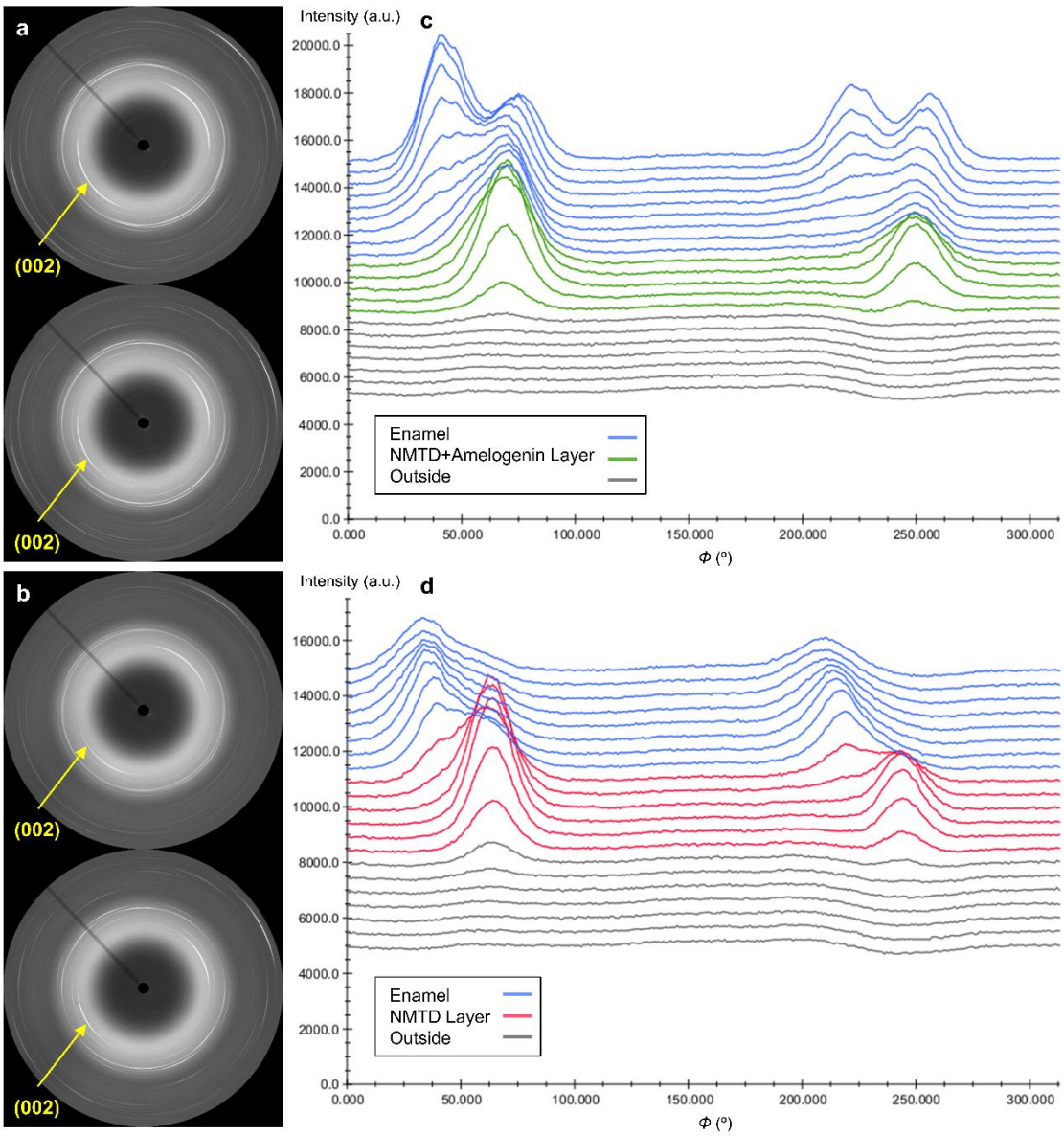

Figure 4. 2D µXRD images from (a) a sample with amelogenin and (b) a sample without amelogenin (enamel point on the top and layer point on the bottom). Representation of the azimuthal plots from a line of (c) a sample with amelogenin and (d) a sample without amelogenin.

In **Figure 5** MCR analysis of the azimuthal plots of the reflection (002) from both treatments (NMTD with amelogenin and NMTD alone) is shown. MCR was developed by imposing non-negativity in both the intensities and azimuthal profiles. The orientation of component 1 (blue) is mostly present in the layer, while component 2 (orange) appears in the outer enamel and component 3 (yellow) becomes more important in the deeper enamel where new preferred orientations appear. Component 4 (purple) belongs to the points outside before reaching the samples. The evolution of the different components confirms that the orientation of the layer with NMTD and amelogenin (**Figure 5a**) follows the enamel underneath better than the layer with only NMTD (**Figure 5b**). In the NMTD layer with amelogenin the change of the components 1 and 2 between the layer and the enamel is more gradual than in the one with NMTD alone, which is consistent with the movement of the peaks in **Figure 4 (c and d)**. The changes in the intensities of the components as they enter deeper into the tooth (**Figure 5a and 5b**) can also be correlated with the intensities of the peaks in the azimuthal plots at different depths. The intensity in the layers of the azimuthal plots in **Figure 4 (c and d)** is also higher than in the enamel. More examples are included in the **Supporting Information Figure S3**.

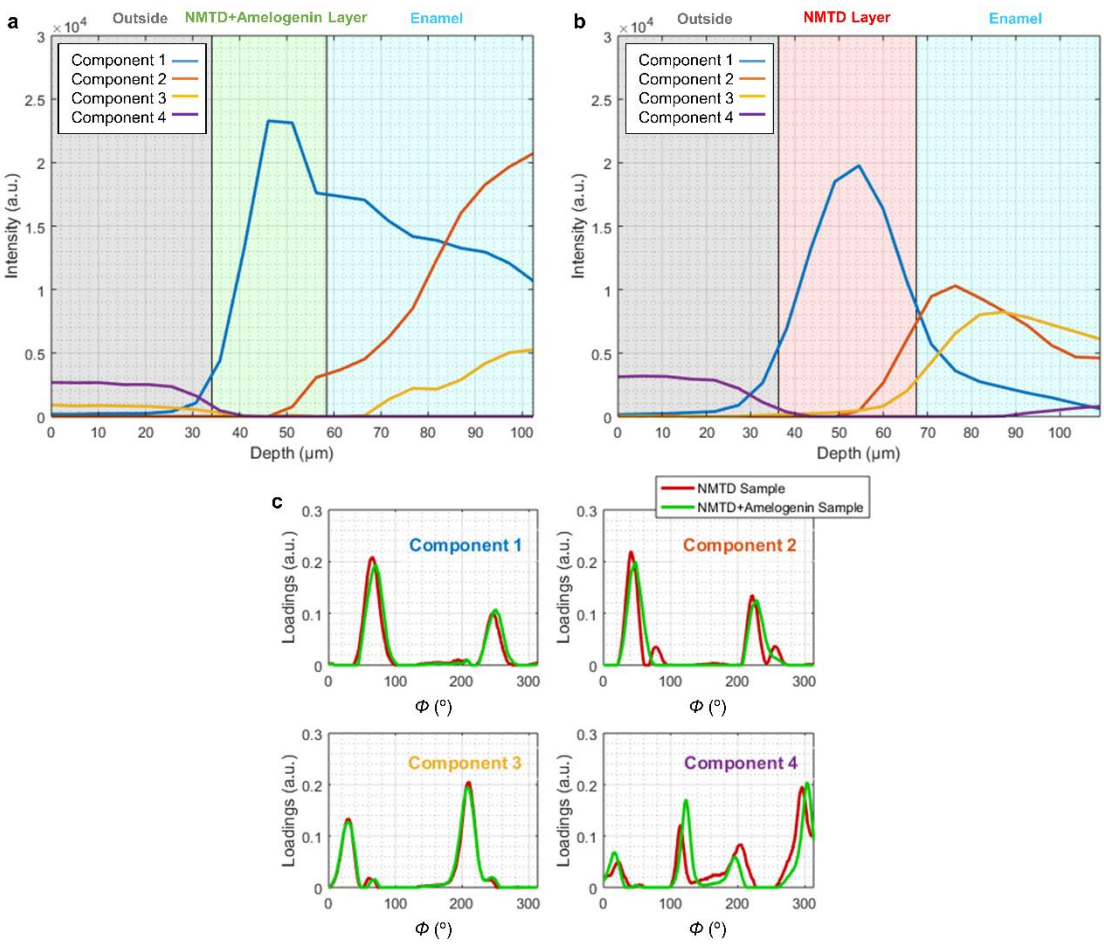

Figure 5. Examples of MCR analysis of the azimuthal plots from a line of (a) the sample with amelogenin and (b) the sample without amelogenin. (c) Loadings for each component of both samples, with amelogenin and without amelogenin.

The loadings in **Figure 5c** show peaks separated by 180º, as the peaks of the original azimuthal plots. The peaks for components 1 and 2 are in similar positions, yet component 3 has them shifted to lower angles. This is consistent with component 3 being predominant in the inner enamel (**Figure 5a and 5b**) where azimuthal peaks appear at lower angles (**Figure 4c and 4d**).

4. CONCLUSIONS

The combination of synchrotron infrared microspectroscopy and micro X-ray diffraction have shown to conform a useful methodology, together with the proper data treatment, to analyze the structure of apatites in samples of hard dental tissues. Infrared microspectroscopy provides information on chemical structural properties such as carbonate substitution, while micro X-ray diffraction allows to study the crystal structure and texture distribution on dental specimens. Synchrotron radiation allows to detect small changes with better resolution and to analyze microzones with high signal intensity.

Since mature tooth enamel does not regenerate after substantial loss, finding a suitable solution for the dental problems is essential.[27,28,47] The NMTD resin with or without amelogenin protein creates a remineralized layer on the surface of acid-etched teeth composed of carbonate free FA that has higher physicochemical stability than tooth HA. Nevertheless, amelogenin is a crucial component of this remineralizing product since it plays a critical role in controlling the preferred orientation of the growing crystal to resemble dental enamel.

Further studies would be desirable to assess the clinical applicability of this biomimetic treatment in humans.

ASSOCIATED CONTENT

Supporting Information

Images of dental specimens prepared for the synchrotron techniques; second derivative spectra of the enamel and the different layers; and additional examples of azimuthal plots and MCR analysis for the different samples.

AUTHOR INFORMATION

Corresponding Author

María-Jesús Sánchez-Martín − GTS Research Group, Department of Chemistry, Faculty of Science, Universitat Autònoma de Barcelona, 08193 Bellaterra, Spain; orcid.org/0000-0003-1678-6055; Phone: +34 93 581 4638; Email: mariajesus.sanchez@uab.cat

Authors

Sandra Diez-García − GTS Research Group, Department of Chemistry, Faculty of Science, Universitat Autònoma de Barcelona, 08193 Bellaterra, Spain; orcid.org/0000-0002-1549-5427

José Manuel Amigo − Chemical and Environmental Engineering Department, School of Engineering, University of the Basque Country, Alameda de Urquijo s/n, E-48013 Bilbao, Spain; orcid.org/0000-0003-1319-1312

Manuel Valiente − GTS Research Group, Department of Chemistry, Faculty of Science, Universitat Autònoma de Barcelona, 08193 Bellaterra, Spain; orcid.org/0000-0003-0766-9922

Notes

The authors declare no competing financial interest.

ACKNOWLEDGEMENTS

This work was supported by the Spanish Ministerio de Economía y Competitividad (project: CTM2015-65414-C2-1-R). Sandra Diez-García acknowledges the FI-2017 fellowship from Agència de Gestió d'Ajuts Universitaris i de Recerca (Generalitat de Catalunya). The SR-μFTIR experiment was performed at MIRAS beamline and the tts-μXRD experiment at MSPD beamline at ALBA Synchrotron (Cerdanyola del Vallès, Spain), with the collaboration of ALBA staff. This work has been funded by ALBA Synchrotron through granted proposals (grant references: 2018093150 and 2020024308).

REFERENCES

(1) Fujisaki, K.; Todoh, M.; Niida, A.; Shibuya, R.; Kitami, S.; Tadano, S. Orientation and Deformation of Mineral Crystals in Tooth Surfaces. *J. Mech. Behav. Biomed. Mater.* **2012**, *10*, 176–182.

(2) Kis, V. K.; Sulyok, A.; Hegedűs, M.; Kovács, I.; Rózsa, N.; Kovács, Z. Magnesium Incorporation into Primary Dental Enamel and Its Effect on Mechanical Properties. *Acta Biomater.* **2021**, *120*, 104–115.

(3) Wei, M.; Evans, J. H.; Bostrom, T.; Grondahl, L. Synthesis and Characterization of Hydroxyapatite, Fluoride-Substituted Hydroxyapatite and Fluorapatite. *J. Mater. Sci. Mater. Med.* **2003**, *14*, 311–320.

(4) Reyes-Gasga, J.; Martínez-Piñeiro, E. L.; Rodríguez-Álvarez, G.; Tiznado-Orozco, G. E.; García-García, R.; Brès, E. F. XRD and FTIR Crystallinity Indices in Sound Human Tooth Enamel and Synthetic Hydroxyapatite. *Mater. Sci. Eng. C* **2013**, *33* (8), 4568–4574.

(5) Derceli, J. dos R.; Faraoni, J. J.; Pereira–da–silva, M. A.; Palma-Dibb, R. G. Analysis of the Early Stages and Evolution of Dental Enamel Erosion. *Braz. Dent. J.* **2016**, *27* (3), 313–317.

(6) Gross, K. A.; Rodríguez-Lorenzo, L. M. Sintered Hydroxyfluorapatites. Part II: Mechanical Properties of Solid Solutions Determined by Microindentation. *Biomaterials* **2004**, *25* (7–8), 1385–1394.

(7) Oliveira, M.; Mansur, H. S. Synthetic Tooth Enamel: SEM Characterization of a Fluoride Hydroxyapatite Coating for Dentistry Applications. *Mater. Res.* **2007**, *10* (2), 115–118.

(8) Aoba, T.; Shimazu, Y.; Taya, Y.; Soeno, Y.; Sato, K.; Miake, Y. Fluoride and Apatite Formation *In Vivo* and *In Vitro*. *J. Electron Microsc. (Tokyo).* **2003**, *52* (6), 615–625.

(9) Campillo, M.; Lacharmoise, P. D.; Reparaz, J. S.; Goñi, A. R.; Valiente, M. On the Assessment of Hydroxyapatite Fluoridation by Means of Raman Scattering. *J. Chem. Phys.* **2010**, *132* (24), 244501.

(10) Poggio, C.; Lombardini, M.; Vigorelli, P.; Ceci, M. Analysis of Dentin/Enamel Remineralization by a CPP-ACP Paste: AFM and SEM Study. *Scanning* **2013**, *35* (6), 366–374.

(11) Soares, R. Assessment of Enamel Remineralisation after Treatment with Four Different Remineralising Agents: A Scanning Electron Microscopy (SEM) Study. *J. Clin. Diagnostic Res.* **2017**, *11* (4), 136–141.

(12) Lopes, C. de C. A.; Limirio, P. H. J. O.; Novais, V. R.; Dechichi, P. Fourier Transform Infrared Spectroscopy (FTIR) Application Chemical Characterization of Enamel, Dentin and Bone. *Appl. Spectrosc. Rev.* **2018**, *53* (9), 747–769.

(13) Mukherjee, S.; Gowen, A. A Review of Recent Trends in Polymer Characterization Using Non-Destructive Vibrational Spectroscopic Modalities and Chemical Imaging. *Anal. Chim. Acta* **2015**, *895*, 12–34.

(14) Acerbo, A. S.; Carr, G. L.; Judex, S.; Miller, L. M. Imaging the Material Properties of Bone Specimens Using Reflection-Based Infrared Microspectroscopy. *Anal. Chem.* **2012**, *84* (8), 3607–3613.

(15) Dumas, P.; Sockalingum, G. D.; Sulé-Suso, J. Adding Synchrotron Radiation to Infrared Microspectroscopy: What's New in Biomedical Applications? *Trends Biotechnol.* **2007**, *25* (1), 40–44.

(16) Deng, Y.; Hsu, C. Y. S. Combined Effect of Fluoride and Laser on the Crystalline Structure of Human Enamel: A Pilot Study. *Lasers Dent. XI* **2005**, *5687*, 42.

(17) Xue, J.; Zhang, L.; Zou, L.; Liao, Y.; Li, J.; Xiao, L.; Li, W. High-Resolution X-Ray Microdiffraction Analysis of Natural Teeth. *J. Synchrotron Radiat.* **2008**, *15* (3), 235–238.

(18) Maritan, L.; Casas, L.; Crespi, A.; Gravagna, E.; Rius, J.; Vallcorba, O.; Usai, D. Synchrotron Tts-MXRD Identification of Secondary Phases in Ancient Ceramics. *Herit. Sci.* **2018**, *6*, 74.

(19) Rodríguez-Martínez, J.; Valiente, M.; Sánchez-Martín, M. Tooth Whitening: From the Established Treatments to Novel Approaches to Prevent Side Effects. *J. Esthet. Restor. Dent.* **2019**, *31* (5), 431–440.

(20) Marquillas, C. B.; Procaccini, R.; Malmagro, M. V. Breaking the Rules: Tooth Whitening by Means of a Reducing Agent. *Clin. Oral Investig.* **2019**, *24*, 2773–2779.

(21) Babot-Marquillas, C.; Sánchez-Martín, M. J.; Rodríguez-Martínez, J.; Estelrich, J.; Busquets, M. A.; Valiente, M. Flash Tooth Whitening: A Friendly Formulation Based on a Nanoencapsulated Reductant. *Colloids Surfaces B Biointerfaces* **2020**, *195*, 111241.

(22) Saads Carvalho, T.; Lussi, A. Chapter 9: Acidic Beverages and Foods Associated with Dental Erosion and Erosive Tooth Wear. *Monogr. Oral Sci.* **2020**, *28*, 91–98.

(23) Yagi, N.; Ohta, N.; Matsuo, T.; Tanaka, T.; Terada, Y.; Kamasaka, H.; To-O, K.; Kometani, T.; Kuriki, T. Evaluation of Enamel Crystallites in Subsurface Lesion by Microbeam X-Ray Diffraction. *J. Synchrotron Radiat.* **2009**, *16* (3), 398–404.

(24) Featherstone, J. D. Prevention and Reversal of Dental Caries: Role of Low Level Fluoride. *Community Dent. Oral Epidemiol.* **1999**, *27* (1), 31–40.

(25) Creeth, J. E.; Karwal, R.; Hara, A. T.; Zero, D. T. A Randomized *In Situ* Clinical Study of Fluoride Dentifrices on Enamel Remineralization and Resistance to Demineralization: Effects of Zinc. *Caries Res.* **2018**, *52* (1–2), 129–138.

(26) Ratanaporncharoen, C.; Tabata, M.; Kitasako, Y.; Ikeda, M.; Goda, T.; Matsumoto, A.; Tagami, J.; Miyahara, Y. pH Mapping on Tooth Surfaces for Quantitative Caries Diagnosis Using Micro Ir/IrOx pH Sensor. *Anal. Chem.* **2018**, *90* (7), 4925–4931.

(27) Ruan, Q.; Moradian-Oldak, J. Amelogenin and Enamel Biomimetics. *J. Mater. Chem. B* **2015**, *3*, 3112–3129.

(28) Fan, Y.; Nelson, J. R.; Alvarez, J. R.; Hagan, J.; Berrier, A.; Xu, X. Amelogenin-Assisted *Ex Vivo* Remineralization of Human Enamel: Effects of Supersaturation Degree and Fluoride Concentration. *Acta Biomater.* **2011**, *7* (5), 2293–2302.

(29) Nelson, K.; Hesse, B.; Addison, O.; Morrell, A. P.; Gross, C.; Lagrange, A.; Suárez, V. I.; Kohal, R.; Fretwurst, T. Distribution and Chemical Speciation of Exogenous Micro- and Nanoparticles in Inflamed Soft Tissue Adjacent to Titanium and Ceramic Dental Implants. *Anal. Chem.* **2020**, *92* (21), 14432–14443.

(30) Aoba, T. The Effect of Fluoride on Apatite Structure and Growth. *Crit. Rev. Oral Biol. Med.* **1997**, *8* (2), 136–153.

(31) Perioli, L.; Nocchetti, M.; Giannelli, P.; Pagano, C.; Bastianini, M. Hydrotalcite Composites for an Effective Fluoride Buccal Administration: A New Technological Approach. *Int. J. Pharm.* **2013**, *454* (1), 259–268.

(32) Hussain, I.; Ahamad, K. U.; Nath, P. Low-Cost, Robust, and Field Portable Smartphone Platform Photometric Sensor for Fluoride Level Detection in Drinking Water. *Anal. Chem.* **2017**, *89* (1), 767–775.

(33) Valiente, M. Remineralizing Material for Organomineral Tissues. USA Patent US 6,413,498 B1, 1999.

(34) Matsunaga, T.; Ishizaki, H.; Tanabe, S.; Hayashi, Y. Synchrotron Radiation Microbeam X-Ray Fluorescence Analysis of Zinc Concentration in Remineralized Enamel *In Situ*. *Arch. Oral Biol.* **2009**, *54* (5), 420–423.

(35) Torrado, A.; Valiente, M. Kinetics Characterization of Ion Release under Dynamic and Batch Conditions. I. Weak Acid and Weak Base Ion Exchange Resins. *J. Solution Chem.* **2008**, *37* (4), 581–594.

(36) Torrado, A.; Valiente, M.; Zhang, W.; Li, Y.; Muñoz, C. A. Remineralization Potential of a New Toothpaste Formulation: An *In-Vitro* Study. *J. Contemp. Dent. Pract.* **2004**, *5* (1), 18–30.

(37) Chatterjee, S.; Singh, B.; Diwan, A.; Lee, Z. R.; Engelhard, M. H.; Terry, J.; Tolley, H. D.; Gallagher, N. B.; Linford, M. R. A Perspective on Two Chemometrics Tools: PCA and MCR, and Introduction of a New One: Pattern Recognition Entropy (PRE), as Applied to XPS and ToF-SIMS Depth Profiles of Organic and Inorganic Materials. *Appl. Surf. Sci.* **2018**, *433*, 994–1017.

(38) Ruckebusch, C.; Blanchet, L. Multivariate Curve Resolution: A Review of Advanced and Tailored Applications and Challenges. *Anal. Chim. Acta* **2013**, *765*, 28–36.

(39) Svensson Bonde, J.; Bulow, L. One-Step Purification of Recombinant Human Amelogenin and Use of Amelogenin as a Fusion Partner. *PLoS One* **2012**, *7* (3), e33269.

(40) Fonseca, R. B.; Haiter-Neto, F.; Fernandes-Neto, A. J.; Barbosa, G. A. S.; Soares, C. J. Radiodensity of Enamel and Dentin of Human, Bovine and Swine Teeth. *Arch. Oral Biol.* **2004**, *49* (11), 919–922.

(41) Fonseca, R. B.; Haiter-Neto, F.; Carlo, H. L.; Soares, C. J.; Sinhoreti, M. A. C.; Puppin-Rontani, R. M.; Correr-Sobrinho, L. Radiodensity and Hardness of Enamel and Dentin of Human and Bovine Teeth, Varying Bovine Teeth Age. *Arch. Oral Biol.* **2008**, *53* (11), 1023–1029.

(42) Ribó, L.; Sics, I.; Gevorgyan, A.; Nicolas, J.; Crisol, A.; Colldelram, C.; Nikitina, L.; Monge, R.; Quispe, M.; Yousef, I.; Dumas, P.; Ellis, G. Mechanical Design of MIRAS, Infrared Microspectroscopy Beam Line at ALBA Synchrotron. *JACoW, Geneva, Switz.* **2017**, 403–408.

(43) Fauth, F.; Peral, I.; Popescu, C.; Knapp, M. The New Material Science Powder Diffraction Beamline at ALBA Synchrotron. *Powder Diffr.* **2013**, *28*, 360–370.

(44) Rius, J.; Vallcorba, O.; Frontera, C.; Peral, I.; Crespi, A.; Miravitlles, C. Application of Synchrotron Through-the-Substrate Microdiffraction to Crystals in Polished Thin Sections. *IUCrJ* **2015**, *2*, 452–463.

(45) Vallcorba, O.; Rius, J. D2Dplot: 2D X-Ray Diffraction Data Processing and Analysis for Through-the-Substrate Microdiffraction. *J. Appl. Crystallogr.* **2019**, *52* (2), 478–484.

(46) Al-Jawad, M.; Addison, O.; Khan, M. A.; James, A.; Hendriksz, C. J. Disruption of Enamel Crystal Formation Quantified by Synchrotron Microdiffraction. *J. Dent.* **2012**, *40* (12), 1074–1080.

(47) Siddiqui, S.; Anderson, P.; Al-Jawad, M. Recovery of Crystallographic Texture in Remineralized Dental Enamel. *PLoS One* **2014**, *9* (10), 1–9.

(48) Aufort, J.; Ségalen, L.; Gervais, C.; Brouder, C.; Balan, E. Modeling the Attenuated Total Reflectance Infrared (ATR-FTIR) Spectrum of Apatite. *Phys. Chem. Miner.* **2016**, *43* (9), 615–626.

(49) Bachmann, L.; Diebolder, R.; Hibst, R.; Zezell, D. M. Infrared Absorption Bands of Enamel and Dentin Tissues from Human and Bovine Teeth. *Appl. Spectrosc. Rev.* **2003**, *38* (1), 1–14.

(50) Garskaite, E.; Gross, K. A.; Yang, S. W.; Yang, T. C. K.; Yang, J. C.; Kareiva, A. Effect of Processing Conditions on the Crystallinity and Structure of Carbonated Calcium Hydroxyapatite (CHAp). *CrystEngComm* **2014**, *16* (19), 3950–3959.

(51) Arboleda, A.; Franco, M.; Caicedo, J.; Tirado, L.; Goyes, C. Synthesis and Chemical and Structural Characterization of Hydroxyapatite Obtained from Eggshell and Tricalcium Phosphate. *Ing. y Compet.* **2016**, *18* (1), 69–71.

(52) Madupalli, H.; Pavan, B.; Tecklenburg, M. M. J. Carbonate Substitution in the Mineral Component of Bone: Discriminating the Structural Changes, Simultaneously Imposed by Carbonate in A and B Sites of Apatite. *J. Solid State Chem.* **2017**, *255*, 27–35.

(53) Brangule, A.; Gross, K. A. Importance of FTIR Spectra Deconvolution for the Analysis of Amorphous Calcium Phosphates. *IOP Conf. Ser. Mater. Sci. Eng.* **2015**, *77* (1), 012027.

(54) Chen, K. H.; Cheng, W. T.; Li, M. J.; Yang, D. M.; Lin, S. Y. Calcification of Senile Cataractous Lens Determined by Fourier Transform Infrared (FTIR) and Raman Microspectroscopies. *J. Microsc.* **2005**, *219* (1), 36–41.

(55) Fan, K.; Bell, P.; Fried, D. Rapid and Conservative Ablation and Modification of Enamel, Dentin, and Alveolar Bone Using a High Repetition Rate Transverse Excited Atmospheric Pressure CO_2 Laser Operating at λ=9.3 Mm. *J. Biomed. Opt.* **2006**, *11* (6), 064008.

(56) Jones, R. S.; Darling, C. L.; Featherstone, J. D. B.; Fried, D. Remineralization of *In Vitro* Dental Caries Assessed with Polarization-Sensitive Optical Coherence Tomography. *J. Biomed. Opt.* **2006**, *11* (1), 014016.

(57) Brundavanam, R. K.; Eddy, G.; Poinern, J.; Fawcett, D. Modelling the Crystal Structure of a 30 nm Sized Particle Based Hydroxyapatite Powder Synthesised under the Influence of Ultrasound Irradiation from X-Ray Powder Diffraction Data. *Am. J. M aterials Sci.* **2013**, *3* (4), 84–90.

(58) Okazaki, M.; Hirata, I.; Matsumoto, T.; Takahashi, J. Advantages of TOF-SIMS Analysis of Hydroxyapatite and Fluorapatite in Comparison with XRD, HR-TEM and FT-IR. *Dent. Mater. J.* **2005**, *24* (4), 508–514.

(59) Zheo, J.; Dong, X.; Bian, M.; Zhao, J.; Zhang, Y.; Sun, Y.; Chen, J.; Wang, X. Solution Combustion Method for Synthesis of Nanostructured Hydroxyapatite, Fluorapatite and Chlorapatite. *Appl. Surf. Sci.* **2014**, *314*, 1026–1033.

(60) Li, L.; Mao, C.; Wang, J.; Xu, X.; Pan, H.; Deng, Y.; Gu, X.; Tang, R. Bio-Inspired Enamel Repair via Glu-Directed Assembly of Apatite Nanoparticles: An Approach to Biomaterials with Optimal Characteristics. *Adv. Mater.* **2011**, *23* (40), 4695–4701.

(61) Fan, Y.; Sun, Z.; Moradian-Oldak, J. Controlled Remineralization of Enamel in the Presence of Amelogenin and Fluoride. *Biomaterials* **2009**, *30* (4), 478–483.

(62) Al-Jawad, M.; Steuwer, A.; Kilcoyne, S. H.; Shore, R. C.; Cywinski, R.; Wood, D. J. 2D Mapping of Texture and Lattice Parameters of Dental Enamel. *Biomaterials* **2007**, *28* (18), 2908–2914.

(63) Al-Mosawi, M.; Davis, G. R.; Bushby, A.; Montgomery, J.; Beaumont, J.; Al-Jawad, M. Crystallographic Texture and Mineral Concentration Quantification of Developing and Mature Human Incisal Enamel. *Sci. Rep.* **2018**, *8* (1), 1–18.

(64) Free, R.; Derocher, K.; Xu, R.; Joester, D.; Stock, S. R. A Method for Mapping Submicron-Scale Crystallographic Order/Disorder Applied to Human Tooth Enamel. *Powder Diffr.* **2020**, *35* (2), 117–123.

SUPPORTING INFORMATION OF THE MANUSCRIPT:

"A Combination of Two Synchrotron Radiation-Based Techniques and Chemometrics to Study an Enhanced Natural Remineralization of Enamel"

Sandra Diez-García[1(¥)], María-Jesús Sánchez-Martín[1*(¥)], José Manuel Amigo[2] and Manuel Valiente[1]

[1] GTS Research Group, Department of Chemistry, Faculty of Science, Universitat Autònoma de Barcelona, 08193 Bellaterra, Spain

[2] Chemical and Environmental Engineering Department, School of Engineering, University of the Basque Country, Alameda de Urquijo s/n, E-48013 Bilbao, Spain

[(¥)] Shared co-first authorship

[*] Author for correspondence e-mail address: mariajesus.sanchez@uab.cat

Table of Contents:

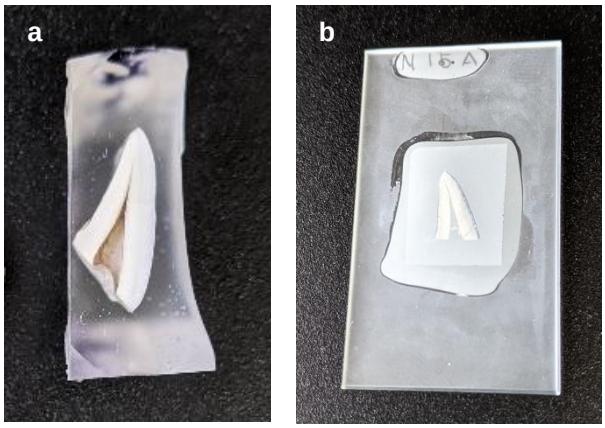

Figure S1. Image of a dental specimen prepared for (a) specular reflectance synchrotron radiation-based Fourier transform infrared microspectroscopy and (b) synchrotron through-the-substrate micro X-ray diffraction.

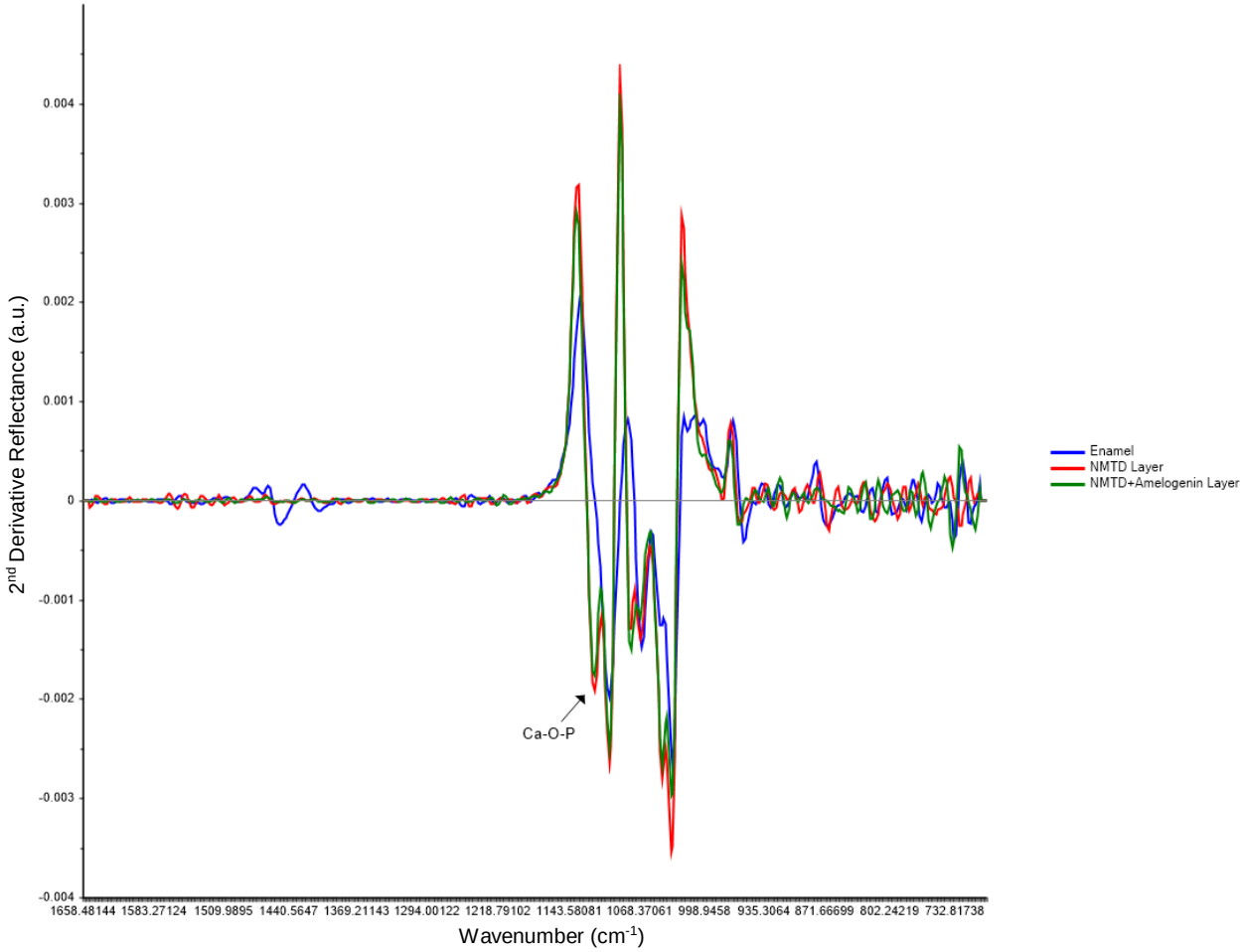

Figure S2. Savitzky-Golay second derivative average spectra of the enamel and the different layers performed with a polynomial order 3 on the region between 1660 and 700 cm^{-1} with Unscrambler X software (n=11).

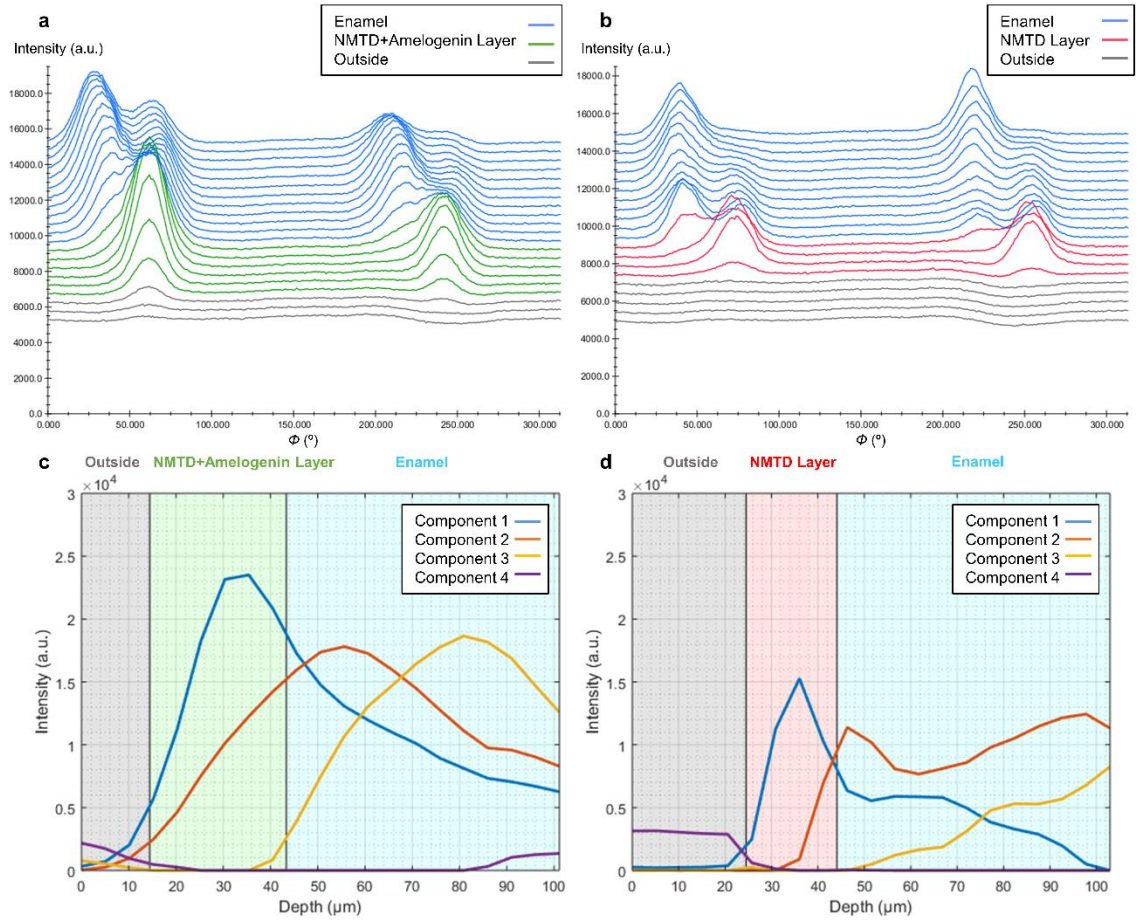

Figure S3. Representation of the azimuthal plots from a line of (a) a sample with amelogenin and (b) a sample without amelogenin. Examples of MCR analysis of the azimuthal plots from a line of (c) the sample with amelogenin and (d) the sample without amelogenin.

Y como dice siempre mi padre:

“Querer es poder”

FIN